Investigating the influence of selected environmental parameters as drivers of CO_2 emissions in the Northwest Territories, Canada

Master thesis, 6th Semester

Supervisor University of Augsburg: Prof. Dr. Wolfgang Buermann

Supervisor MPI-BGC: Dr. Mathias Goeckede

Co-Supervisor MPI-BGC: Kseniia Ivanova

Küchenmeister, Annelen

Registration number: 2110994

Climate and Environmental Sciences (M.Sc.), 6th semester

E-Mail: annelen.kuechenmeister@uni-a.de

Submission deadline: 02.05.2024

Acknowledgement

Abstract

Arctic wetlands play a critical role in the global carbon cycle. Although they account for only small parts of the global terrestrial areas, wetlands, in particular peatlands store large amounts of CO_2 while they are also severely affected by climate change at the same time. Rising temperatures can lead to the degradation and drying out of wetlands releasing CO_2 to the atmosphere and hence contribute to global warming. Furthermore, arctic ecosystems including vegetation, soil and hydrodynamics that are known for their complex relation towards CO_2 fluxes, are also experiencing a high impact of global climate change. Therefore, it is important to understand the dynamics between CO_2 and its response to environmental changes in these complex arctic ecosystems. This study investigates CO_2 flux dynamics in polygonal mires, focusing on how environmental parameters like thaw depth, soil temperature, soil moisture, soil pH, vegetation and NDVI influence CO_2 in the Northwest Territories, Canada. To do so, closed chamber measurements, which are a common approach for measuring NEE and ER fluxes were conducted at two polygonal mires close to the Trail Valley Creek (TVC) research camp in July. GPP was calculated using NEE and ER determined in the field. To investigate the influence of various environmental parameters collected during measurements, a statistical analysis was applied using linear regression, R^2, RMSE, MAE and a GAM model. The results showed that the relations are very complex and non-linear, highlighting the need for nuanced and careful interpretation. NDVI influenced CO_2 fluxes, with stronger correlations observed in certain vegetation compositions and moisture conditions. Surprisingly, correlations with PAR and air temperature were not significant, possibly due to data limitations and constant temperature conditions during the measurement period. Environmental parameters like soil moisture or pH interact in intricate ways to influence carbon dynamics. This study enhances our understanding of CO_2 flux dynamics in polygonal mires, providing valuable insights into the role of environmental parameters. Further research incorporating longer study durations and more comprehensive data collection could deepen our understanding of these complex ecosystems and their contribution to the global carbon cycle.

Table of Contents

List of figures

List of tables

Abbreviations

ER	Ecosystem Respiration
GAM	General Additive Model
GPP	Gross Primary Production
MAE	Mean Absolute Error
NDVI	Normalized Difference Vegetation Index
NEE	Net Ecosystem Respiration
PAR	Photosynthetically Active Radiation
R^2	Coefficient of Determination
RMSE	Root Mean Square Error
TD	Thaw depth
TVC	Trail Valley Creek

1 Introduction

1.1 The Arctic and global climate change

The Arctic, delimited by the Arctic Circle 66 ° 33'N in the South, describes the region spreading across the North Pole and covers only 5% of the Earth's land surface. Low temperatures (< 10°C) and permafrost soils are characteristic of this region (UNIVERSITY OF LAPLAND, 2024). Permafrost describes frozen ground with temperatures that stay below zero degrees for at least two consecutive years. This soil is typically covered by an active layer, that thaws every summer. Most of the biochemical and biological processes occur in this uppermost layer of permafrost soils (AWI, 2024). Due to the inhibition of mineralization, permafrost is also responsible for the carbon sink that arctic ecosystems provide (KWON et al., 2016). About 50% of the global soil organic carbon (SOC) is retained in these permafrost soils (LI et al., 2021). HUGELIUS et al. (2014) estimated that approximately 1307 Pg of SOC are stored in the first 0 to 3 m of permafrost soils and around 272 Pg below 3 m depth. CO_2 exchange between biosphere and atmosphere plays an important role in regulating these stocks and the carbon balance in general, whereby the process of photosynthesis and respiration is from great importance (VIRKKALA et al., 2018). During photosynthesis, light energy, CO_2 and H_2O are used by plants, algae and cyanobacteria to release oxygen (O_2) and to generate glucose ($C_6H_{12}O_6$, STIRBET et al., 2020). In contrast, respiration describes the process in reverse when CO_2 is released and O_2 is reduced to H_2O (HUNT, 2003; MILLAR et al., 2011). While the uptake of CO_2 during photosynthesis is called gross primary production (GPP), ecosystem respiration (ER) describes the release of CO_2 to the atmosphere due to plant but also microbial respiratory losses. The net ecosystem exchange (NEE) represents the balance between these two fluxes (VIRKKALA et al., 2018).

Global warming and climate change can impact these fluxes in various ways. Due to arctic surface temperatures, which have doubled more than the average worldwide over the last 20 years and increasing permafrost soil temperatures (IPCC, 2022), permafrost regions are severely affected by global climate change. The observed warming trends result in rapid thawing and with that

1

increasing mineralization and decomposition of the carbon stored in permafrost soils (KWON et al., 2016; VIRKKALA et al., 2018). This can lead to the increased release of greenhouse gases, such as carbon dioxide, causing a positive feedback loop between global warming and permafrost thawing, contributing to rising carbon concentrations in the atmosphere (LINDGREN et al., 2016). Consequently, the previously existing tendency of arctic ecosystems to store more CO_2 than releasing it changes, turning permafrost soils and the Arctic to a carbon source (KWON et al., 2016). Former studies investigating flux measurements in arctic environments confirmed this assumption that arctic tundra ecosystems provide a source to atmospheric carbon (BIASI et al., 2014; NATALI et al., 2019; OECHEL et al., 2014). However, other studies found that these ecosystems can also serve as sink and source (BRUHWILER et al., 2021; KITTLER et al., 2017).

Due to the harsh arctic conditions, data collection in these extreme and remote environments is more complicated and currently leads to a scarcity of data limiting the ability to assess CO_2 fluxes. (OECHEL et al., 2014; SCHUUR & ABBOTT, 2011). While commonly used Eddy Covariance (EC) towers measure carbon fluxes continuously, these technique averages over fine-scale heterogeneity and requires technical knowledge, high costs and maintenance as well as logistical challenges such as access to electricity. In contrast, chamber measurements, which are further explained in chapter 2.2, are very labour-intensive and time-consuming but cost-efficient and allow to capture fine-scale spatial-variability (VIRKKALA et al., 2018). However, models for estimating carbon release usually do not consider important processes like rapid permafrost thawing as they only focus on rising air temperature leading to uncertainties in the estimation of carbon fluxes (BRUHWILER et al., 2021; SCHUUR & ABBOTT, 2011).

1.2 CO2 emissions of polygon mires in the Arctic tundra

Arctic wetlands play an important ecological role in filtering drinking water, buffering heavy rainfall and contributing to biodiversity by providing habitats and breeding areas for e.g. birds and fish (CAFF, 2021). Almost half of the world's wetlands are concentrated in the Arctic, where they account for approximately 60% of the Arctic ecosystems and include a mix of peatlands, wet tundra, open water and seashore areas. Despite covering only a small fraction of the world's terrestrial area, wetlands store with 20% more terrestrial carbon than forests (CAFF, 2021). Canada comprises about a quarter of the world's wetlands with about 1,29 km^2 (GOVERNMENT OF CANADA, 2016). At the same time, Canadas peatlands store about 147 Gt soil organic carbon (TARNOCAI, 2009).

Wetlands are defined as areas, that experiences regular inundation or saturation by water, sustaining emergent plant life adapted to such conditions. Additionally, the Ramsar Convention, an international Convention on Wetlands providing a framework for the conservation of wetlands, extends this definition to open freshwaters as well as marine waters up to a depth of six meters at low tide (BARTHELMES et al., 2015; THE RAMSAR CONVENTION, 2024). There are many different approaches to the classification of wetlands and their subcategories around the world (JOOSTEN & CLARKE, 2002). Polygonal mires are a complex form of peatlands, that describe a wetland area with an accumulated peat layer at the surface. Peat is an accumulated material consisting of a minimum of 30 % dead organic material. A peatland in a state in which peat is currently being formed is called a mire. Polygon mires can be found in arctic environments with continuous permafrost (JOOSTEN & CLARKE, 2002). These wetlands are caused by thermal contraction and expansion in the active layer when tension cracks spread through the frozen active layer into the deeper permafrost layer during the winter months. During summer, water from snow melt runs in these open cracks and freezes before they close leading to an expansion of the vertical ice veins to ice wedges due to the annually repeating circle. While these ice wedges grow, they force the surrounding soil upward resulting in polygonal structures. This effect is intensified when occurring in

peat, leading to deep, ice-filled cracks which provide water sources that maintain the mire and peat formation (MINAYEVA et al., 2016). In addition to low-centre polygons, which represent the early stages of polygon development, high-centre polygons signify the matured forms of polygonal mires with domes that rise from the polygonal trenches (Figure 1). In Canadian wetland terminology, low-centre polygons are classified as fens, while high-centre polygons correspond to bogs (CANADA COMMITTEE ON ECOLOGICAL (BIOPHYSICAL) LAND CLASSIFICATION, 1988).
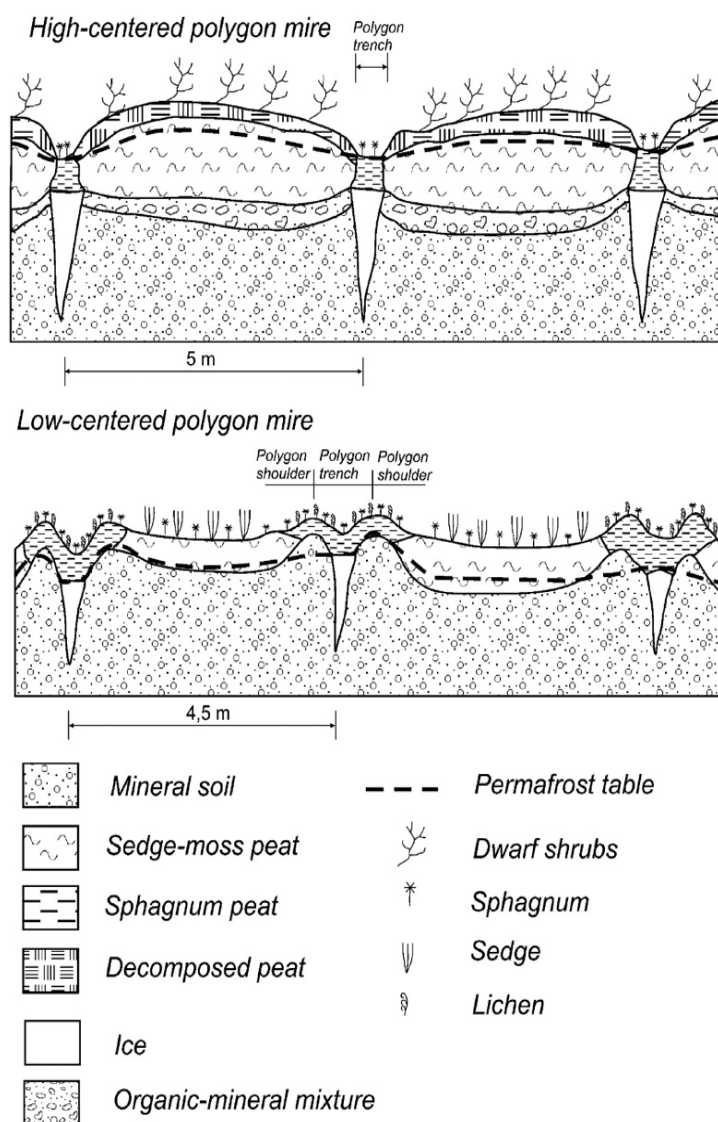
Figure 1: Cross-section of a high-centre polygonal mire (a) and a low-centre polygon mire (b) showing the different component and development stages of polygon mires (MINAYEVA et al., 2016).

While they are important for preventing permafrost thaw, wetlands are also influenced by climate change and global warming resulting in the degradation of arctic wetland ecosystems (CAFF, 2021). A peat sensitivity model run by TARNOCAI (2009) confirmed that 675.540 km^2 will experience an extreme impact of climate change affecting approximately 75.05 Gt of organic carbon. While these wetlands are expected to become drier due to climate change, the number of wildfires is also likely to increase as a result. Consequently, peatlands could release large amounts of carbon into the atmosphere. Moreover, the degradation of SOC in wetlands, especially peatlands, can also lead to strong feedback mechanisms that further support the process of climate change (TARNOCAI, 2009).

1.3 Impact of global warming on CO_2 and environmental parameters in arctic ecosystems

In the context of climate change, the Arctic is experiencing a warming trend effecting environmental conditions in various ways (CALVIN et al., 2023). The terrestrial warming trend leads to rising ground temperatures (KOKELJ et al., 2017; KOVEN et al., 2015) that initiate thawing of permafrost soils and change the hydrology of arctic ecosystems like peatlands at the same time (ANDRESEN et al., 2020; TARNOCAI, 2009). Hydrology plays a crucial role in permafrost landscapes as it controls the complex interactions between e.g. biogeochemical cycles. Permafrost significantly impacts hydrology by determining water distribution, storage and flow patterns both on the surface and subsurface. It inhibits vertical water movement, leading to saturated ground conditions in continuous permafrost areas, while in discontinuous permafrost areas it constrains subsurface flow through unfrozen layers. However, with the observed and predicted thawing of permafrost, considerable uncertainties arise regarding future hydrological conditions and their impacts, including the carbon-climate feedback of permafrost. Changes in surface hydrology, particularly influenced by soil moisture, play a critical role in determining the nature and extent of carbon emissions from thawing soils and microbial decomposition, which affects CO_2 dynamics (ANDRESEN et al., 2020). By using the Community Land

Model, Lawrence et al. (2020) found that drying of the landscape due to permafrost thaw significantly increases CO_2 emissions and soil respiration rates. At the same time, when ice-rich peat soils thaw, water-saturated conditions occur in permafrost soils, which, together with higher temperatures, intensify anaerobic decomposition (TARNOCAI, 2009).

Changes in temperatures also enhance Arctic greening, which is determined via the Normalized Difference Vegetation Index (NDVI, MCPARTLAND et al., 2019). This Index measures the difference between the surface reflection of near-infrared light by vegetation and red light absorbed by vegetation. Due to warming temperatures and changes in the hydrology, maximum summer NDVI increases in Arctic regions resulting in the expansion of shrub cover (BERNER et al., 2020; BRUHWILER et al., 2021). However, while some studies show that the drying out of peatlands leads to a reduction in GPP fluxes (CHURCHILL et al., 2015), other studies indicate that carbon uptake can increase with a positive greening trend (ANDRESEN et al., 2020).

1.4 Research objective and motivation

Given the complexity of parameters that contribute to the changes in the Arctic environment und associated uncertainties in the response like the permafrost carbon-climate-feedback (ANDRESEN et al., 2020; BRUHWILER et al., 2021), this study aims to investigate the influence of soil- and vegetation-related environmental parameters on NEE, ER and GPP on a small-scale by using chamber measurements at two polygonal mires close to Trail Valley Creek (TVC) Research Station in the Northwest Territories (NWT) Canada. Soil temperature, soil moisture, soil pH, thaw depth, NDVI as well as air temperature and photosynthetically active radiation (PAR) are also assessed at the different study sites. We hypothesize that soil temperature and soil moisture have a positive impact on CO_2 fluxes. Furthermore, thaw depth is expected to have a positive effect on ecosystem respiration while negatively influencing carbon uptake. The relation between CO_2 fluxes and NDVI is expected to depend on vegetation composition. However, the study is limited due to the reasonable

working and the remoteness of the study areas. Further limitation due to missing investigation during spring, autumn and winter periods contribute to the missing requirements for a comprehensive study.

While chamber flux studies are mainly concentrated in Alaska, Fenoscandinavia or Russia, Canada has not received much consideration until a few years ago (VIRKKALA et al., 2018). Studies regarding carbon emissions of polygonal mires are often found in regions of the Siberian Arctic (ECKHARDT et al., 2019, 2019; KITTLER et al., 2017; KWON et al., 2016; VIRTANEN et al., 2016). Other studies that were conducted in Canada focus on the Hudson Bay Lowland (HARRIS et al., 2020; HELBIG et al., 2019; HUMPHREYS et al., 2014). This study concentrates on polygonal mires in the Northwest Territories aiming to contribute to a better understanding on CO_2 dynamics in the Arctic ecosystems of northern Canada.

2 Methodology

2.1 Study Area

2.1.1 Trail Valley Creek

The study area is located in the Trail Valley Creek (TVC) research basin (68°45'N, 133°30'W) approximately 55 km north of Inuvik, the Northwest Territories (Figure 2) and east of the Mackenzie River Delta (MARSH & POMEROY, 1996). The studied transects 2 and 5 are located in two polygonal mires to the east and north-west of the TVC camp (Figure 2).

TVC has an area of about 57 km^2 and is in the zone of low Arctic climate with continuous permafrost including deeply incised river valleys, gently rolling hills and elevations that range from 9 to 187 m.a.s.l. (MARSH et al., 2010; POHL et al., 2005; POMEROY et al., 1998).

The mean annual air temperature and precipitation for Inuvik in the period from 1991 – 2020 was -7.6 °C and around 249.8 mm respectively, with mean temperatures in Canada continuing to rise especially in the north of the country (A1; GOVERNMENT OF CANADA, 2024a, 2024b). While the inland is characterized by warmer and wetter conditions, climate gets colder and drier with increasing proximity to the coast resulting in a steep climate gradient for the region (KOKELJ et al., 2017). The highest temperatures and precipitation in Inuvik are in July and August (A1) with the highest temperature of 33°C measured on July 4th, 2023 (Government of Canada, 2024c). The snow cover lasts from September to May with decreasing precipitation in winter and the lowest temperatures in January (A1; Pomeroy et al., 1998). During measurements, air temperature did not fall below 20°C (A2).
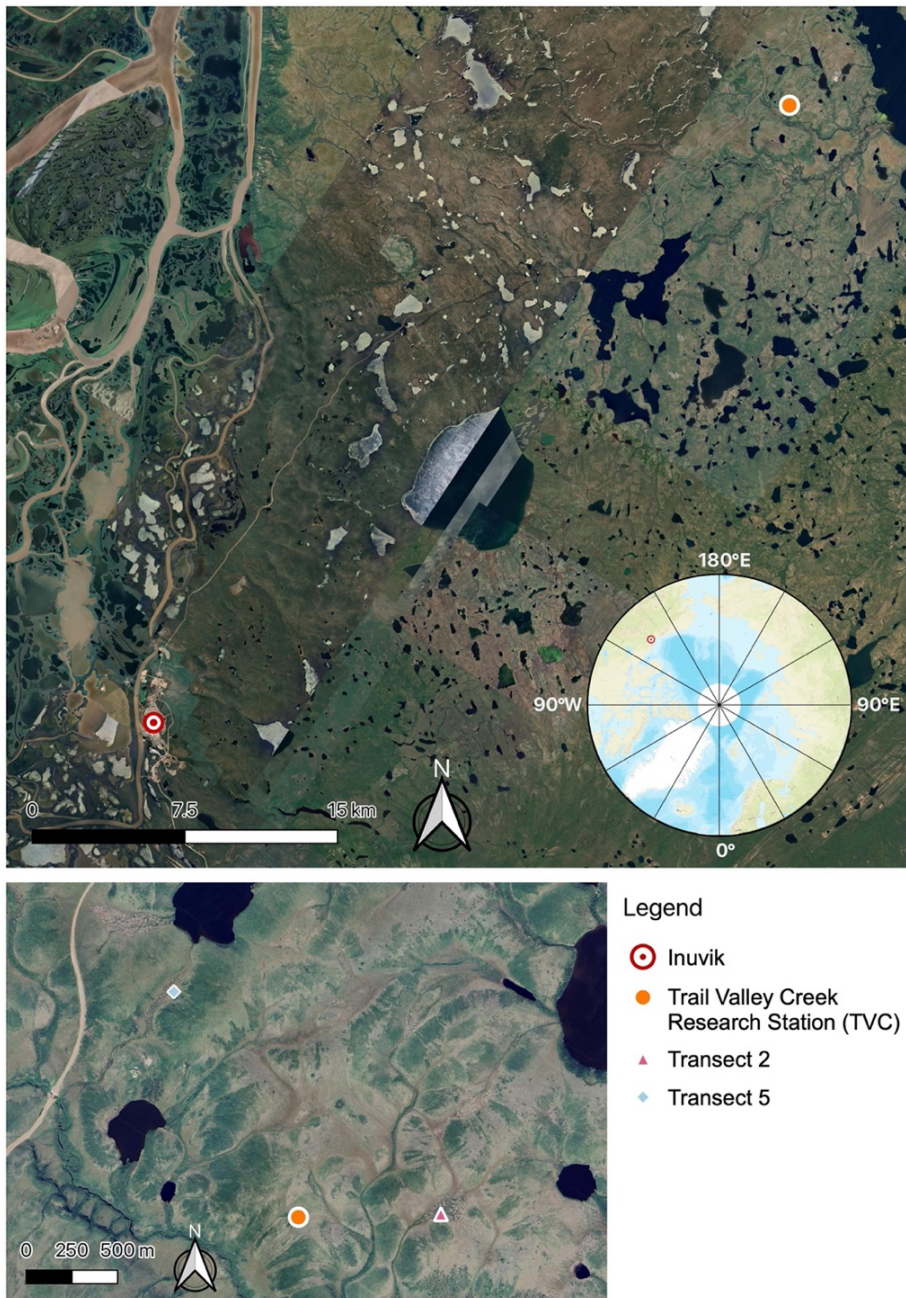
Figure 2: Location of the TVC study site. The study site is located appr. 55 km north of Inuvik (68°45'N, 133°30'W). Transects 2 and 5 are in close distance to TVC camp.

About 25,000 to 30,000 years ago, the study region east of the Mackenzie River delta was covered by Wisconsin glacial ice and, together with later lake drainage during the Holocene, left behind polygonal peat plateaus that are characteristic of the landscape today (KOKELJ et al., 2017). Hence, different polygonal structures including high- and low-centre polygons can be found in the study

area (CANADA COMMITTEE ON ECOLOGICAL (BIOPHYSICAL) LAND CLASSIFICATION, 1988). Furthermore, the investigated area is characterized by mineral earth hummocks with diameters ranging from 0.4 to 1 meter and crests varying from 0.1 to 0.4 cm in height. Overall, peat thickness in the inter-hummock areas ranges between 0.3 and 0.5 meters, with living vegetation and lightly decomposed peat in the upper 0.2 meters, followed by highly decomposed peat below this layer. In addition, the fine-grained material varies only slightly in particle size distribution with depth, but has large clay-containing fractions (QUINTON et al., 2000). This landscape in the forest-tundra transition zone consists of many different types of tundra vegetation, with forest patches still to be found in some locations. Prevailing vegetation types include trees, tall shrub tundra, dwarf shrubs, riparian shrubs, tussocks and lichen (Figure 3; Grünberg et al., 2020; Marsh et al., 2010).

Tree patches consist mainly of white and black spruce (*Picea glauca* and *P. mariana*) with an undergrowth of dwarf-birch (*Betula glandulosa*) and green alder (*Alnus crispa*; Palmer et al., 2012). These small forest areas are located near river channels, but also grow in isolated patches, which can reach a height of up to 10 m or between 0.5 m and 2 m respectively (ANTONOVA et al., 2019; GRÜNBERG et al., 2020). With regard to the study area, these patches account for approximately 2% of the TVC landscape. Dwarf shrubs growing on hilltops and slopes, and tussocks represent the most common types of vegetation, covering approximately 24% and 37% of the TVC area, respectively. With a height ranging from 0.2 to 0.5 m dominant species like the dwarf birch form a dense canopy. Other vegetation species also found in dwarf shrub tundra are shorter dwarf shrubs such as Labrador tea (*Ledum palustre*) and mountain cranberry (*Vaccinium vitis-idaea*), forbs (e.g. sweet coltsfoot, *Petasites frigidus*) and lichen. Tussock tundra grows mostly in flat and poorly drained areas. Cotton grasses (*Eriophorum spp.*) and sedges (*Carex spp.)* dominate forming the tussocks often grow with mosses between the tussocks as well as other species such as dwarf shrubs, willows (*Salix* spp.), Labrador tea, mountain cranberry, bilberry (*Vaccinium uliginosum*), crowberry (*Empetrum nigrum*) and cloudberry (*Rubus chamaemorus*). Tall shrub tundra covers around 11% of the area and consists of green alder (*Alnus viridis*), dwarf birch (*Betula glandulosa* Michx.,

B.) as well as Salix species. Close to streams, vegetation species like Willows (*Salix spp.*) are part of the riparian shrub tundra, which accounts for about 14 % of the TVC area. Lichen-dominated vegetation covers approximately 10% of the TVC landscape with further occurrence of Labrador tea, mountain cranberry, crowberry, bearberry, and cloudberry (GRÜNBERG et al., 2020; GRÜNBERG & BOIKE, 2019; STREET et al., 2018).
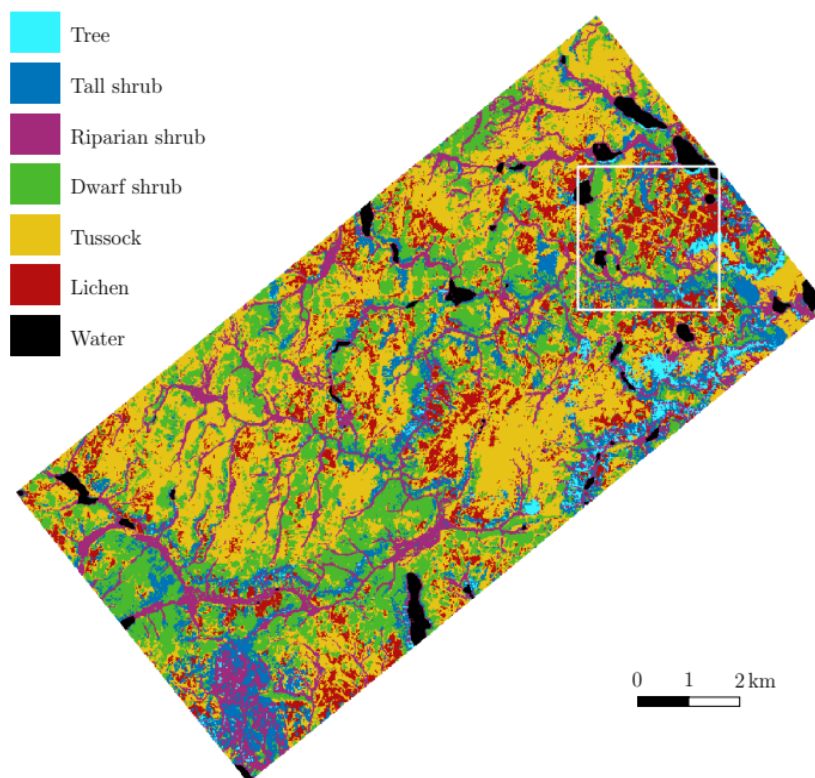
Figure 3: Vegetation of TVC (GRÜNBERG AND BOIKE, 2019).

2.1.2 Transect 2

Transect 2, located east of the TVC camp (Figure 2), is a polygonal complex measuring 120 to 320 m in size. The polygon has a wet degraded center that extends for approximately 30 to 70 m (Figure 4). In addition to flat, mainly quadrangular lichen polygons, which cover most of this area, there are also trenches with different soil moisture levels found in this polygon (A4).
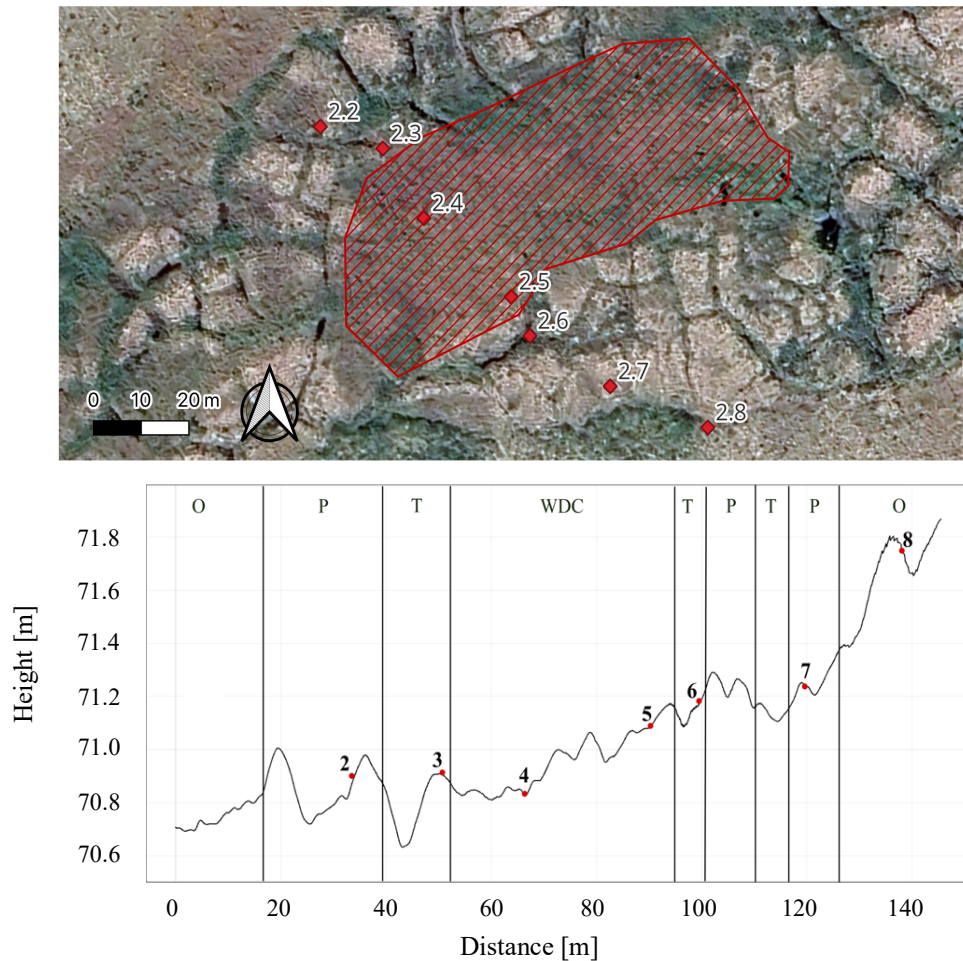
Figure 4: a) Overview of the collar locations of Transect 2. The red hatched area symbolizes the wet degraded center of the polygonal mire b) Profile of transect 2 and position of the sites in the sections of the polygon complex: Outside (O), Polygon (P), Trench (T) and wet degraded center (WDC).

As polygonal centers are mostly flat, the surrounding rims are not clearly distinct. Measurement site 2.8 is located outside the polygonal complex on a drier upslope position within the upland tundra (Figure 4). Vegetation in this collar consists of dwarf shrubs like Labrador tea, crowberry bilberry, mosses as well as sedges and lichens (A3), which are considered indicators for drier conditions (CHESTER, 2016). Site 2.7 was installed inside a minor depression in the flat center of a polygon (Figure 4) showing wetter conditions than the surrounding lichen community (A4). *Sphagnum squarrosum* and *Sphagnum russowi* cover most of the collar followed by a small proportion of dwarf shrubs (A3). The flat degraded wet center contains collars 2.4 and 2.5, which show

12

characteristics of wet tussock tundra including high tussocks and wet inter-tussock areas. However, moisture conditions and vegetation indicate drier conditions with green mosses covering large parts of these sites followed by few dwarf shrubs. The wettest sites are collars 2.2, 2.3 and 2.6 (A4), whereby the last two sites are permanently waterlogged and located in trenches surrounding the flat lichen centers. Moss layers consisting of *Hypnum* species as well as *Carex* tufts and *Betula nana* are the prevailing vegetation at these sites (A3). In contrast, site 2.2 shows wet conditions with green mosses forming the main vegetation followed by several dwarf shrubs and different *Carex* tufts (A3; A4).

2.1.3 Transect 5

Transect 5 was set up to the north-west of the TVC research camp. In contrast to transect 2, this polygonal mire does not have a wet degraded center and is located in a gully with proximity to the closest lake (Figure 2). The complex is approximately 50 to 400 m with the polygon elements clearly visible due to its low stage of degradation (Figure 5).

Sites 5.1, 5.2 and 5.3 are located in a trench that slightly slopes downward towards a waterfilled gulley (Figure 5), whereby 5.1 is placed furthest away from the water and 5.2 and 5.3. getting progressively wetter (A5). Compared to the other sites in this trench, which all are mainly covered by *Sphagnum* mosses, green mosses and *Carex* spp., collar 5.1 shows a higher occurrence of e.g. *Rubus chamaemorus* and *Vaccinium vitis-idaea* (A3). The other locations are placed in different polygonal centers of the complex (Figure 5) showing different degrees of wetness (A5). Sites 5.4, 5.5 and 5.6 are located in a low-centered polygon with a wet center. Collar 5.4 is close to the rim of the polygon and shows a vegetation composition with high proportion of lichen. Due to its closer proximity to the wet center, the vegetation of collar 6 includes mainly *Sphagnum balticum* (A3). Sites 5.9 and 5.10 are placed at the outer margins of this polygonal complex with 5.9 further away from the wet center (Figure 5).
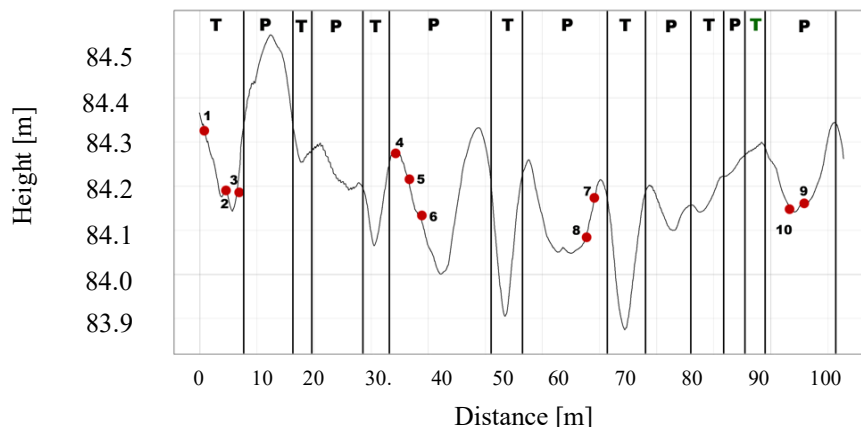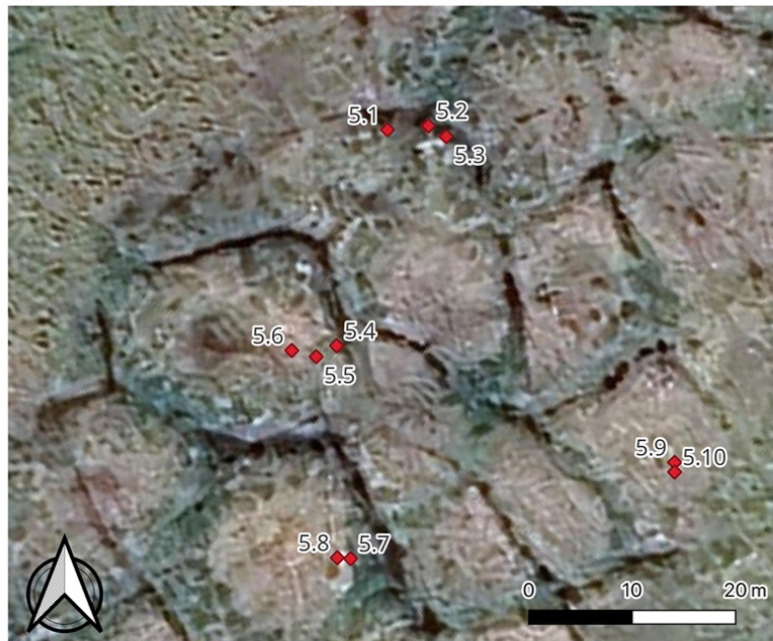
Figure 5: a) Overview of the collar locations of Transect 5 b) Profile of transect 2 and position of the sites in the sections of this polygon complex: Trench (T), Polygon (P).

2.2 Chamber installation and chamber measurements

The chamber measuring method used in this study is based on a closed dynamic chamber consisting of a collar that is installed into the ground and a portable chamber which is placed on top of the collar during each measurement. Operating in a fully closed mode, air is continuously sampled from the chamber air space. At the same time, this air is drawn to a gas analyzer and then returned to the chamber measuring changes in CO_2 concentrations over a short time period. The calculate the fluxes from these changes, a linear fitting model is used. The collar provides stability for the chamber and ensures an airtight

sealing during flux measurements. The chamber is further equipped with sensors that allow measurements of parameters like air and soil temperature, soil moisture or PAR (PAVELKA et al., 2018).

To measure CO_2 fluxes in different study areas of Trail Valley Creek in July, a setup of closed chambers, a portable Licor LI-7810 gas analyzer as well as a Datalogger CR1000X and various sensors were used (Table 1). The chamber system consisted of a UV-resistant circular plastic glass tube, 25 cm in diameter and 25 cm in height, and a PVC collar, also 25 cm in diameter. An amount of 5 mm was subtracted from the diameter to take into account the thickness of the walls. The soil collars were set up in 2022 and were installed at least 0.09 cm into the ground and extend no more than 0.30 cm above the soil surface (Figure 6).
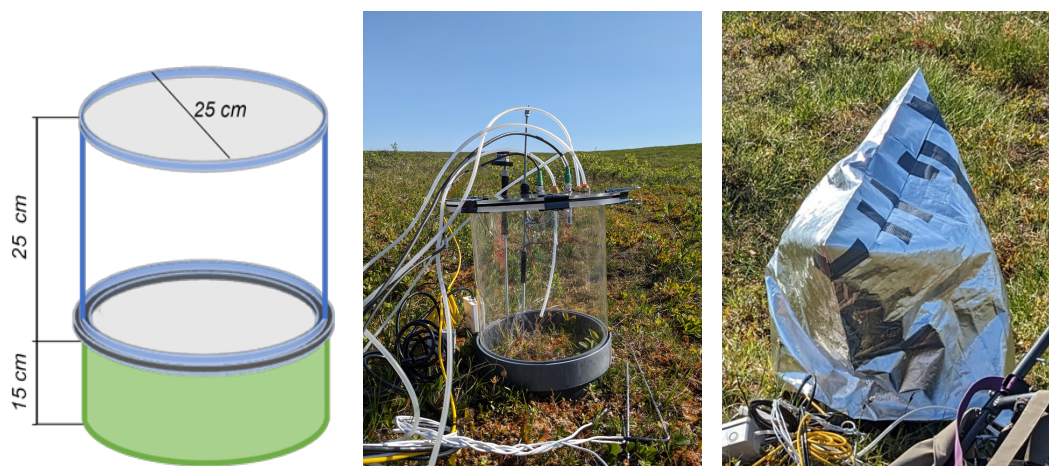
Figure 6: Dimensions (left) of the chamber system and setup for light (middle) and dark (right) measurements in the field (photos: KÜCHENMEISTER, 2023).

Further instruments included in the chamber measurement system involve an air temperature and humidity sensor, an air pressure transmitter and a fan for mixing the air inside the chamber. Photosynthetically active radiation and other supporting measurements like thaw depth, soil moisture and temperature, soil pH and vegetation analysis (Table 1) were conducted close to each chamber setup. All instruments and the gas analyzer were connected to the data logger

(A6), which used a WIFI connection to send all collected data to one tablet for further processing.

Table 1: Supporting measurements and instruments in addition to the chamber measurements.

Method	Parameter	Range of value	Precision
Portable gas analyser LI-7810	CO_2	1 – 10000 ppm	3,5 ppm /1 s
Datalogger CR1000X	Data storage		
Temperature and humidity sensor KPK1_9-ME	Relative humidity air temperature	0 – 100% -30 – 70 °C	2% 0,2°C
Air pressure transmitter 61402V	Air pressure	500 – 1100 hPa	0,2 hPa
Sensor for photosynthetically active radiation (PAR) PQS1	Irradiance	0 – 10000 mmol/m^2/s	1 mmol/m^2/s
Soil temperature profile probe CS230	Soil temperature:	-55 – 85°C	0,2°C
Soil moisture probe CS655-DS, CS650-DS	Volumetric water content 12 and 30 cm	0 – 100%	3%
pH logger PCE-228SLUR-ICA	Soil pH	0 – 14	0,02
GPS 16X-HVS	Geographic position		15 m
Steel rod with calibrated markings	Thaw depth	0 – 50 cm	1 cm

After all instruments were installed close around the chamber system, three light and two dark measurements were conducted. Each measurement took two minutes with a 30 to 60 seconds break to ventilate the chamber and remove all water vapor inside. While conducting dark measurements to investigate ER, the PAR level was reduced close to 0 by using an opaque cover sheet (A6; Figure 6). Following the light and dark measurements at each chamber, the minimum and maximum height of the collar inside was measured for later chamber and collar volume calculations (Figure 7). NDVI was determined using the bands of the aerial imagery dataset provided by (RETTELBACH et al., 2018. It was calculated by using the reflectance of the red and near-infrared spectral bands and applying the formula (JESPERSEN et al., 2023) :

$$NDVI = \frac{R_{nir} - R_{red}}{R_{nir} + R_{red}} \tag{1}$$

Furthermore, pictures were taken vertically above the collar and samples of mosses and shrubs were also collected for the identification of the vegetation in the collar.
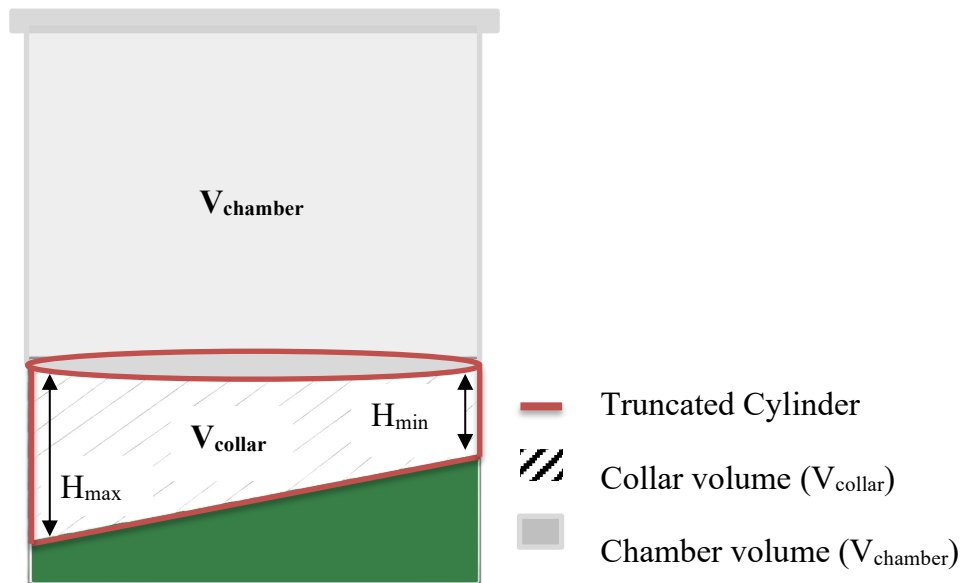
Figure 7: Minimum (H$_{max}$) and maximum (Hmin) height within the collar and the subsequently calculated volume fractions of chamber and collar relevant for calculating the CO$_2$ fluxes.

2.2.1 Collar volume and chamber surface area

In order to determine the CO_2 fluxes, the chamber volume $V_{chamber}$ and the collar volume V_{collar} as well as the surface area A of the chamber inside the collar had to be calculated based on the previous height measurements of each collar. While the chamber has a constant volume of $V_{chamber} = 0.01414 \text{ m}^3$ due to its fixed dimensions, the volume of the collar and surface area were calculated for each individual location. As the vegetation and wetness inside the collar vary spatially, it could not be assumed that the ground is completely horizontal. Therefore, a truncated cylinder was assumed for calculating the collar volume (Figure 7), using the measurements of H_{min} and H_{max} at each location and a radius r of 12.25 cm (HARRIS, 1998):

$$V_{collar} = \frac{\pi\, r^2}{2} \times (H_{min} + H_{max}) \tag{2}$$

By adding both volumes, the total volume of the chamber system can be determined. The calculation of the chamber surface area is based on the lateral surface area formula of an truncated cylinder (HARRIS, 1998) using again H_{min} and H_{max} as well as an radius of 12.25 cm which is converted to m^2 by dividing the difference of H_{min} and H_{max} by 100:

$$A = \pi r \left[\sqrt{r^2 + \left(\frac{\frac{H_{min} - H_{max}}{100}}{2} \right)^2} \right] \tag{3}$$

2.3 Data processing

After all the data was collected and stored in one file by the datalogger, it got prepared for further processing using a routine run in R Studio. In a first step, after reading the raw output file the time series was cut into segments

representing the individual measurements. In the next step the script analyzed the input data from each single file for a stable gradient of concentration change over time while fitting a mean slope. Since the gradient fitting did not work well in all cases, the script generated not only numerical output but also panel plots for each measurement. In case the time period for gradient fitting did not fit, each plot was checked individually whereby the time period was manually adjusted when necessary.

The final step involves the processing of the gradients for each timestamp by repeating the previous steps of the script, taking into account the changes made for some of the gradient time windows. This process aggregates the data points and calculates the flux component slopes, which were then used to compute net ecosystem exchange and ecosystem respiration.

2.3.1 Calculating Net Ecosystem Exchange and Ecosystem Respiration

After processing the field data and calculating different volumes of the chamber system, CO_2 fluxes were determined using a general formula for flux calculations that includes the mean slope of gas concentration change over time:

$$CO_2\ flux\ =\ slope\ \frac{\frac{V_{ch}}{A_{ch}}p_{air}}{RT_{air}} \tag{4}$$

V_{ch} (m^3) and A_{ch} (m^2) are the volume of the whole chamber system and the surface area of the chamber, respectively. T_{air} and p_{air} denote the mean air temperature (K) and pressure (Pa) within the previous defined time windows. R is the universal gas constant with 8.3144 JK^{-1}mol^{-1}. All fluxes are expressed in µg C m^{-2} s^{-1}.

NEE and ER fluxes were calculated using the respective light and dark chamber measurements. However, to calculate GPP, the portion of photosynthetic uptake of the CO_2 flux, the daily mean of ER was calculated for each specific collar. To determine the GPP in the next step, the daily mean value of ER was added

to the negative NEE value of each of the three light measurements on the respective day. This was done for each site and each date.

2.4 Grouping of the data

In order to compare the influence of various environmental parameters, results were subdivided into Groups representing different moisture categories. The separation of Groups was performed using the coverage fractions of plant species as a proxy for the prevailing hydrologic status (Virkkala et al., 2018). To do so, grasses, shrubs, lichens and mosses inside the different collars were identified (Kseniia Ivanova, personal communication) based on vegetation family and species using the samples collected during field measurements. The identification process was based on several key morphological features such as size and shape of stem and branch leaves, visual characteristics of the mosses, habitat, coloration of the stems, specific pattern of leaf arrangement, and type of capitulum (GOVERNMENT OF NORTHWEST TERRITORIES, 2024; NOSKOVA, 2016). In the subsequent grouping of the different collars, the coverage of a particular vegetation family or species was estimated and assigned a scale number from 1 to 5 (Table 2). This was done by analyzing the photos taken in the field with close reference to the Braun-Blanquet scale for estimating species richness for plant populations (KALUSCHE, 2016).

Table 2: Estimation of the coverage of vegetation families and species in order to Group the collars (KALUSCHE, 2016).

Scale	Frequency of Occurrence [%]
1	< 5
2	5 – 25
3	25 - 50
4	50 - 75
5	75 - 100

In this way, the collars of transects 2 and 5 were assigned to specific Groups based on their vegetation composition and richness (A3), which were named as follows: Group 1, Group 2, Group 3 and Group 4. Overall, due to the limited quantity of data from Group 1 and the lack of significant differences in soil properties between Groups 1 and 2, the data were merged based on similarities in soil moisture and vegetation conditions to facilitate later statistical analysis.

2.5   Statistical Analysis

For visualizing and comparing the CO_2 fluxes with soil moisture, soil temperature, NDVI, pH, thaw depth and PAR, a linear regression model was fitted using the "lm" function of the package "stats" in R Studio (R CORE TEAM, 2023), which estimates the relationship between each parameter and the different fluxes. The *p* values were corrected using Holm's method (FISCHER et al., 2022) and were considered significant when $p < 0.05$. To support the analysis and the model's predictive accuracy, further metrics were included such as the coefficient of determination (R^2), Root Mean Square Error (RMSE) and Mean Absolute Error (MAE). As some of the data showed more complex patterns, a non-linear approach in the form of a general additive model was also applied. The GAM model was executed using the "mgcv" function in R Studio (R CORE TEAM, 2023).

2.5.1   Coefficient of Determination

The coefficient of determination (R^2) is a fundamental indicator in statistical analysis that illustrates the extent of agreement between the observed data and the model predictions. Its formula, as explained by Krause et al. (2005), involves the comparison of observed values *x* and predicted values *y* with their respective means $\bar{x}$ and $\bar{y}$. The equation is expressed as follows (KRAUSE et al., 2005):

$$R^2 = \left(\frac{\sum_{i=1}^{n}(x_i - \bar{x})(y_i - \bar{y})}{\sqrt{\sum_{i=1}^{n}(x_i - \bar{x})^2}\sqrt{\sum_{i=1}^{n}(y_i - \bar{y})^2}} \right)^2 \qquad (5)$$

R² values range from 0 to 1, representing the strength of correlation between predicted and observed time series. A score of 1 indicates perfect alignment, while 0 signifies no correlation. However, relying solely on R² to assess model performance has limitations, as it predominantly captures dispersion without discerning between over- or underestimation by the model (KRAUSE et al., 2005).

2.5.2 Root Mean Square Error

The Root Mean Square Error (RMSE) is defined as the square root of the mean squared error, serving as a ubiquitous metric in assessing model performance. Its computation involves utilizing observations y and corresponding predictions across a sample size n (HODSON, 2022):

$$RMSE = \sqrt{\frac{1}{n}\sum_{1}^{n}(y_i - \hat{y}_i)^2} \tag{6}$$

2.5.3 Mean Absolute Error

The Mean Absolute Error (MAE) is calculated as the average of the absolute differences between independent values y and predicted values $\hat{y}$ (WILLMOTT et al., 2009):

$$MAE = \frac{1}{n}\sum_{i=1}^{n}|x_i - \hat{y}_i| \tag{7}$$

In contrast to RMSE, MAE is independent of sample size and equally weighs the variance in the errors (CHAI & DRAXLER, 2014).

2.5.4 General Additive Model

In a generalized additive model, the relationship between the dependent variable and the predictor variables is modeled as a sum of smooth functions of the predictors, rather than assuming a linear relationship between the variables. Each function represents the effect of a predictor variable on the dependent variable, allowing for more flexible modeling of nonlinear relationships. (HASTIE et al., 2009):

$$E(Y \mid X_1, X_2, \ldots, X_p) = \alpha + f_1(X_1) + f_2(X_2) + \cdots + f_p(X_p) \tag{8}$$

While α represents the intercept term when all predictor variables are 0, X_1, X_2, …, X_p act as predictors, Y represents the continuous response and $f_1(.) + f_2(.) +$ …$+ f_p(X_p)$ are unspecified smooth functions. GAMs are particularly useful when the relationships between the variables are complex and nonlinear, as they can capture these relationships more effectively than traditional linear regression models (AMIN et al., 2024; HASTIE et al., 2009).

3 Results

3.1 Environmental characteristics of the different Groups

Grouping the flux data into moisture categories according to vegetation type as described in Section 2.4 resulted in four Groups, which in many cases showed differences in each environmental parameter investigated. However, based on this classification, Groups 1 and 2 indicated no significant differences regarding the presence of lichens (A3) and also had much lower soil moisture values than Groups 3 and 4 (A7). Due to the small amount of data in Group 1 and the similarities to Group 2 in terms of vegetation composition while also taking other parameters like soil moisture, soil temperature, thaw depth or NDVI into account (A7), the Groups were merged (now called Group 1) resulting in three Groups with varying environmental characteristics (Figure 8). Hence, for further analysis, Group 1 and 2 are now called Group 1, while Group 3 and 4 retain their names (A3).

The overall vegetation composition of Group 1 includes a high occurrence of lichens and mosses of the species *Pleurozium schreberi, Polytrichum* and the genus *Tomentypnum* as well as other green mosses. Group 2 inhabits large proportions of *Sphagnum* mosses as well as grasses and shrubs such as *Empetrum nigrum, Rubus chamaemorus, Eriophorum* sp*., Sphagnum capillifolium* or *Sphagnum squarrosum.* Contrasting with Groups 1 and 2, Group 3 shows the occurrence of different plant species such as Carex *aquatilis*, *Hypnum* sp., and *Sphagnum inundatum*, which could not be found in Groups 1 and 2 (A3).

A comparison of environmental conditions across different Groups reveals significant variations in moisture levels, soil temperature, thaw depth, pH, and NDVI. The above-mentioned moisture gradient is clearly visible at both 12 and 30 cm. Group 1 shows the driest moisture level and Group 3, in contrast, the wettest moisture characteristics with a difference of almost 52%. All Groups demonstrate significant differences in moisture content. A small gradient from warmer to colder soil temperature conditions can be seen at 5 cm depth, with Group 1 exhibiting the warmest conditions ($\hat{\mu} = 14.75°C$). However, it should

be mentioned that the temperature differences are small. In 10 cm depth, Group 2 shows the highest soil temperature ($\hat{\mu} = 10.5°C$). Similar conditions can be found at 20 cm and 30 cm depth. No significant differences are observed at 10 cm depth among the Groups. Apart from 10 cm depth, significant differences could be found between Groups 1 and 3 in the remaining depths, whereby Groups 2 and 3 only showed significant differences in 5 cm. Thaw depth shows a similar gradient as soil moisture with Group 3 having the deepest TD at $\hat{\mu} = 30.00$ cm. Significant differences between the Groups can be found between Groups 1 and 2 and Groups 1 and 3. Furthermore, pH shows very acidic conditions in Group 2 ($\hat{\mu} = 3.79$) and thus differs significantly from the other Groups. In the case of NDVI all Groups reveal significant differences exhibiting the lowest value with the highest variability in Group 2 (Figure 8).
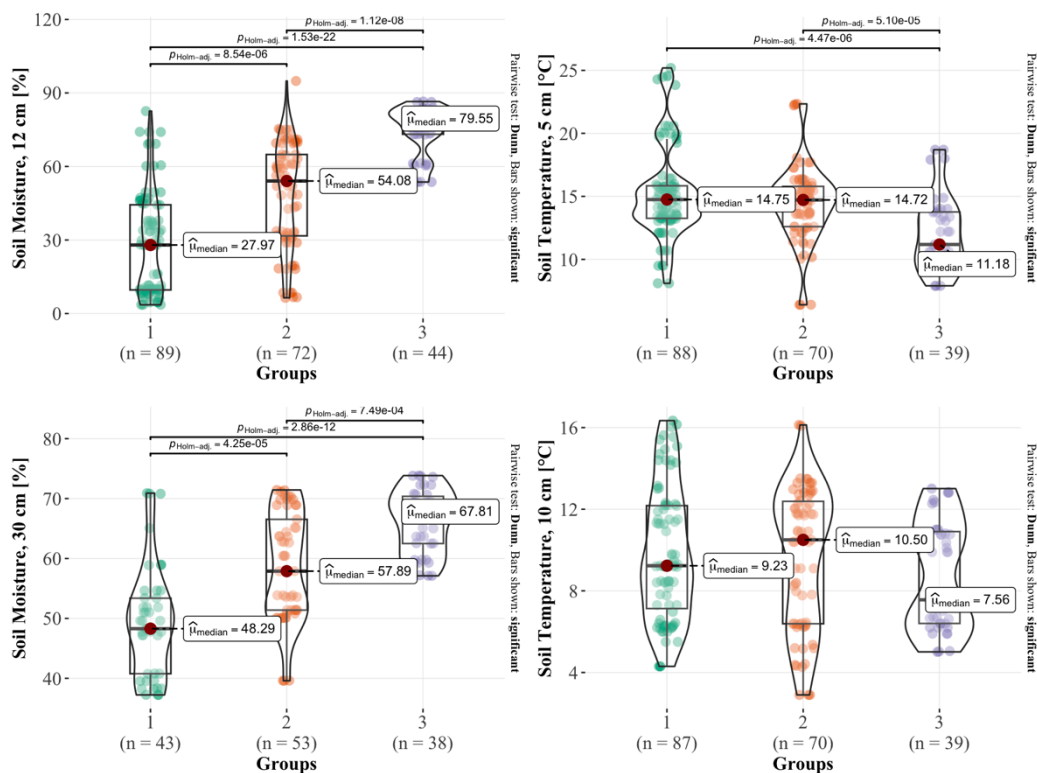
Figure 8: Differences in environmental conditions between Group 1,2 and 3. The plots show the median value and variance of each environmental parameter according to each Group. Moreover, statistically significant differences between the Groups are shown in the bars above the violin plots.
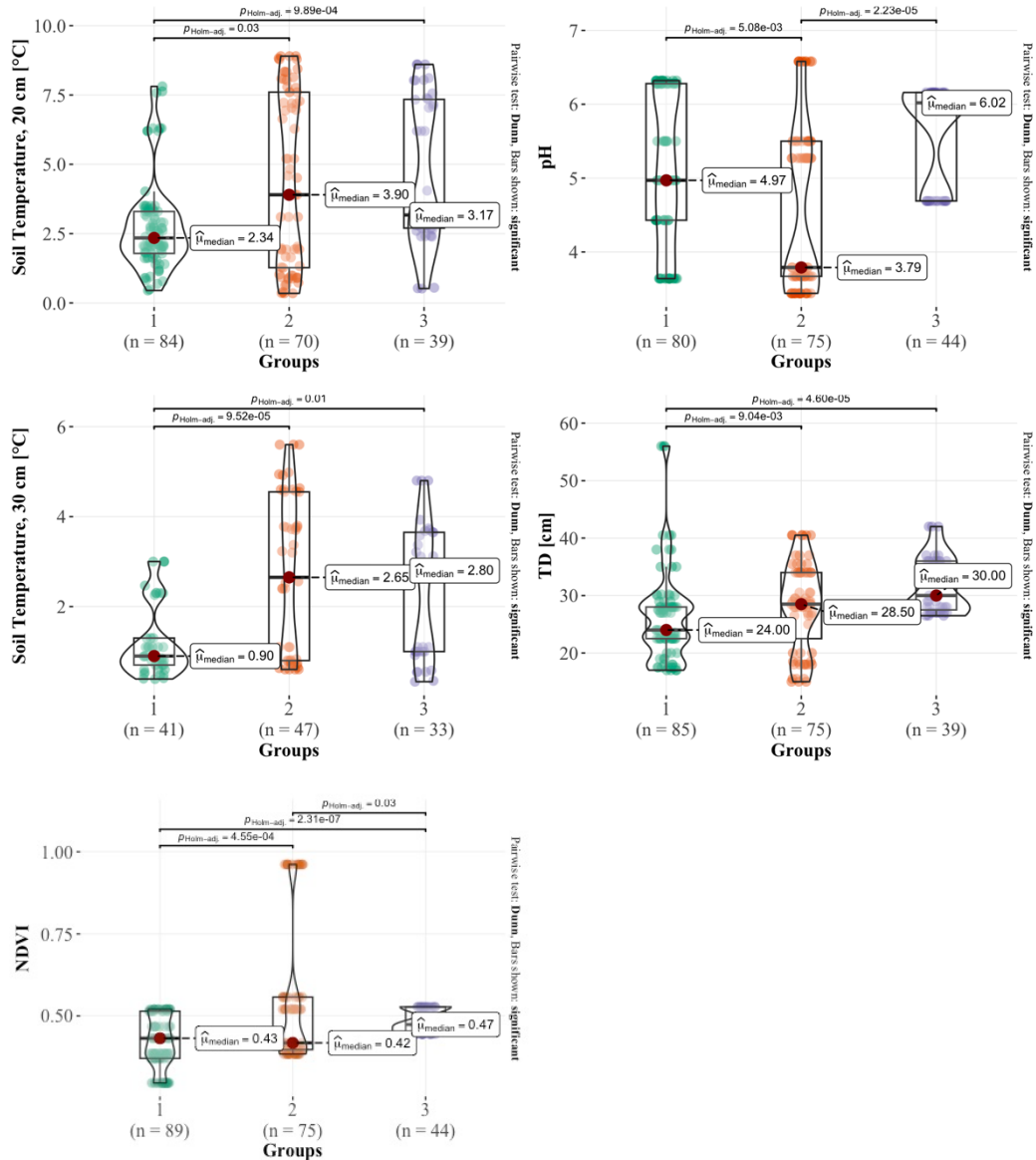
Continuing plot figure 8: Differences in environmental conditions between Group 1,2 and 3. The plots show the median value and variance of each environmental parameter according to each group. Moreover, statistically significant differences between the groups are shown in the bars above the violin plots.

In summary, the clustering of the data resulted in 3 different groups, that are mainly separated by moisture conditions and related effects on e.g. soil temperature or TD. Significant variations exist among the groups in terms of moisture levels, soil temperature, thaw depth, pH and NDVI highlighting the varying environmental conditions across the study area. Above all, soil moisture and NDVI show the greatest differences between the three Groups (Figure 8).

Furthermore, air temperature and PAR show relatively constant conditions during the 2023 measurement period with no significant differences between the Groups. However, a wide range of PAR values was recorded during the measurements, varying between approximately 350 and 2077 mmol/m2/s (Figure 9). This shows that, despite sampling on different measurement days, the average conditions for the different categories were equal when the fluxes were sampled.
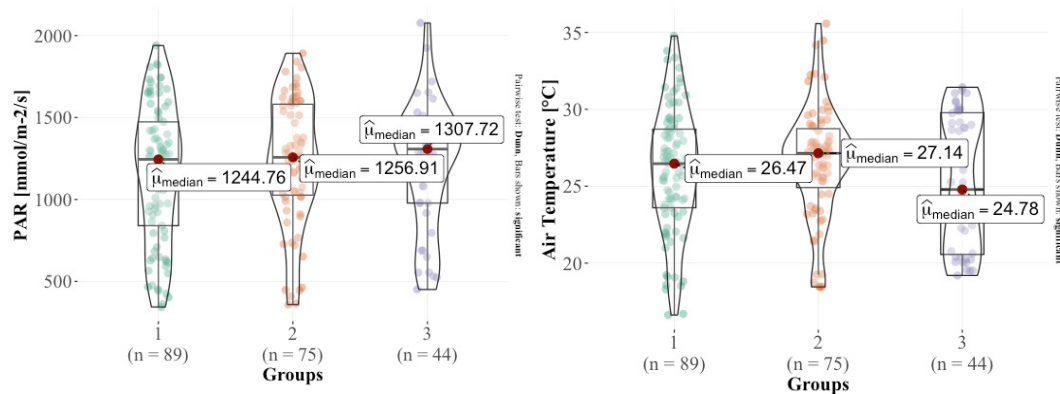
Figure 9: Median air temperature and PAR for each Group. The violin plots show the conditions and variability during the measuring period 2023.

3.2 CO₂ fluxes of the different Groups

Mean flux values for NEE, ER, and GPP of the different ecosystem Groups were calculated to represent the overall carbon exchange dynamics (Figure 10, Table 3).
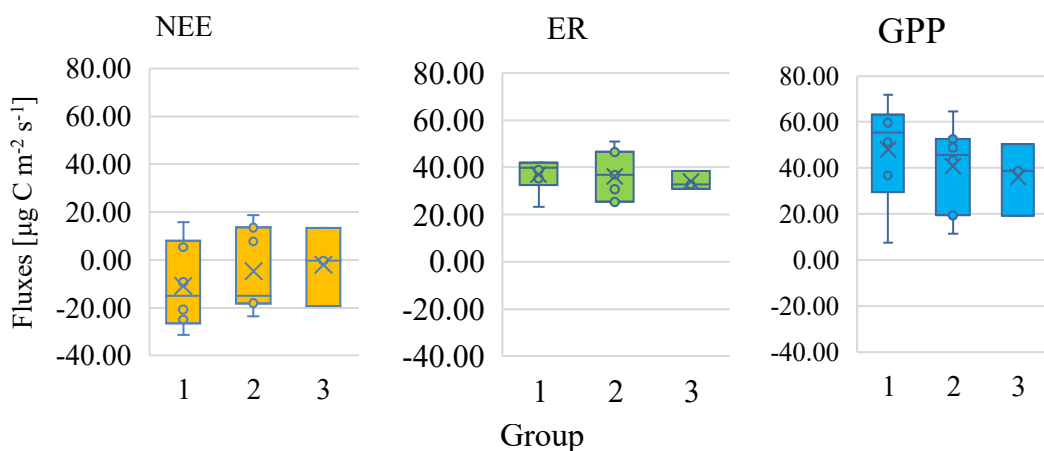

Figure 10: Mean NEE, ER and GPP fluxes of each Group for the measuring period 2023.

In this study, negative NEE values are considered as carbon uptake by the ecosystem. Group 1 exhibited the most negative mean NEE value (- 10.86 $\mu g \, C \, m^{-2} \, s^{-1}$), indicating a substantial carbon sink capacity. Group 3 showed a higher mean NEE value (-2.1 $\mu g \, C \, m^{-2} \, s^{-1}$) compared to Group 1 and 2, suggesting the smallest carbon uptake by the ecosystem. However, this Group also demonstrates a balance between carbon release through ecosystem respiration (mean ER: 34.04 $\mu g \, C \, m^{-2} \, s^{-1}$) and carbon uptake through gross primary productivity (mean GPP: 36.1 $\mu g \, C \, m^{-2} \, s^{-1}$), highlighting their carbon exchange dynamics. All groups demonstrated carbon sequestration potential, with mean GPP exceeding mean ER. Lookin at ER fluxes, it can be seen that ER was quite constant during the measuring period (Figure 10; Table 3).

Table 3: Mean flux values and standard deviation of NEE, ER and GPP [$\mu g \, C \, m^{-2} \, s^{-1}$] for the whole measuring period 2023.

	NEE	ER	GPP
Group 1	-10.9(+/-30.3)	37.1 (+/- 22.2)	47.9 (+/- 44.0)
Group 2	- 4.6 (+/- 22.1)	36.3 (+/- 13.7)	40.9 (+/- 32.0)
Group 3	- 2.1 (+/- 19.33)	34.04 (+/- 10.0)	36.1 (+/- 26.4)

The timeline of CO_2 fluxes showed similar curve progressions for NEE, ER and GPP across all three Groups. The fluxes stayed quite constant during the measuring period. Group 1 showed an increase in NEE, ER and GPP at the beginning of the study which decreases later on. GPP exhibits an increase in fluxes at the end of the measuring period. The highest variability shows Group 3 with a peak in fluxes in mid July (A8; A9; A10).

The carbon exchange dynamics reveals variations in NEE, ER as well as GPP fluxes between the different Groups. Group 1 demonstrates the lowest mean NEE value, indicating a noticeable tendency towards a carbon sink. Group 2 and 3 showed a tendency towards higher NEE values. However, ER generally

reveals higher values than NEE in all groups, albeit it is balanced out by GPP (Figure 10).

3.3 Statistical Analysis of environmental parameters and CO2 fluxes

The statistical analysis, which includes linear regression analysis, a General Additive Model as well as R^2, RMSE, and MAE, shows different relationships between the individual CO_2 fluxes and environmental parameters based on their Groups, which are determined mainly by vegetation composition but also moisture conditions.

### 3.3.1 Soil parameters

3.3.1.1 Soil temperature

The analysis between NEE and soil temperature demonstrates weak correlations in the linear regression analysis (A14). Only at 20 cm depth, a significant relation was modelled by both, the linear and the GAM model, whereby the GAM model showed higher explanatory power ($R^2 = 0.11$), albeit only weak. The linear model fit and the corresponding significance of the relations between soil temperature and NEE improves in Group 2 with a p-value below 0.05 at and the highest R^2 of 0.34 at 20 cm depth. Notably, in Group 3, the GAM model shows a significant improvement, with R^2 values exceeding 0.5 for soil temperature at 30 cm depth while also showing a better model fit than the linear regression model. Hence, the significance of relationships varies across groups and soil depths, with Group 3 showing the most consistent and significant results. Furthermore, RMSE and MAE values are relatively high especially in Group 1 and 2, suggesting modest predictive accuracy despite some improvements with the GAM model (A14). GPP exhibits slightly stronger correlations with soil temperature compared to NEE, particularly in Group 2. In Group 1, the GAM model produced a moderate R^2 values at 10 cm, 20 cm and 30 cm depth, although significant differences were found in both models. Significance and explanatory power of both models improve in Group 2 and 3. The GAM model further enhances the fit, particularly evident in Group 3, with

29

R^2 values surpassing 0.73 for soil temperature at 30 cm depth. Equivalent to NEE, GPP shows significant relations in all depths with the GAM model representing the better model fit. The highest values could be found in 20 cm depth and 30 cm depth. However, high RMSE and MAE values especially in Group 1 and in shallower depths indicate limited predictive accuracy even with the GAM model (A16). The linear regression analysis for ER and soil temperature resulted in low R^2 values in all soil depths and Groups, none of which exceeded 0.2. In Group 1, only the relationship between ER and soil temperature at 30 cm depth is significant, indicating a stronger influence of deeper soil temperatures on ER. However, the R^2 value shows only weak significance with an explanatory power of 0.44. Despite some improvements, both linear and GAM models show high RMSE and MAE values, indicating limited predictive accuracy for ER. However, the values slightly improve in Group 3 (A15).

The GAM plots reveal a general carbon uptake with rising soil temperatures across all depths and groups. Photosynthetic activity increases with increasing temperatures especially in Group 3, while ER shows an increase in 30 cm depth in Group 1 (Figure 11). Furthermore, in Group 1 a decrease in GPP and increase in NEE could be observed with rising soil temperatures in 10 cm depth.

In general, the linear regression analysis of ER, NEE, and GPP with soil temperature at various depths reveals generally low R^2 values, with only occasional significant correlations, particularly in Group 3 and in deeper soil layers. This is also confirmed by the regression plots A36 to A44 in the Appendix. However, GAM models tend to exhibit slightly higher R^2 values and lower RMSE and MAE values indicating a potentially better fit, although significance varies. In some cases, such as NEE and GPP in Group 3, GAM models show strong correlations. Nonetheless, both linear and GAM models demonstrate relatively high RMSE and MAE values across all Groups, suggesting limited predictive accuracy. However, RMSE and MAE are lower in the GAM model for NEE as well as GPP.

Group 1
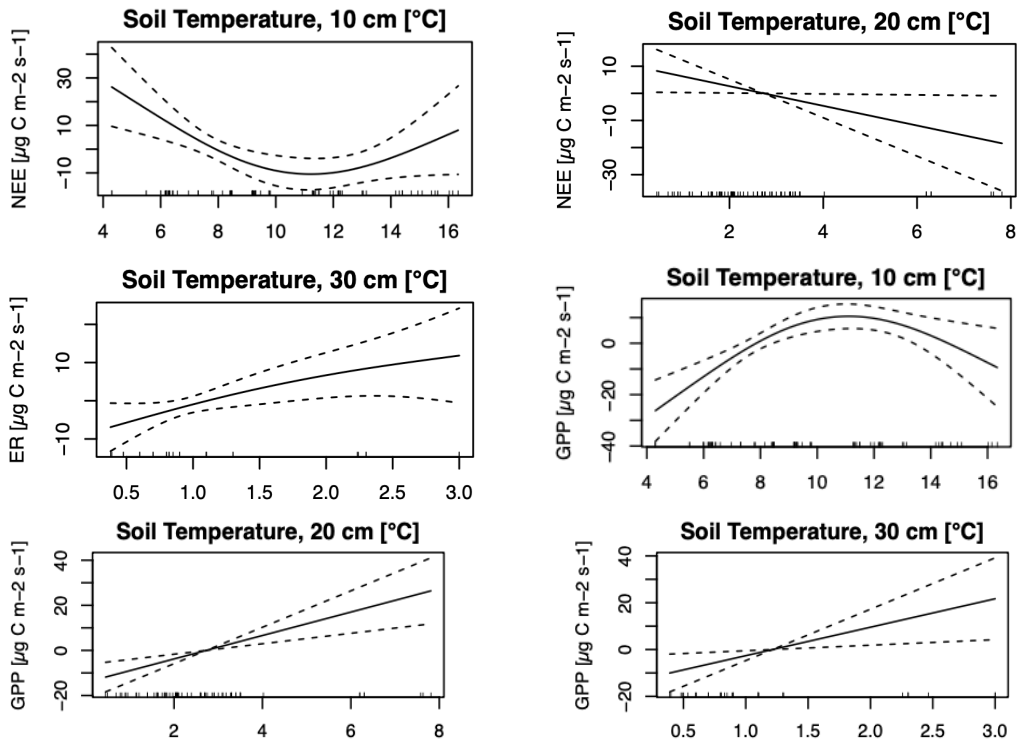
Group 2

Figure 11: Significant non-linear relations in all groups between soil temperature across all depths and CO₂ fluxes produced by the GAM model for the measuring period 2023.

Group 3

Continuing plot Figure 11: Significant non-linear relations between soil temperature across all depths and CO₂ fluxes produced by the GAM model for the measuring period 2023.

3.3.1.2 Soil moisture

Using linear regression models and GAM model, the statistical analysis for the relation between soil moisture in 12 cm and 30 cm depths is characterized by minimal correlations and non-significant p-values (> 0.05) across both soil moisture depths especially in Groups 1 and 2. The interaction between soil moisture, ER, NEE and GPP remains unclear, with many R^2 values below 0.1

32

indicating a limited explanatory power of the linear regression in Group 1 and 2. However, in most cases the GAM model showed a better fit with higher R^2 values than determined in the linear model (A11, A12, A13). For example, NEE and soil moisture at a depth of 30 cm show an R^2 of 0.77 and a significant correlation of > 0.05 in Group 1, while the linear model shows no explanatory power in Group 1 or 2 (A11; Figure 12). A similar pattern could be observed in Group 2 as well as for GPP in Group 1 indicating non-linear relations between these fluxes and soil moisture in 30 cm depth (A13, Figure 12). In contrast, ER contains limited explanatory power of soil moisture on ER variation in Group 1 and 2, as evidenced by negligible R-squared values (< 0.1) in the linear regression models and GAM model. Moreover, non-significant p-values further underscore the absence of statistically significant relationships between soil moisture and ER (A12). In contrast, GPP and NEE showed much stronger correlations emphasized by much higher R^2 values and significant p-values highlighted in the GAM models and the linear model in Group 3. Looking at NEE and soil moisture in 12 cm depth, R^2 is 0.17 and 0.37 for the linear model and the GAM model, respectively. In 30 cm depth, the values include 0.75 for the linear model and 0.76 for the GAM model. GPP contains higher R^2 values in 30 cm depth of 0.55 produced by the GAM model. ER showed only significant results but with little explanatory power for soil moisture at 30 cm depth modelled by the GAM model indicating that the relationship between soil moisture and ER appears to be weak in all Groups, as only the GAM model in Group 3 produced statistically significant results. In addition, the models have relatively high MAE and RMSE suggesting limited predictive accuracy. However, smaller MAE and RMSE of the GAM model indicate a better fit than the linear model and a tendency towards a non-linear relationship between soil moisture and ER. This was also observed for RMSE and MAE of GPP and NEE in Group 1 to Group 3. In general, a gradient from higher to lower RMSE and MAE at 30 cm depth than at 12 cm depth could be observed (A11; A12, A13).
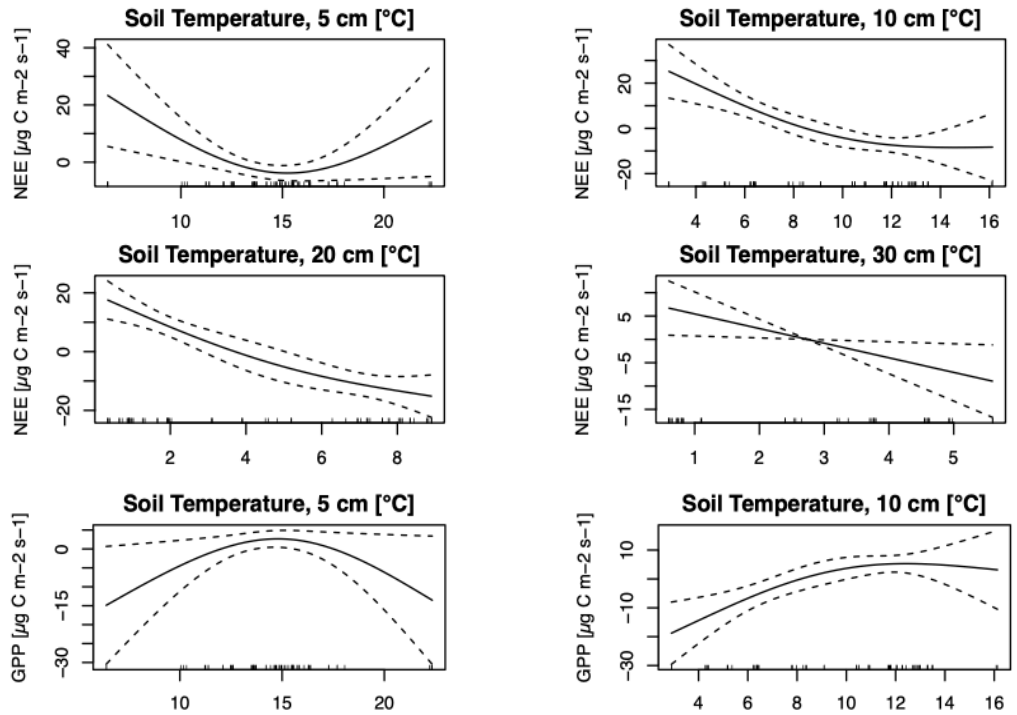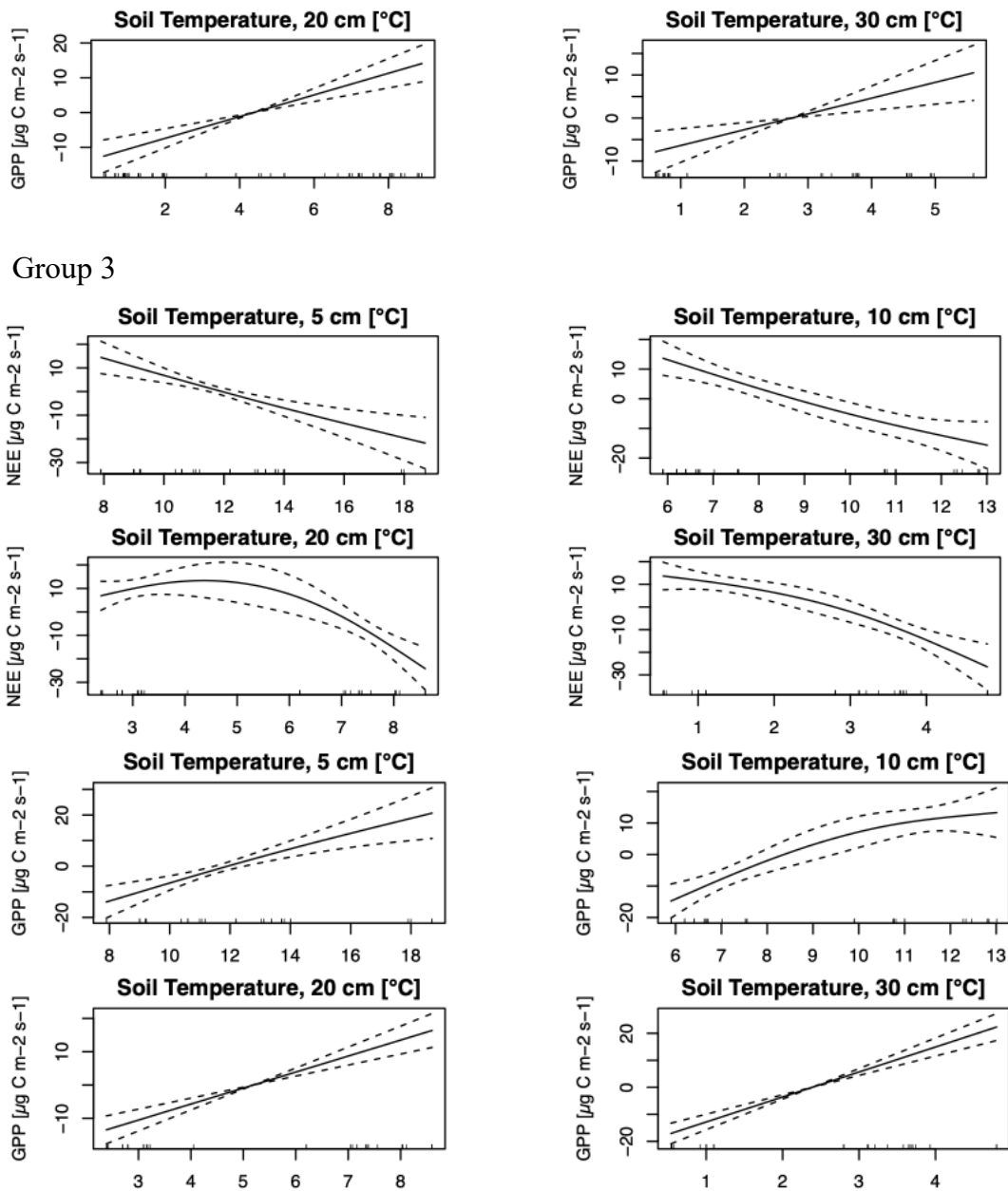
Group 1

Group 2

Group 3

Figure 12: Significant non-linear relations in all groups between soil moisture across all depths and CO₂ fluxes produced by the GAM model for the measuring period 2023.
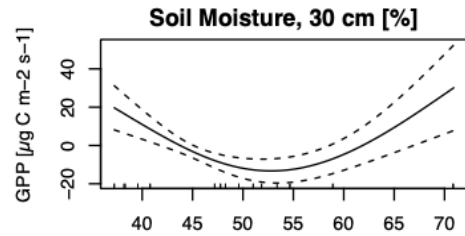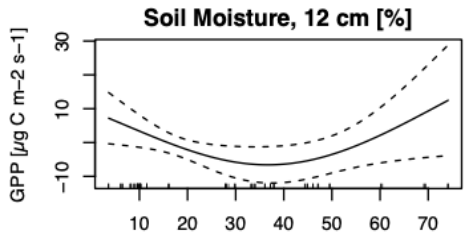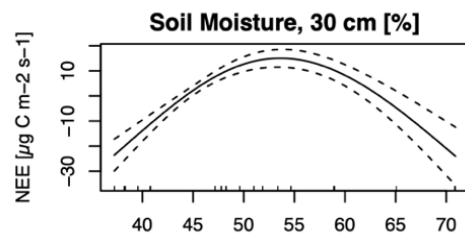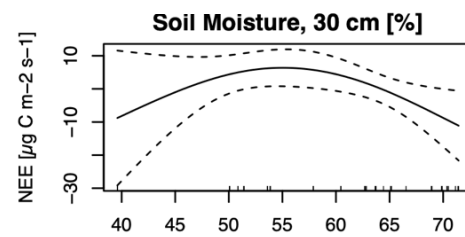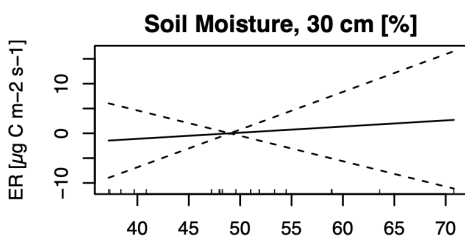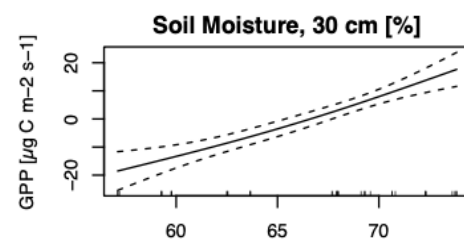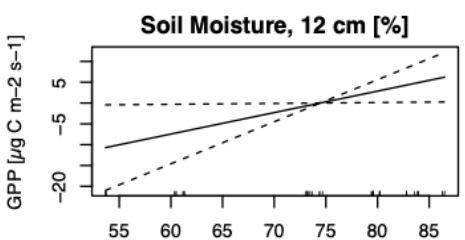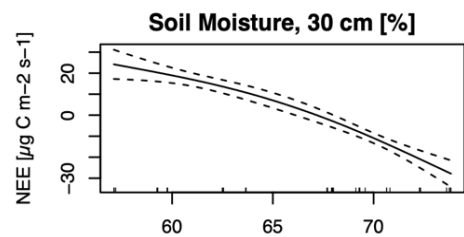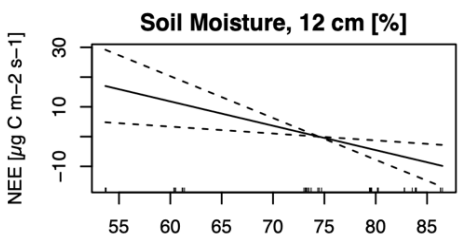
While minimal correlations and non-significant p-values are observed in most cases, especially in Groups 1 and 2, the GAM models generally show higher R-squared values and a better fit, indicating potential non-linear relationships between soil moisture and ecosystem processes. Despite the higher predictive accuracy of the GAM models, the RMSE and MAE remain relatively high in Groups 1 and 2, while they show better values in Group 3 for all three fluxes. In general, Group 3 shows the highest correlation between NEE, GPP and soil moisture, with soil moisture at 30 cm standing out in both cases. Furthermore, higher soil moisture led to carbon uptake in the GAM plots (Figure 12). Contrary to NEE and GPP, both models produced only weak to no relations between ER and soil moisture.

3.3.1.3 Soil pH

Considering the relation between soil pH, NEE, ER and GPP the statistical analysis revealed different findings similar to soil temperature and soil moisture. Looking at NEE, both the linear and GAM models revealed a significant correlation between pH and NEE in Group 1. The linear model demonstrated a moderate R^2 value (0.24) and significant p-value, while the GAM model showed an even better model fit with a high relation of 0.79 and highly significant p-value. With that, Group 1 shows the highest correlation between pH and NEE. Similarly, in Group 2, pH showed a significant correlation with NEE in both models, with the GAM model computing a weaker R^2 of 0.38 but also a significant relation between pH and NEE. In Group 3, pH also demonstrated a significant correlation with NEE, with both linear and GAM models producing significant but moderate R^2 values of 0.39 and 0.62, respectively. However, just as Groups 1 and 2, the GAM model represents a better model fit than the linear model taking R2 as well as RMSE and MAE into account (A17). Similar to NEE, the GAM model represented a better model fit than the linear regression model for GPP showing significant correlations across all groups. However, in this case Group 2 showed the weakest relation with an R^2 value of 0.15. The strongest relation could be observed in Group 3 with an R^2 of 0.52 an RMSE of 10.42 and MAE of 8.32 produced by the GAM model (A19). The investigation

of ER and soil pH revealed that in Group 1, neither the linear nor the GAM model exhibited significant correlations. Similar non-significant relationships were observed in Group 2. Despite a slight improvement in Group 3, the correlation between pH and ER remained weak and statistically non-significant. As with NEE and GPP, the GAM model produces a better model fit than the linear model (A18).

In general, higher pH values resulted in an increase in NEE. Only in group 2, a decrease after a threshold of 5.5 could be observed. However, in Group 1 rising pH values resulted in declining carbon uptake capacity. GPP values tend to decrease with increasing pH, but increases in Group 3 after a threshold of 5.5 (Figure 13).
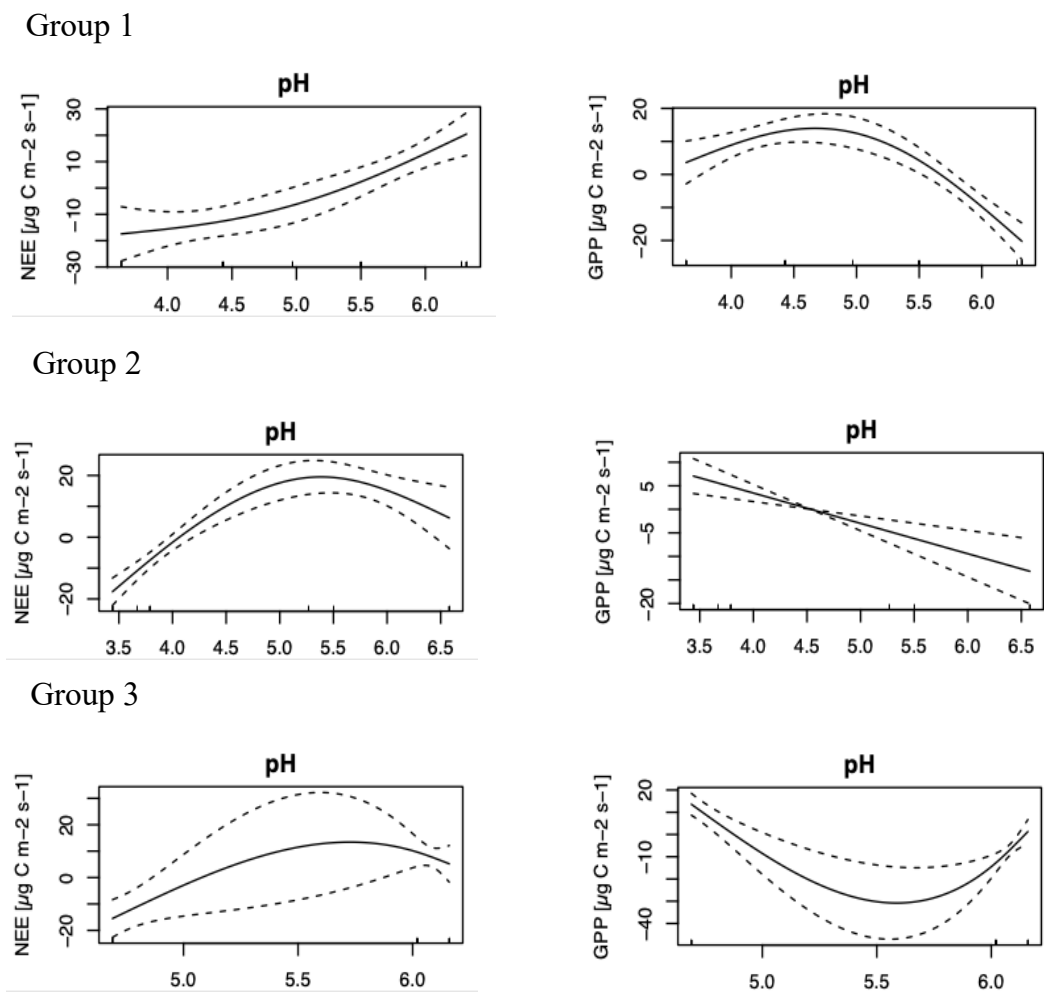
Group 1

Group 2

Group 3

Figure 13: Significant non-linear relations in all groups between pH and CO_2 fluxes produced by the GAM model for the measuring period 2023.

In conclusion, the analysis unveiled varying relationships between soil pH and ecosystem fluxes across different groups. While ER exhibited no correlations with pH, NEE and GPP demonstrated more pronounced correlations, particularly in Groups 1 and 2. The overall stronger statistical values produced by the GAM model suggest a non-linear relation between NEE, GPP and soil pH.

3.3.2 Thaw depth (TD)

The statistical analysis revealed significant correlations between NEE, GPP and TD across all groups (A17). Notably, the linear model shows a moderate relation and p-values of less than 0.05, indicating a strong correlation for NEE. However, the GAM model presents a substantially higher R2 of 0.79 with a significant p-value, suggesting an even better fit. MAE and RMSE of the GAM model are lower compared to the linear model emphasizing the better model fit produced by the GAM model. The values improve in Group 2 and 3, whereby in Group 2 the linear model shows a higher R^2 od 0.27. In both cases a significant relation exists. In Group 3 a strong and significant correlation could be observed for both models, albeit the GAM model showed a higher significant correlation with an R^2 of 0.62 and lower RMSE and MAE values of 13.82 and 11.03 respectively. Looking at GPP, the models indicate significant relations and moderate explanatory power produced by both models (A19). The GAM model exhibits slightly lower RMSE and MAE values in Group 1, suggesting better predictive accuracy. In Group 3, GAM model and linear model show similar predictive power and a significant correlation, whereby the linear model demonstrates a slightly higher significance than the GAM model. RMSE and MAE values are comparable between the two models, indicating similar predictive accuracy. In contrast, both models produced no significant relation for ER across all three groups (A18). However, a better model fit is represented by the GAM model, showing higher R^2 and lower RMSE and MAE values than the linear regression model. The best R^2 of 0.65 could be found in Group 1, although no significance

was determined. As for NEE and GPP lower RMSE and MAE values in all groups imply a better fit by the GAM model.

Considering the modelled relation visualized by the GAM plots, NEE showed overall carbon uptake in all groups, while photosynthetic activity increased with deeper thaw depth (Figure 14).

Overall, NEE demonstrates significant correlations across all groups, with the GAM model outperforming the linear model, as emphasized by lower RMSE and MAE values. Similarly, GPP exhibits significant relationships in Group 1 to 3, with the GAM model showing similar results to the linear model. In contrast, ER shows limited explanatory power, with non-significant results in most groups, highlighting the complexity of its relationship with environmental factors.

Group 1
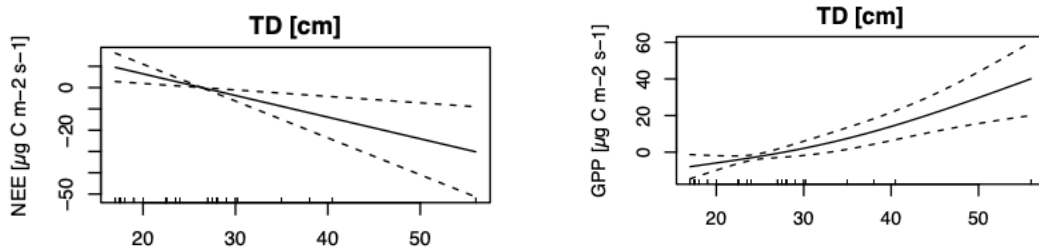
Group 2
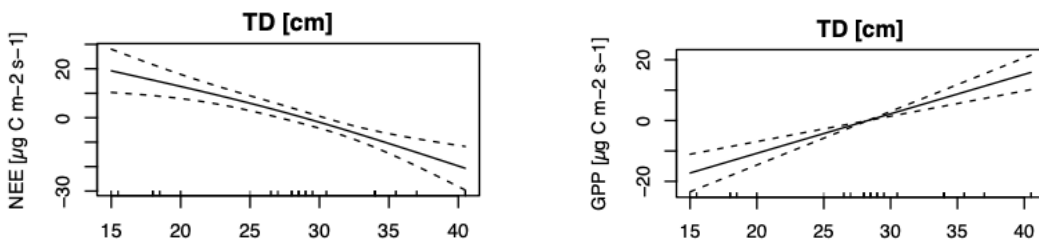
Group 3
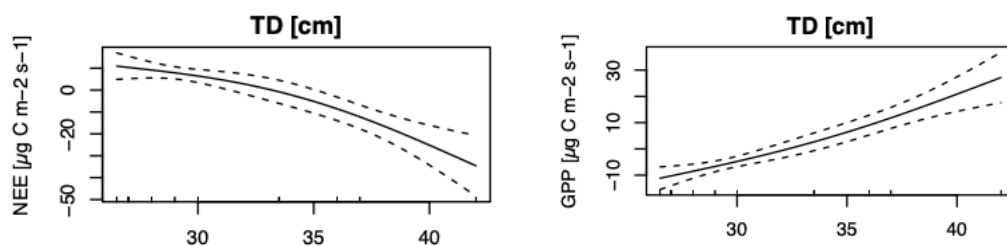
Figure 14: Significant non-linear relations in all groups between TD and CO2 fluxes produced by the GAM model for the measuring period 2023.

3.3.3 NDVI

In the analysis of NEE, significant correlations were observed between NEE and NDVI, particularly across all Groups (A20). The GAM model exhibited higher explanatory power than the linear model, as indicated by higher R^2 values. Notably, in Group 1, the GAM model produced a moderate R^2 of 0.36, with a highly significant p-value. The highest significant R^2 of 0.58 could be found in Group 2. Additionally, RMSE and MAE were considerably lower in the GAM model compared to the linear model across all Groups, suggesting higher predictive accuracy. For GPP, the analysis revealed a similar trend, with the GAM model outperforming the linear model (A22). In Group 3, the GAM model shows the highest R^2 of 0.64, indicating a strong relationship between GPP and NDVI. Furthermore, the p-values for the GAM model were highly significant across all Groups, underscoring the robustness of the observed correlations. In Group 1, the GAM model also achieved a substantially higher R^2 than the linear model with a value of 0.15, demonstrating the better fit of the model and implying a non-linear relation between GPP and NDVI. ER exhibited varying degrees of correlation with NDVI across different Groups (A21). In Group 1 and 2, the linear model yielded no correlation, indicating no relation between ER and NDVI, with a non-significant p-value. However, in Group 2, while the linear model showed no improvement, the GAM model produced a weak but significant relation between ER and NDVI with an R^2 value of 0.19. Conversely to NEE and GPP, Group 3 shows no improvement by the GAM model. The linear model produces significant results, albeit the explanatory power is non-existent.

The visualization of the GAM model revealed increasing photosynthetic activity with increasing NDVI in Group 1 and 3, but also declining ER. In general, the groups show an increase in carbon uptake with increasing NDVI values (Figure 15).

Overall, the analysis reveals significant correlations between NDVI and ecosystem processes across all Groups. NDVI influences GPP and NEE by showing significant correlations with NDVI especially in Groups 2 and 3.

Although ER exhibits weaker elations, NDVI still influences it, particularly in Group 2.

Group 1

Group 2
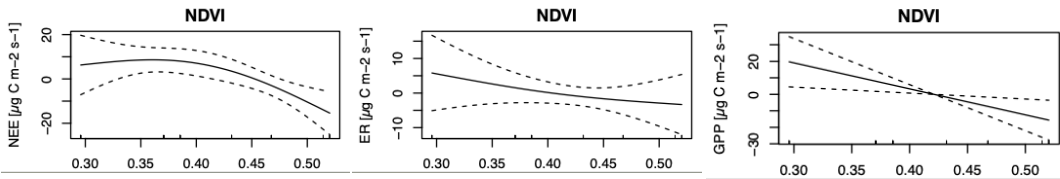
Group 3
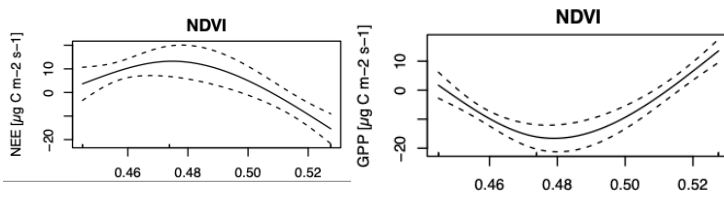
Figure 15: Significant non-linear relations in all groups between NDVI and CO₂ fluxes produced by the GAM model for the measuring period 2023.
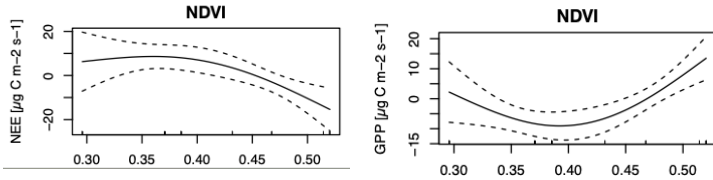
3.3.4 PAR & Air Temperature

For all three fluxes, neither the linear regression model nor the GAM model showed significant correlations between PAR and air temperature (A23; A24; A25). This could also be seen in the regression plots A54, A55 and A56 as well as A57, A58 and A59 in the Appendix. Only Group 2 showed significant relations between air temperature, NEE, ER and GPP as well as GPP and PAR (Figure 16), albeit the explanatory power of the models is very weak. Both models showed almost no capability of predicting air temperature or PAR based on very low R^2 and high RMSE and MAE values. However, as the values in the GAM model improved slightly, suggesting a non-linear relationship between the fluxes, air temperature and PAR, NEE and ER showed stronger significance values of 0.03 and 0.04, respectively, compared to GPP (0.05).
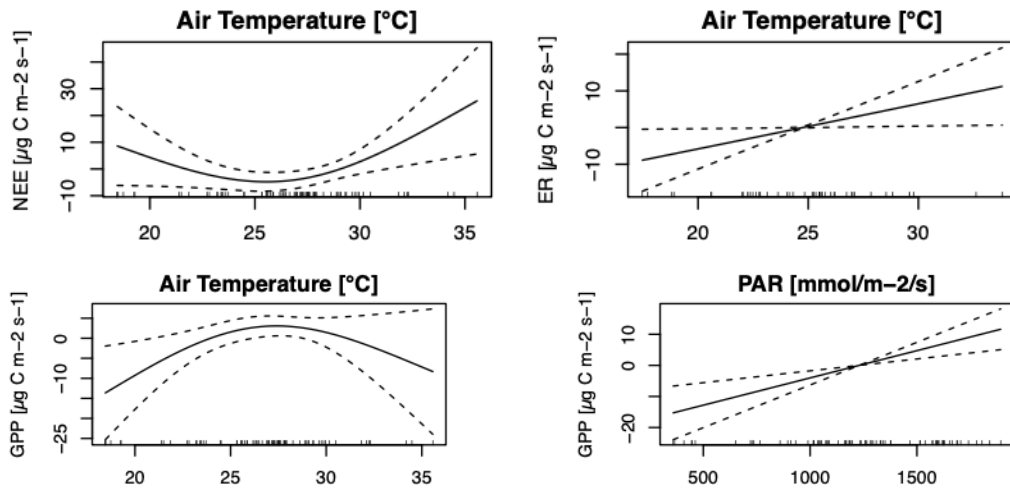
Figure 16: Significant non-linear relations in Group 2 between air temperature, PAR and CO₂ fluxes produced by the GAM model for the measuring period 2023. The plots are sorted by CO2 fluxes (NEE, ER, GPP).

3.4 Similarities and Differences between different Groups

In the analysis of the relationship between CO_2 fluxes and environmental parameters across different Groups, several similarities and differences between the Groups emerge.

Across various environmental parameters, the GAM model in most cases demonstrates better performance in terms of explanatory power, RMSE and MAE compared to the linear regression model. A visual representation of the regression analysis in the form of regression models can be found in the Appendix A33 to A59. The better performance by the GAM model is mainly observed in soil temperature, soil moisture, soil pH, thaw depth indicating a non-linear relation between these parameters, NEE and GPP across all three Groups. Significance levels of the relationships between CO_2 fluxes and environmental parameters also vary across different Groups. In some cases, significant correlations are observed across all Groups e.g. between NEE and pH as well as TD, while in others, significance is limited to specific Groups or not observed at all. For example, in the analysis of soil temperature, soil moisture, and soil pH, Group 3 mostly exhibits stronger and more significant correlations

compared to Groups 1 and 2. While linear regression models often demonstrate weak correlations, the GAM model suggests non-linear relationships between CO_2 fluxes especially for NEE, GPP and environmental parameters, particularly evident in Group 3. This non-linear relation is more pronounced for certain parameters such as soil moisture and soil pH, but also between NEE, GPP and soil moisture in Groups 1 and 3.

The analysis revealed that while linear regression models often yielded weak correlations, the GAM model mostly suggested non-linear relationships between CO_2 fluxes and environmental parameters, particularly pronounced in Group 2 and 3. This non-linear relationship was particularly notable for parameters such as soil moisture, soil pH, TD, NDVI and soil temperature underscoring the complexity of their interactions with NEE, ER and GPP.

4 Discussion

4.1 Challenges with CO_2 flux measurements

Using closed flux chambers is a common approach to assess CO_2 fluxes and to quantify their interactions between soil and atmosphere. However, this common measuring method involves also several limitations, that have been reviewed and summarized by KUTZBACH et al. (2007). When performing chamber measurements, driving parameters including soil and vegetation can be disturbed and are therefore not constant during data collection. By closing the chamber, concentrations gradients between the overlying air, soil or vegetation can be altered leading to uncertainties in the flux measurements due to inconsistent conditions during the experiments. Furthermore, leaks during the measurements can be caused by the chamber setup itself or by the space in soil pores. Air and soil temperature changes underneath the chamber can further alter the conditions during measurements and prevent consistency. Additionally, soil compression or insufficient pressure relief during the experiment can disturb pressure gradients between the soil and atmosphere. Also, suppressing the natural pressure fluctuation or eliminating advection and turbulence and modify diffusion resistance of the soil-or plant-atmosphere boundary layer. Errors in calculating the volume of the chamber should also be considered. However, unless they can be quantified, calculations are based on the assumption that these sources of error do not influence the CO_2 fluxes (KUTZBACH et al., 2007). However, it should also be noted that these uncertainties cannot be eliminated either.

To take these problems in this study into account and to avoid large temperature and pressure changes, closing times of the chamber were not longer than 2 minutes. Furthermore, breaks between measurements were at least 1 minute to prevent and reduce condensation inside the chamber. A fan and valve were used to mix the air inside the chamber during measurements and to prevent pressure effects when placing the chamber on the collar. To prevent ground disturbances, especially at collars with wetter conditions, a board next to the collar was used to avoid sinking into the ground. For chamber volume calculations, the concept and formula of a truncated cylinder was used to consider the surface condition

in the collar as accurately as possible. But despite taking care to always measure at the same point, variability in the minimum and maximum height measurements due to measurements at different points on the collar during the experiment cannot be excluded.

It should be mentioned, that is also very common that study sites are considered homogenous when they are heterogenous. Hence fluxes may vary between a few meters, pointing out the importance of considering the number of chambers that is needed to capture the variance and mean at the selected sites. Often the variation is at the scale of centimetres, reflecting e.g. disturbances by soil fauna or pockets of fine root proliferation. Chamber measurements can contribute to resolve these differences as they measure on a small-scale. However, when averaging over several chambers under the assumption of homogeneity, the previously mentioned problems can occur (DAVIDSON et al., 2002; VIRKKALA et al., 2018). These small-scale heterogeneity is common for the Arctic and tundra environments and may be caused by microtopographical conditions, soil properties or vegetation characteristics (AALTO et al., 2013; ZONA et al., 2011). In this study, we grouped the data based on vegetation while considering soil moisture conditions in order to account for heterogeneity and combine sites with similar conditions.

4.2 CO$_2$ fluxes in similar ecosystems

Comparing the fluxes assessed in this study to studies in similar environments, the values are within the range of the fluxes listed in Table 4. However, when comparing the fluxes, inter- and intra-annual variability typical for CO$_2$ fluxes as well as variations of environmental conditions should be taken into consideration. Also the presentation and timescales complicate the comparison between studies, because most studies cover larger time periods (CALVIN et al., 2023; LÓPEZ-BLANCO et al., 2017). Values assessed by HUMPHREYS et al. (2014) are from the period from 01st November, 2011 to 31st October, 2012, covering a timeframe of a year. Also the study conducted by LUND et al. (2010) investigates data from 12 different peatland ranging from wet tundra sites to

northern peatlands. Therefore, careful interpretation is important when comparing fluxes from this study directly with fluxes from other sources that might use different processing and representation methods in differing environmental conditions.

Table 4: Comparison of mean NEE, ER and GPP fluxes of different studies [µg C/m²/s]. Differing units were converted to the units used in this study.

	NEE	ER	GPP	Ecotype
This study Group 1	-10.9(+/-30.3)	37.1 (+/- 22.2)	47.9 (+/- 44.0)	Polygonal mire
This study Group 2	- 4.6 (+/- 22.1)	36.3 (+/- 13.7)	40.9 (+/- 32.0)	Polygonal mire
This study Group 3	- 2.1 (+/- 19.33)	34.04 (+/- 10.0)	36.1 (+/- 26.4)	Polygonal mire
Lund et al. (2010)	- 3.3 (+/- 3.26)	13.0 (+/- 4.1)	16.3 (+/- 6.5)	Arctic wet tundra, Sub-arctic fen, temperate and boreal bog
Eckhardt et al. (2019)	- 26 (+/- 19)	35 (+/- 9)	61 (+/- 17)	Polygonal tundra
Humphreys et al. (2014)	- 5.61 (+/- 0.3)	21.3 (+/- 0.4)	26.9 (+/- 0.5)	Temperate bog

4.3 Influence of environmental parameters on CO_2 fluxes in polygonal mires

When discussing the various environmental parameters and their influence on CO_2 fluxes among different groups, it's noteworthy that soil temperatures measured at 30 cm depth often exceeded 0°C, while thaw depth were sometimes assessed at shallower depths. This suggests that the manually measured thaw depth does not always match the depth of the temperature sensor. Moreover, since thaw depth, soil temperature and soil moisture are measured right next to the chamber setup, they do not reflect the exact conditions below the collar.

4.3.1 Soil parameters

4.3.1.1 Soil moisture and soil temperature

The results for soil moisture show gradually increasing moisture levels from group 1 to group 3 (Figure 8). Group 3 contains the highest occurrence of Sphagnum mosses as well as Hypnum species at sites 2.6 and 5.3 (A3). These mosses tend to promote water retention leading to a higher moisture content in the soil (GORNALL et al., 2007; RIXEN & MULDER, 2005), which could be observed especially in Group 3 (Figure 8). Soil moisture plays a crucial role in CO_2 and soil dynamics (ECKHARDT et al., 2019; LAWRENCE et al., 2015). Particularly in Group 3, a significant influence of soil moisture in 12 cm depth as well as in 30 cm depth could be found showing that moisture conditions have a notable impact especially on NEE and GPP in deeper layers. NEE showed a non-linear decrease in Group 2 and 3 indicating carbon uptake when soil moisture increases. In Group 1, carbon uptake only sets in after soil moisture is higher than 55%. In addition, Group 1 showed a decrease in GPP and an increase after 55%, while Group 3, exhibiting generally higher soil moisture content, shows increasing GPP together with still decreasing NEE (Figure 12). The authors MAURITZ et al. (2017) stated that higher soil moisture can stimulate decomposition but also increase carbon uptake in response to reduced water stress experienced by vegetation when the soil is not fully saturated. Together with declining ER and increasing moisture content in Group 3, an overall carbon uptake in connection with rising soil moisture could be observed especially in

46

30 cm depth (Figure 12). In a study by ECKHARDT et al. (2019), who also investigated the differences in CO_2 fluxes at a wet polygonal center and a dry polygonal rim, the authors found that mean GPP and carbon uptake was higher at the sites with higher soil moisture content than at the drier locations. At the same time, waterlogged conditions together with colder soil temperature, which could also be found in Group 2 but especially 3 in the topsoil (Figure 8), lead to slower decomposition rates and hence to reduced respiration (ECKHARDT et al., 2019). However, in this study, mean GPP and mean carbon uptake is higher at the sites with drier conditions (Figure 10; Figure 8). Furthermore, a significant non-linear response of ER on soil moisture changes could only be detected in 30 cm depth indicating a stronger influence of soil moisture on NEE and GPP, which is further supported by a very poor model quality fit (A12). This is contradictory to other studies like SJÖGERSTEN et al. (2006), ECKHARDT et al. (2019) and ILLERIS et al. (2004) who found significant relations between ecosystem respiration and soil water content. The study by ILLERIS et al. (2004) found, that soil moisture levels significantly influence GPP and ER, whereby GPP is more sensitive to soil moisture changes than ER. In general, GPP fluxes and carbon uptake in this study tend to increase with higher moisture content, which is similar to the results of the study by MAURITZ et al. (2017) and is probably related to the reduction in water stress in connection with the plant community composition.

Additionally, the authors ILLERIS et al. (2004) found a soil temperature dependency on soil moisture for GPP and ER with stronger relations in wetter conditions. In this study, soil temperature sensitivity also increased with wetter conditions which is represented by stronger significance and explanatory power in Group 3 indicating that soil moisture could impact soil temperature sensitivity and hence GPP flux in this study. However, the lack of correlation could be due to other influencing factors, but also to the lack of data caused by a short measurement period in July and quite constant air temperature conditions, which exceeded 20°C during most measurements. Also soil temperature was found to be no predictor of ER in this study which is also contrary to findings of other studies (HELBIG et al., 2019; LIU et al., 2019). In a study conducted by HELBIG et al. (2019) in peatlands of the Hudson Bay Lowlands, the authors found that

increasing soil temperatures in response to warming air temperatures result in a significant increase in ER and a decline in CO_2 uptake as well as photosynthetic activity. Although, only in Group 1 at 30 cm depth a very weak and positive significant influence of soil temperature on ER could be observed in this study indicating a stronger relation between ER and soil temperature in deeper soil layers. In contrast, soil temperature proved to be an important predictor with similar significance for NEE as well as GPP in all groups. These results generally correspond to the study by LIU et al. (2019), which also determined non-linear relations between NEE, GPP and soil temperature. In this study, GPP was found to increase with increasing soil temperature in all groups, which was also observed in the study by NATALI et al. (2015) who concluded that carbon uptake can increase when GPP exceeds ER under drier conditions. KWON et al. (2016) also found increasing carbon uptake in 2013, when they investigated the effect of long-term drainage on CO_2 uptake and emissions. They further highlight, that the responses of CO_2 fluxes to changing moisture conditions can differ between ecosystems. In general, the results of this study show, that increasing soil temperature leads to decreasing NEE indicating a general carbon uptake by the ecosystem (Figure 11).

4.3.1.2 Thaw depth

Additionally, CO_2 fluxes as well as soil temperature and moisture are strongly affected by thawing of the permafrost (MINER et al., 2022), which is recognized in several studies (VIRKKALA et al., 2018). A study by VOGEL et al. (2009) which investigated permafrost thaw in a tussock tundra in Alaska found significant relations between active layer depth and NEE, GPP as well as ER. The authors found that GPP and ER will increase with thawing of the soil with NEE also positively related to increasing TD. Rising CO_2 emissions due to thawing permafrost is linked to drying out of the soils due to increased heterotrophic respiration rates (ANDRESEN et al., 2020). However, LAWRENCE et al. (2015) who investigated the effect of permafrost-thaw induced soil drying on CO_2 fluxes, found an positive drying impact on decomposition rates starting from 0.5 m thawing depth. In this study TD does not exceed a depth over 0.5 m

indicating that this drying effect on carbon fluxes is not as extensive. Furthermore, NEE shows a non-linear decrease indicating carbon uptake, which is comparable to the results from MAURITZ et al. (2017), who showed that in deeper thawed soils moisture content is usually highest, which was also observed in this study (Figure 8). As already mentioned above, these non-saturated soil conditions can stimulate CO_2 uptake as a result (MAURITZ et al., 2017). TD influenced GPP only in Group 3 further supporting possible connections to soil moisture or vegetation composition. Moreover, GPP increases non-linearly with increasing TD values, which corresponds to the findings by MAURITZ et al., 2017 who found greater GPP values with deeper thaw depth depending on plant community composition. But since ER did not show any significant influence by TD, which was not expected in this study and is unusual compared to other studies (ANDRESEN et al., 2020; MAURITZ et al., 2017; VOGEL et al., 2009), final conclusions on CO_2 uptake or release due to deeper thawing soils cannot be made with certainty. However, decreasing NEE fluxes in response to deeper TD suggests a carbon uptake by the ecosystem probably due to the counteracting effect of water stress and higher moisture availability (MAURITZ et al., 2017).

4.3.1.3 Soil pH

PH was found to be an important parameter in explaining CO_2 fluxes (LUND et al., 2010). Values of pH were lowest at Group 2 and generally highest at sites of Group 3 (Figure 8). Group 2 shows the highest abundance of *Sphagnum* species compared to the other Groups (A3). The abundance of *Sphagnum* mosses can lead to increases in pH and impact CO_2 fluxes (MALHOTRA & ROULET, 2015). In this study, Group 3 exhibiting the highest pH also shows the lowest carbon uptake capacity compared to the Groups with lower pH and higher Sphagnum abundance (Figure 8; Figure 10; A3). In the study conducted by LUND et al., 2010, pH showed a significant influence on GPP and NEE. The authors investigated 12 different peatlands and tried to find out how differences in CO_2 fluxes can be explained by climatic and environmental variables. In this context, higher values of pH lead to increasing CO_2 uptake, whereby ER showed no

correlation with soil pH. This study supports these results only in some extend, albeit the relation between NEE, GPP and pH are non-linear. However, higher pH first lead to an increase of NEE while tend to sequester CO_2 after a threshold of 5 in Group 2. In contrast, GPP decreases with higher soil pH in all groups. Both results underline the non-linear relation of pH, GPP and NEE (Figure 13). In general, increasing pH values are connected to an increase of NEE flux, suggesting a promotion of CO_2 release at sites with higher pH conditions. LUND et al., 2010 observed, that higher pH values lead to carbon uptake in the ecosystems, which was only observed to a limited extent in Group 2 of this study. It should also be noted, that pH was only measured once at each side leading to a limited amount of data, which is why these results should be interpreted with caution.

4.3.2 NDVI

According to several studies that also investigated which environmental parameters drive CO_2 fluxes, NDVI was additionally considered as an important influencing factor (BRUHWILER et al., 2021; JESPERSEN et al., 2023; MCPARTLAND et al., 2019; POYATOS et al., 2014; VIRKKALA et al., 2018). The authors JESPERSEN et al. (2023) conducted a study in northern Alaska, where they investigated the impact of NDVI changes on CO_2 fluxes based on chamber measurements of vegetation structure and ecosystem functioning. They found significant relations between NEE, GPP and ER, whereby NEE negatively and GPP as well as ER positively correlated with NDVI. Furthermore, higher shrub abundance improved the correlation between fluxes and NDVI. POYATOS et al. (2014) also observed significant relations between NDVI, GPP, NEE and ER in a sub-arctic forest-mire in northern Finland, albeit they found a positive relation between ER and NDVI. They stated that autotrophic respiration might have contributed greatly to ecosystem respiration leading to a positive correlation with NDVI. In this study a significant influence of NDVI on NEE, GPP and ER could also be observed, albeit the GAM model showed the better predictability compared to the linear model, which suggests more complex non-linear relations between CO_2 fluxes and NDVI. The relation between NDVI and NEE was found

to be strongest in Group 2, where grasses and shrubs are part of the vegetation composition. This observation is similar to the stronger correlation in higher shrub abundance observed by JESPERSEN et al. (2023). In Group 1 and 3 a carbon uptake by NEE with increasing NDVI could be observed with mainly decreasing values of ER (Figure 15), which was expected. Furthermore, GPP increased with increasing NDVI in Group 1 and 3, which also corresponds to the studies mentioned above. However, decreasing GPP with rising NDVI values like it could be observed in Group 2 is rather unexpected and contrary to previous studies (JESPERSEN et al., 2023; POYATOS et al., 2014). However, the results underline the non-linear and complex relation between NDVI and these fluxes. NDVI relations vary between Groups indicating the dependence of NDVI on vegetation composition but also moisture conditions, which was also found in other studies (JESPERSEN et al., 2023; MCPARTLAND et al., 2019). However, it should be noted that changes in GPP and hence NDVI are more prominent at sites with higher moss abundance based on varying photosynthesis rates between vascular plants and mosses leading to higher NDVI results and possible misinterpretations additionally contributing to the uncertainties in CO_2 dynamics (MAY et al., 2018). This should be considered when interpreting the results especially of Group 3, which contains the highest NDVI but also the highest moss abundance (A3; Figure 8).

4.3.3 Problems in determining relations with PAR, air temperature and ER

PAR and air temperature are considered driving factors of NEE, GPP and ER (VIRKKALA et al., 2018). Especially NEE and GPP usually show highly significant relations with PAR and air temperature as shown by many studies (KARELIN et al., 2013; LIU et al., 2019; VOGEL et al., 2009). LIU et al., 2019 identified linear and non-linear relations between PAR, air temperature and CO_2 fluxes in a peatland in Zoige. KARELIN et al. (2013) found significant positive correlations of PAR with temperature, TD and CO_2 fluxes in a tundra ecosystem in Vorkuta, Russia. These findings are in line with several other studies showing the same positive correlated relations (MALHOTRA & ROULET, 2015; VIRKKALA et al., 2018). However, in this study no correlation or non-linear relation could

be determined between PAR, air temperature and CO_2 fluxes. In particular, ER showed no correlations with PAR and air temperature, nor with various parameters such as soil temperature and soil moisture. This was very surprising and does not correspond to the results of the studies already mentioned above. Only Group 2 showed a very weak influence of soil temperature and a very weak relation between PAR and GPP, which shows a potential of the ecosystem to respond to changes in air temperature and PAR.

However, model quality and explanatory power are not very meaningful (A23; A24; A25). During the study period air temperatures during measuring times were usually above 20°C while the lowest mean air temperature was not below 24.78°C determined for Group 3 (Figure 9). Furthermore, GPP was calculated for each site from the respective daily mean value of NEE and ER, which resulted in very few data points for the entire measurement period. This also accounts for NEE and ER, albeit these fluxes included more data since they were measured directly. However, ER showed constant fluxes without much variability during the whole measuring period. Additionally, the lack of data together with data gaps, which occur in the data for several parameters together with quite constant temperature conditions and a short measuring period only in July could result in insufficient correlations between different environmental parameters and CO_2 across the groups. Further data collection over longer periods could help to complete the data set and might allow comparison between different years and seasons while also allow to capture the relation between PAR and air temperature.

5 Conclusion

In conclusion, the discussion highlights the complexities and challenges associated with measuring CO_2 fluxes in ecosystems, particularly in polygonal mires. Using closed flux chambers is a common approach and presents limitations due to disturbances in driving parameters such as soil and vegetation, leaks, and temperature changes. Despite efforts to mitigate these challenges, uncertainties persist, emphasizing the need for careful interpretation of results.

The study found that the investigated environment mainly acts as a carbon sink whose carbon uptake capacity depends on several environmental parameters like soil moisture, soil temperature or vegetation underlining the complexity of Arctic ecosystems found also in other studies as well as the importance of including several microtopographical and micrometerological parameters (BRUHWILER et al., 2021; POYATOS et al., 2014).

Regarding the influence of environmental parameters on CO_2 fluxes, soil moisture emerges as a critical factor, impacting NEE and GPP significantly, particularly in deeper soil layers. The study underscores the non-linear relationship between soil moisture as well as soil temperature and CO_2 fluxes, with varying responses observed across different vegetation groups. Thaw depth also influences CO_2 fluxes, with deeper thawing soils potentially leading to carbon uptake by the ecosystem in this study, albeit these result exhibit great uncertainties because increasing thaw depth is usually linked to CO_2 emissions (MAURITZ et al., 2017). PH levels and NDVI are identified as important parameters affecting CO_2 fluxes, with higher pH promoting carbon release in most cases, and NDVI showing complex, non-linear relationships with fluxes, influenced by vegetation composition and moisture conditions. However, limitations in data collection and analysis underscore the need for cautious interpretation of these findings. Furthermore, while PAR and air temperature are typically considered driving factors for CO_2 fluxes, this study finds limited correlations, particularly with ER. Data gaps and short measurement periods contribute to uncertainties, highlighting the importance of long-term data collection for comprehensive understanding.

Looking ahead, future research in the field of CO_2 flux measurement in polygonal mires holds promise for advancing our understanding of carbon dynamics and ecosystem responses to environmental changes. Continued advancements in measurement techniques, long-term monitoring efforts, integration of remote sensing technologies, refinement of modeling approaches, collaborative multi-disciplinary studies, and assessments of climate change impacts are key priorities. By addressing these further, the knowledge of CO_2 dynamics in polygonal mires can be improved contributing to more accurate carbon budget assessments while providing strategies that aim at mitigating the impacts of climate change on these valuable ecosystems.

6 References

AALTO, J., LE ROUX, P.C., LUOTO, M. (2013): Vegetation Mediates Soil Temperature and Moisture in Arctic-Alpine Environments. Arctic, Antarctic, and Alpine Research 45, 429–439.

ALFRED-WEGENER-INSTITUT (2024): Permafrost - An introduction - AWI. URL: https://www.awi.de/en/focus/permafrost/permafrost-an-introduction.html (accessed 3.04.2024).

AMIN, R., AR SALAN, M.S., HOSSAIN, M.M. (2024): Measuring the impact of responsible factors on CO2 emission using generalized additive model (GAM). Heliyon 10, e25416.

ANDRESEN, C.G., LAWRENCE, D.M., WILSON, C.J., MCGUIRE, A.D., KOVEN, C., SCHAEFER, K., JAFAROV, E., PENG, S., CHEN, X., GOUTTEVIN, I., BURKE, E., CHADBURN, S., JI, D., CHEN, G., HAYES, D., ZHANG, W. (2020): Soil moisture and hydrology projections of the permafrost region – a model intercomparison. The Cryosphere 14, 445–459.

ANTONOVA, S., THIEL, C., HÖFLE, B., ANDERS, K., HELM, V., ZWIEBACK, S., MARX, S., BOIKE, J. (2019): Estimating tree height from TanDEM-X data at the northwestern Canadian treeline. Remote Sensing of Environment 231, 111251.

BARTHELMES, A., COUWENBERG, J., RISAGER, M., TEGETMEYER, C., JOOSTEN, H. (2015): Peatlands and Climate in a Ramsar context : A Nordic-Baltic Perspective.

BERNER, L.T., MASSEY, R., JANTZ, P., FORBES, B.C., MACIAS-FAURIA, M., MYERS-SMITH, I., KUMPULA, T., GAUTHIER, G., ANDREU-HAYLES, L., GAGLIOTI, B.V., BURNS, P., ZETTERBERG, P., D'ARRIGO, R., GOETZ, S.J. (2020): Summer warming explains widespread but not uniform greening in the Arctic tundra biome. Nat Commun 11, 4621.

BIASI, C., JOKINEN, S., MARUSHCHAK, M.E., HÄMÄLÄINEN, K., TRUBNIKOVA, T., OINONEN, M., MARTIKAINEN, P.J. (2014): Microbial Respiration in Arctic Upland and Peat Soils as a Source of Atmospheric Carbon Dioxide. Ecosystems 17, 112–126.

BRUHWILER, L., PARMENTIER, F.-J.W., CRILL, P., LEONARD, M., PALMER, P.I. (2021): The Arctic Carbon Cycle and Its Response to Changing Climate. Curr Clim Change Rep 7, 14–34.

CALVIN, K., DASGUPTA, D., KRINNER, G., MUKHERJI, A., THORNE, P.W., TRISOS, C., ROMERO, J., ALDUNCE, P., BARRETT, K., BLANCO, G., CHEUNG, W.W.L., CONNORS, S., DENTON, F., DIONGUE-NIANG, A., DODMAN, D., GARSCHAGEN, M., GEDEN, O., HAYWARD, B., JONES, C., JOTZO, F., KRUG, T., LASCO, R., LEE, Y.-Y., MASSON-DELMOTTE, V., MEINSHAUSEN, M., MINTENBECK, K., MOKSSIT, A., OTTO, F.E.L., PATHAK, M., PIRANI, A., POLOCZANSKA, E., PÖRTNER, H.-O., REVI, A., ROBERTS, D.C., ROY, J., RUANE, A.C., SKEA, J., SHUKLA, P.R., SLADE,

R., SLANGEN, A., SOKONA, Y., SÖRENSSON, A.A., TIGNOR, M., VAN VUUREN, D., WEI, Y.-M., WINKLER, H., ZHAI, P., ZOMMERS, Z., HOURCADE, J.-C., JOHNSON, F.X., PACHAURI, S., SIMPSON, N.P., SINGH, C., THOMAS, A., TOTIN, E., ARIAS, P., BUSTAMANTE, M., ELGIZOULI, I., FLATO, G., HOWDEN, M., MÉNDEZ-VALLEJO, C., PEREIRA, J.J., PICHS-MADRUGA, R., ROSE, S.K., SAHEB, Y., SÁNCHEZ RODRÍGUEZ, R., ÜRGE-VORSATZ, D., XIAO, C., YASSAA, N., ALEGRÍA, A., ARMOUR, K., BEDNAR-FRIEDL, B., BLOK, K., CISSÉ, G., DENTENER, F., ERIKSEN, S., FISCHER, E., GARNER, G., GUIVARCH, C., HAASNOOT, M., HANSEN, G., HAUSER, M., HAWKINS, E., HERMANS, T., KOPP, R., LEPRINCE-RINGUET, N., LEWIS, J., LEY, D., LUDDEN, C., NIAMIR, L., NICHOLLS, Z., SOME, S., SZOPA, S., TREWIN, B., VAN DER WIJST, K.-I., WINTER, G., WITTING, M., BIRT, A., HA, M., ROMERO, J., KIM, J., HAITES, E.F., JUNG, Y., STAVINS, R., BIRT, A., HA, M., ORENDAIN, D.J.A., IGNON, L., PARK, S., PARK, Y., REISINGER, A., CAMMARAMO, D., FISCHLIN, A., FUGLESTVEDT, J.S., HANSEN, G., LUDDEN, C., MASSON-DELMOTTE, V., MATTHEWS, J.B.R., MINTENBECK, K., PIRANI, A., POLOCZANSKA, E., LEPRINCE-RINGUET, N., PÉAN, C. (2023): IPCC, 2023: Climate Change 2023: Synthesis Report. Contribution of Working Groups I, II and III to the Sixth Assessment Report of the Intergovernmental Panel on Climate Change [Core Writing Team, H. Lee and J. Romero (eds.)]. IPCC, Geneva, Switzerland. Intergovernmental Panel on Climate Change (IPCC).

CANADA COMMITTEE ON ECOLOGICAL (BIOPHYSICAL) LAND CLASSIFICATION (ED.) (1988): Wetlands of Canada, Ecological land classification series. Minister of Supply and Services Canada, Hull, Quebec.

CHAI, T., DRAXLER, R.R. (2014): Root mean square error (RMSE) or mean absolute error (MAE)? (preprint). Numerical Methods.

CHESTER, S.R. (2016): The arctic guide: wildlife of the far north, 1st edition. ed. Princeton University Press, Princeton, NJ.

CHURCHILL, A.C., TURETSKY, M.R., MCGUIRE, A.D., HOLLINGSWORTH, T.N. (2015): Response of plant community structure and primary productivity to experimental drought and flooding in an Alaskan fen. Can. J. For. Res. 45, 185–193.

CONSERVATION OF ARCTIC FLORA AND FAUNA (CAFF) (2021): Resilience and management of Arctic wetlands: phase 2 report.

DAVIDSON, E.A., SAVAGE, K., VERCHOT, L.V., NAVARRO, R. (2002): Minimizing artifacts and biases in chamber-based measurements of soil respiration. Agricultural and Forest Meteorology, FLUXNET 2000 Synthesis 113, 21–37.

ECKHARDT, T., KNOBLAUCH, C., KUTZBACH, L., HOLL, D., SIMPSON, G., ABAKUMOV, E., PFEIFFER, E.-M. (2019): Partitioning net ecosystem exchange of CO_2 on the pedon scale in the Lena River Delta, Siberia. Biogeosciences 16, 1543–1562.

FISCHER, W., THOMAS, C.K., ZIMOV, N., GÖCKEDE, M. (2022): Grazing enhances carbon cycling but reduces methane emission during peak growing season in the Siberian Pleistocene Park tundra site. Biogeosciences 19, 1611–1633.

GORNALL, J.L., JÓNSDÓTTIR, I.S., WOODIN, S.J., VAN DER WAL, R. (2007): Arctic mosses govern below-ground environment and ecosystem processes. Oecologia 153, 931–941.

GOVERNMENT OF CANADA (2024a): Canadian Climate Normals 1991-2020 Data - Climate - Environment and Climate Change Canada. URL: https://climate.weather.gc.ca/climate_normals/results_1991_2020_e.html?searchType=stnName_1991&txtStationName_1991=inuvik&searchMethod=contains&txtCentralLatMin=0&txtCentralLatSec=0&txtCentralLongMin=0&txtCentralLongSec=0&stnID=408000000&dispBack=1 (accessed 23.02.2024).

GOVERNMENT OF CANADA (2024b): Temperature change in Canada - Canada.ca. URL: https://www.canada.ca/en/environment-climate-change/services/environmental-indicators/temperature-change.html (accessed 23.02.2024).

GOVERNMENT OF CANADA (2024c): Daily Data Report for July 2023 - Climate - Environment and Climate Change Canada. URL: https://climate.weather.gc.ca/climate_data/daily_data_e.html?StationID=41883&Month=7&Day=1&Year=2023&timeframe=2&StartYear=1840&EndYear=2023 (accessed 23.02.2024).

GOVERNMENT OF CANADA (2016): Extent of Canada's wetlands. URL: https://www.canada.ca/en/environment-climate-change/services/environmental-indicators/extent-wetlands.html (accessed 5.04.2024).

GOVERNMENT OF NORTHWEST TERRITORIES (2024): NWT Species Search. URL: https://www.gov.nt.ca/species-search/ (accessed 22.02.2024).

GRÜNBERG, I., BOIKE, J. (2019): Vegetation map of Trail Valley Creek, Northwest Territories, Canada.

GRÜNBERG, I., WILCOX, E.J., ZWIEBACK, S., MARSH, P., BOIKE, J. (2020): Linking tundra vegetation, snow, soil temperature, and permafrost. Biogeosciences 17, 4261–4279.

HARRIS, J.W. (1998): Handbook of mathematics and computational science. Springer, New York [u.a.].

HARRIS, L.I., ROULET, N.T., MOORE, T.R. (2020): Mechanisms for the Development of Microform Patterns in Peatlands of the Hudson Bay Lowland. Ecosystems 23, 741–767.

HASTIE, T., TIBSHIRANI, R., FRIEDMAN, J. (2009a): Additive Models, Trees, and Related Methods, in: The Elements of Statistical Learning, Springer Series in Statistics. Springer New York, New York, NY, pp. 295–336.

HASTIE, T., TIBSHIRANI, R., FRIEDMAN, J. (2009b): The Elements of Statistical Learning, Springer Series in Statistics. Springer New York, New York, NY.

HELBIG, M., HUMPHREYS, E.R., TODD, A. (2019): Contrasting Temperature Sensitivity of CO2 Exchange in Peatlands of the Hudson Bay Lowlands, Canada. Journal of Geophysical Research: Biogeosciences 124, 2126–2143.

HODSON, T.O. (2022): Root-mean-square error (RMSE) or mean absolute error (MAE): when to use them or not. Geosci. Model Dev. 15, 5481–5487.

HUMPHREYS, E.R., CHARRON, C., BROWN, M., JONES, R. (2014): Two Bogs in the Canadian Hudson Bay Lowlands and a Temperate Bog Reveal Similar Annual Net Ecosystem Exchange of CO2. Arctic, Antarctic, and Alpine Research 46, 103–113.

HUNT, S. (2003): Measurements of photosynthesis and respiration in plants. Physiol Plant 117, 314–325.

ILLERIS, L., CHRISTENSEN, T.R., MASTEPANOV, M. (2004): Moisture Effects on Temperature Sensitivity of CO2 Exchange in a Subarctic Heath Ecosystem. Biogeochemistry 70, 315–330.

INTERGOVERNMENTAL PANEL ON CLIMATE CHANGE (IPCC) (2022): The Ocean and Cryosphere in a Changing Climate: Special Report of the Intergovernmental Panel on Climate Change, 1st ed. Cambridge University Press.

JESPERSEN, R.G., ANDERSON-SMITH, M., SULLIVAN, P.F., DIAL, R.J., WELKER, J.M. (2023): NDVI changes in the Arctic: Functional significance in the moist acidic tundra of Northern Alaska. PLoS ONE 18, e0285030.

JOOSTEN, H., CLARKE, D. (2002): Wise use of mires and peatlands: background and principles including a framework for decision-making. International Peat Society ; International Mire Conservation Group, Jyväskylä.

KALUSCHE, D. (2016): Ökologie in Zahlen: Eine Datensammlung in Tabellen mit über 10.000 Einzelwerten. Springer, Berlin, Heidelberg.

KARELIN, D.V., ZAMOLODCHIKOV, D.G., ZUKERT, N.V., CHESTNYKH, O.V., POCHIKALOV, A.V., KRAEV, G.N. (2013): Interannual changes in PAR and soil moisture during warm season may be more important than temperature fluctuations in directing annual carbon balance in Tundra. Biol Bull Rev 3, 371–387.

KITTLER, F., HEIMANN, M., KOLLE, O., ZIMOV, N., ZIMOV, S., GÖCKEDE, M. (2017): Long-Term Drainage Reduces CO2 Uptake and CH4 Emissions in a Siberian Permafrost Ecosystem. Global Biogeochemical Cycles 31, 1704–1717.

KOKELJ, S.V., PALMER, M.J., LANTZ, T.C., BURN, C.R. (2017): Ground Temperatures and Permafrost Warming from Forest to Tundra, Tuktoyaktuk Coastlands and Anderson Plain, NWT, Canada: Permafrost

temperatures across tree line northwestern Canada. Permafrost and Periglac. Process. 28, 543–551.

KOVEN, C.D., SCHUUR, E.A.G., SCHÄDEL, C., BOHN, T.J., BURKE, E.J., CHEN, G., CHEN, X., CIAIS, P., GROSSE, G., HARDEN, J.W., HAYES, D.J., HUGELIUS, G., JAFAROV, E.E., KRINNER, G., KUHRY, P., LAWRENCE, D.M., MACDOUGALL, A.H., MARCHENKO, S.S., MCGUIRE, A.D., NATALI, S.M., NICOLSKY, D.J., OLEFELDT, D., PENG, S., ROMANOVSKY, V.E., SCHAEFER, K.M., STRAUSS, J., TREAT, C.C., TURETSKY, M. (2015): A simplified, data-constrained approach to estimate the permafrost carbon–climate feedback. Phil. Trans. R. Soc. A. 373, 20140423.

KRAUSE, P., BOYLE, D.P., BÄSE, F. (2005): Comparison of different efficiency criteria for hydrological model assessment. Adv. Geosci. 5, 89–97.

KUTZBACH, L., SCHNEIDER, J., SACHS, T., GIEBELS, M., NYKÄNEN, H., SHURPALI, N.J., MARTIKAINEN, P.J., ALM, J., WILMKING, M. (2007): CO_2 flux determination by closed-chamber methods can be seriously biased by inappropriate application of linear regression. Biogeosciences 4, 1005–1025.

KÜCHENMEISTER, ANNELEN (2023): Photos of the chamber setup during light and dark measurements, Trail Valley Creek.

KWON, M.J., HEIMANN, M., KOLLE, O., LUUS, K.A., SCHUUR, E.A.G., ZIMOV, N., ZIMOV, S.A., GÖCKEDE, M. (2016): Long-term drainage reduces CO_2 uptake and increases CO_2 emission on a Siberian floodplain due to shifts in vegetation community and soil thermal characteristics. Biogeosciences 13, 4219–4235.

LAWRENCE, D.M., KOVEN, C.D., SWENSON, S.C., RILEY, W.J., SLATER, A.G. (2015): Permafrost thaw and resulting soil moisture changes regulate projected high-latitude CO_2 and CH_4 emissions. Environ. Res. Lett. 10, 094011.

LI, Z.-L., MU, C.-C., CHEN, X., WANG, X.-Y., DONG, W.-W., JIA, L., MU, M., STRELETSKAYA, I., GREBENETS, V., SOKRATOV, S., KIZYAKOV, A., WU, X.-D. (2021): Changes in net ecosystem exchange of CO_2 in Arctic and their relationships with climate change during 2002–2017. Advances in Climate Change Research 12, 475–481.

LINDGREN, A., HUGELIUS, G., KUHRY, P., CHRISTENSEN, T.R., VANDENBERGHE, J. (2016): GIS-based Maps and Area Estimates of Northern Hemisphere Permafrost Extent during the Last Glacial Maximum. Permafrost & Periglacial 27, 6–16.

LIU, X., ZHU, D., ZHAN, W., CHEN, H., ZHU, Q., HAO, Y., LIU, W., HE, Y. (2019): Five-Year Measurements of Net Ecosystem CO_2 Exchange at a Fen in the Zoige Peatlands on the Qinghai-Tibetan Plateau. JGR Atmospheres 124, 11803–11818.

LÓPEZ-BLANCO, E., LUND, M., WILLIAMS, M., TAMSTORF, M.P., WESTERGAARD-NIELSEN, A., EXBRAYAT, J.-F., HANSEN, B.U., CHRISTENSEN, T.R. (2017): Exchange of CO2 in Arctic tundra: impacts of meteorological variations and biological disturbance. Biogeosciences 14, 4467–4483.

LUND, M., LAFLEUR, P.M., ROULET, N.T., LINDROTH, A., CHRISTENSEN, T.R., AURELA, M., CHOJNICKI, B.H., FLANAGAN, L.B., HUMPHREYS, E.R., LAURILA, T., OECHEL, W.C., OLEJNIK, J., RINNE, J., SCHUBERT, P., NILSSON, M.B. (2010): Variability in exchange of CO2 across 12 northern peatland and tundra sites. Global Change Biology 16, 2436–2448.

MALHOTRA, A., ROULET, N.T. (2015): Environmental correlates of peatland carbon fluxes in a thawing landscape: do transitional thaw stages matter? Biogeosciences 12, 3119–3130.

MARSH, P., BARTLETT, P., MACKAY, M., POHL, S., LANTZ, T. (2010): Snowmelt energetics at a shrub tundra site in the western Canadian Arctic. Hydrological Processes 24, 3603–3620.

MARSH, P., POMEROY, J.W. (1996): MELTWATER FLUXES AT AN ARCTIC FOREST-TUNDRA SITE. Hydrol. Process. 10, 1383–1400.

MAURITZ, M., BRACHO, R., CELIS, G., HUTCHINGS, J., NATALI, S., PEGORARO, E., SALMON, V., SCHÄDEL, C., WEBB, E., SCHUUR, E. (2017): Non-linear CO 2 flux response to seven years of experimentally induced permafrost thaw. Global Change Biology 23.

MAY, J.L., PARKER, T., UNGER, S., OBERBAUER, S.F. (2018): Short term changes in moisture content drive strong changes in Normalized Difference Vegetation Index and gross primary productivity in four Arctic moss communities. Remote Sensing of Environment 212, 114–120.

MCPARTLAND, M.Y., KANE, E.S., FALKOWSKI, M.J., KOLKA, R., TURETSKY, M.R., PALIK, B., MONTGOMERY, R.A. (2019): The response of boreal peatland community composition and NDVI to hydrologic change, warming, and elevated carbon dioxide. Global Change Biology 25, 93–107.

MILLAR, A.H., WHELAN, J., SOOLE, K.L., DAY, D.A. (2011): Organization and Regulation of Mitochondrial Respiration in Plants. Annu. Rev. Plant Biol. 62, 79–104.

MINAYEVA, T., SIRIN, A., KERSHAW, P., BRAGG, O. (2016): Arctic Peatlands, in: Finlayson, C.M., Milton, G.R., Prentice, R.C., Davidson, N.C. (Eds.), The Wetland Book. Springer Netherlands, Dordrecht, pp. 1–15.

MINER, K.R., TURETSKY, M.R., MALINA, E., BARTSCH, A., TAMMINEN, J., MCGUIRE, A.D., FIX, A., SWEENEY, C., ELDER, C.D., MILLER, C.E. (2022): Permafrost carbon emissions in a changing Arctic. Nat Rev Earth Environ 3, 55–67.

NATALI, S., SCHUUR, T., MAURITZ, M., SCHADE, J., CELIS, G., CRUMMER, K., JOHNSTON, C., KRAPEK, J., PEGORARO, E., SALMON, V., WEBB, E. (2015): Permafrost thaw and soil moisture drive CO_2 and CH_4 release from upland tundra. Journal of Geophysical Research: Biogeosciences.

NATALI, S.M., WATTS, J.D., ROGERS, B.M., POTTER, S., LUDWIG, S.M., SELBMANN, A.-K., SULLIVAN, P.F., ABBOTT, B.W., ARNDT, K.A., BIRCH, L., BJÖRKMAN, M.P., BLOOM, A.A., CELIS, G., CHRISTENSEN, T.R., CHRISTIANSEN, C.T., COMMANE, R., COOPER, E.J., CRILL, P., CZIMCZIK, C., DAVYDOV, S., DU, J., EGAN, J.E., ELBERLING, B., EUSKIRCHEN, E.S., FRIBORG, T., GENET, H., GÖCKEDE, M., GOODRICH, J.P., GROGAN, P., HELBIG, M., JAFAROV, E.E., JASTROW, J.D., KALHORI, A.A.M., KIM, Y., KIMBALL, J.S., KUTZBACH, L., LARA, M.J., LARSEN, K.S., LEE, B.-Y., LIU, Z., LORANTY, M.M., LUND, M., LUPASCU, M., MADANI, N., MALHOTRA, A., MATAMALA, R., MCFARLAND, J., MCGUIRE, A.D., MICHELSEN, A., MINIONS, C., OECHEL, W.C., OLEFELDT, D., PARMENTIER, F.-J.W., PIRK, N., POULTER, B., QUINTON, W., REZANEZHAD, F., RISK, D., SACHS, T., SCHAEFER, K., SCHMIDT, N.M., SCHUUR, E.A.G., SEMENCHUK, P.R., SHAVER, G., SONNENTAG, O., STARR, G., TREAT, C.C., WALDROP, M.P., WANG, Y., WELKER, J., WILLE, C., XU, X., ZHANG, Z., ZHUANG, Q., ZONA, D. (2019): Large loss of CO_2 in winter observed across the northern permafrost region. Nat. Clim. Chang. 9, 852–857.

NOSKOVA, M.G. (2016): Полевой атлас-определитель сфагновых мхов таежной зоны Европейской России. Aquarius, Tula City.

OECHEL, W.C., LASKOWSKI, C.A., BURBA, G., GIOLI, B., KALHORI, A.A.M. (2014): Annual patterns and budget of CO_2 flux in an Arctic tussock tundra ecosystem. Journal of Geophysical Research: Biogeosciences 119, 323–339.

PALMER, M.J., BURN, C.R., KOKELJ, S.V. (2012): Factors influencing permafrost temperatures across tree line in the uplands east of the Mackenzie Delta, 2004–2010. Can. J. Earth Sci. 49, 877–894.

PAVELKA, M., ACOSTA, M., KIESE, R., ALTIMIR, N., BRÜMMER, C., CRILL, P., DARENOVA, E., FUß, R., GIELEN, B., GRAF, A., KLEMEDTSSON, L., LOHILA, A., LONGDOZ, B., LINDROTH, A., NILSSON, M., JIMÉNEZ, S.M., MERBOLD, L., MONTAGNANI, L., PEICHL, M., PIHLATIE, M., PUMPANEN, J., ORTIZ, P.S., SILVENNOINEN, H., SKIBA, U., VESTIN, P., WESLIEN, P., JANOUS, D., KUTSCH, W. (2018): Standardisation of chamber technique for CO_2, N_2O and CH_4 fluxes measurements from terrestrial ecosystems. International Agrophysics 32, 569–587.

PCE INSTRUMENTS (2024): Schlamm-pH-Meter PCE-228SLUR-ICA inkl. ISO-Kalibrierzertifikat vom Hersteller. URL: https://www.pce-instruments.com/deutsch/messtechnik/messgeraete-fuer-alle-parameter/ph-meter-ph-messgeraet-pce-instruments-schlamm-ph-

meter-pce-228slur-ica-inkl.-iso-kalibrierzertifikat-det_5856771.htm (accessed 5.02.2024).

POHL, S., DAVISON, B., MARSH, P., PIETRONIRO, A. (2005): Modelling spatially distributed snowmelt and meltwater runoff in a small Arctic catchment with a hydrology land-surface scheme (WATCLASS). Atmosphere-Ocean 43, 193–211.

POMEROY, J.W., GRAY, D.M., SHOOK, K.R., TOTH, B., ESSERY, R.L.H., PIETRONIRO, A., HEDSTROM, N. (1998): An evaluation of snow accumulation and ablation processes for land surface modelling. Hydrological Processes 12, 2339–2367.

POYATOS, R., HEINEMEYER, A., INESON, P., EVANS, J.G., WARD, H.C., HUNTLEY, B., BAXTER, R. (2014): Environmental and Vegetation Drivers of Seasonal CO2 Fluxes in a Sub-arctic Forest–Mire Ecotone. Ecosystems 17, 377–393.

QUINTON, W.L., GRAY, D.M., MARSH, P. (2000): Subsurface drainage from hummock-covered hillslopes in the Arctic tundra. Journal of Hydrology 237, 113–125.

R CORE TEAM (2023): R: A language and environment for statistical computing. R Foundation for Statistical Computing, Vienna, Austria. URL: https://www.R-project.org/ (accessed 26.02.2024).

RETTELBACH, T., NITZE, I., GRÜNBERG, I., HAMMAR, J., SCHÄFFLER, S., HEIN, D., GESSNER, M., BUCHER, T., BRAUCHLE, J., HARTMANN, J., SACHS, T., BOIKE, J., GROSSE, G. (2018): Super-high-resolution aerial imagery, digital surface models and 3D point clouds of Trail Valley Creek, Canada.

RIXEN, C., MULDER, C.P.H. (2005): Improved water retention links high species richness with increased productivity in arctic tundra moss communities. Oecologia 146, 287–299.

SCHUUR, E.A.G., ABBOTT, B. (2011): High risk of permafrost thaw. Nature 480, 32–33.

SJÖGERSTEN, S., VAN DER WAL, R., WOODIN, S.J. (2006): Small-scale hydrological variation determines landscape CO2 fluxes in the high Arctic. Biogeochemistry 80, 205–216.

STIRBET, A., LAZÁR, D., GUO, Y., GOVINDJEE, G. (2020): Photosynthesis: basics, history and modelling. Annals of Botany 126, 511–537.

STREET, L.E., SUBKE, J.-A., BAXTER, R., DINSMORE, K.J., KNOBLAUCH, C., WOOKEY, P.A. (2018): Ecosystem carbon dynamics differ between tundra shrub types in the western Canadian Arctic. Environ. Res. Lett. 13, 084014.

TARNOCAI, C. (2009): The Impact of Climate Change on Canadian Peatlands. Canadian Water Resources Journal 34, 453–466.

THE RAMSAR CONVENTION (2024): Home page | The Convention on Wetlands, The Convention on Wetlands. URL: https://www.ramsar.org/ (accessed 6.04.2024).

UNIVERSITY OF LAPLAND (2024): Arctic Region. Uni of Lapland. URL: https://www.arcticcentre.org/EN/arcticregion (accessed 2.04.2024).

VIRKKALA, A.-M., VIRTANEN, T., LEHTONEN, A., RINNE, J., LUOTO, M. (2018): The current state of CO2 flux chamber studies in the Arctic tundra: A review. Progress in Physical Geography: Earth and Environment 42, 162–184.

VIRTANEN, R., OKSANEN, L., OKSANEN, T., COHEN, J., FORBES, B.C., JOHANSEN, B., KÄYHKÖ, J., OLOFSSON, J., PULLIAINEN, J., TØMMERVIK, H. (2016): Where do the treeless tundra areas of northern highlands fit in the global biome system: toward an ecologically natural subdivision of the tundra biome. Ecology and Evolution 6, 143–158.

VOGEL, J., SCHUUR, E.A.G., TRUCCO, C., LEE, H. (2009): Response of CO2 exchange in a tussock tundra ecosystem to permafrost thaw and thermokarst development. Journal of Geophysical Research: Biogeosciences 114.

WILLMOTT, C.J., MATSUURA, K., ROBESON, S.M. (2009): Ambiguities inherent in sums-of-squares-based error statistics. Atmospheric Environment 43, 749–752.

ZONA, D., LIPSON, D.A., ZULUETA, R.C., OBERBAUER, S.F., OECHEL, W.C. (2011): Microtopographic controls on ecosystem functioning in the Arctic Coastal Plain. Journal of Geophysical Research: Biogeosciences 116.

7. Appendix

A 1: Mean monthly precipitation and temperature for Inuvik in the period from 1991-2020 (GOVERNMENT OF CANADA, 2024a).
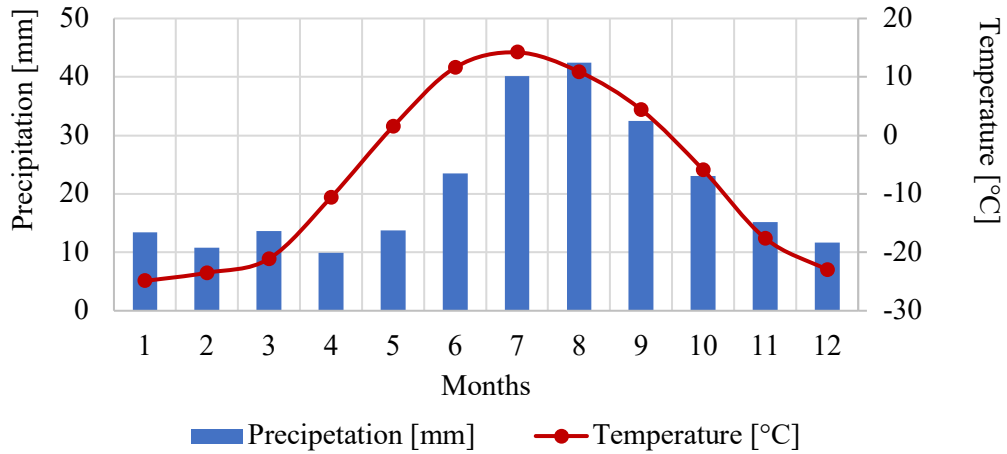
A 2: Mean temperature [°C] at the study sites during the measuring period in July 2023.
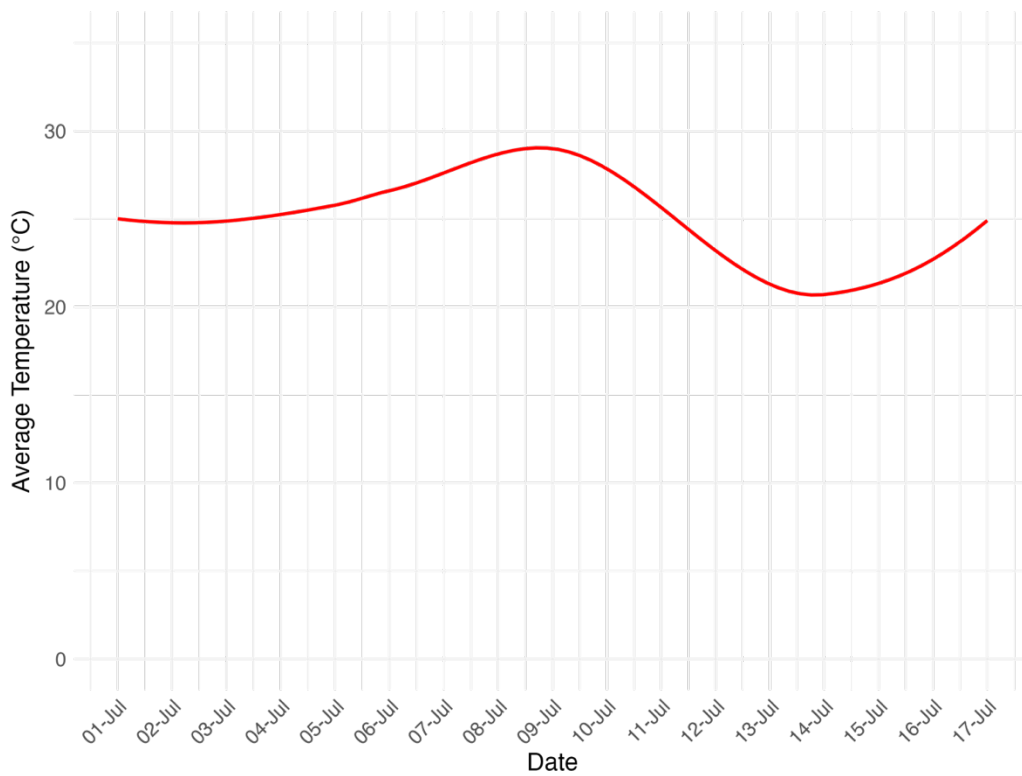
A 3: Vegetation groups of the collars from transect 2 and 5. The groups are based on the Braun-Blanquet scale for estimating species richness for plant populations (KALUSCHE, 2016). Collars with similar vegetation compositions were combined in one group. The groups written in light gray (1 to 4) are the groups assigned at the beginning. The groups in bold (1 to 3) are the merged groups that are used for the further analysis.

		Group 1		Group 2						Group 3						Group 4		
		Group 1								**Group 3**						**Group 4**		
Form	Name	5.4	5.7	2.2	2.4	2.5	2.8	5.2	5.9	5.1	2-7	5.10	5.8	5.5	5.6	2.3	2.6	5.3
Grass	*Carex aquatilis*			0	0	0	0	0		0	0	0				1	4	1
Shrub	*Andromeda polifolia*			0	0	0	0	0		0	0	0	1			0	0	0
Grass	*Oxycoccus palustris*			0	0	0	0	0	1	0	0	0	1	1	1	0	0	0
Shrub	*Empetrum nigrum*			1	1	1	1	1	1		1		1			0	0	0
Grass	*Rubus chamaemorus*	2	2			1			1	3	1			1	1	0	0	1
Shrub	*Vaccinium vitis-idaea*	2	2		1	3	3		1	2	1	1	1	1	1	0	0	0
Shrub	*Vaccinium uliginosum*				1		1		1							0	0	0
Grass	*Carex sp.*			2	1	3	3	2	2		1	2				0	0	0
Grass	*Eriophorum sp.*											4	1		2	0	0	1
Grass	*Pelasites frigidus*										1					0	0	0
Shrub	*Arctostaphylos alpina*	1							2	1		1		1		0	0	0
Lichens	*Flavocetraria spp.*	1	2			1			1	1								
Lichens	*Cladonia sp.*	5	4			1												
Lichens	*Peltigera sp.*						1											
Lichens	*Cetraria sp.*						1											
Lichens	*Stereocaulon spp.*																	
Moss	*Sphagnum inundatum*																	5
Moss	*Hypnum sp*															5	5	
Moss	*Sphagnum sp.*																	
Moss	*Sphagnum capillifolium*																	
Moss	*Sphagnum squarrosum*										2							
Moss	*Sphagnum russowi*										4							
Moss	*Pleurozium schreberi*			5	5													
Moss	*Green mosses*		1			4	5	5		2								
Moss	*Tomentypnum sp*					2												
Moss	*Polytrichum sp.*			1				1										1
Moss	*Sphagnum sp.*																	
Grass	*Dryas octopetala*																	
Grass	*Pyrola grandiflora*			1														
Grass	*Selaginella selaginoides*																	
Shrub	*Salix sp.*																	
Grass	*Equisetum scirpoides / Equisetum variegatum*																	
Shrub	*Betula glandulosa*		3	1							1						1	
Shrub	*Ledum palustre*			1			2			1		2	1	1	1			
Moss	*Mnium spp*																	
Moss	*Sphagnum balticum*					1			1	3			5		5			
Moss	*Sphagnum capillifolium*																	
Moss	*Sphagnum fuscum*								4					5				
Moss	*Sphagnum rubellum*								1									
Moss	*Sphagnum subnitens*																	

A 4: Average soil moisture in 12 cm [%] of transect 2 for the whole measuring period 2023.
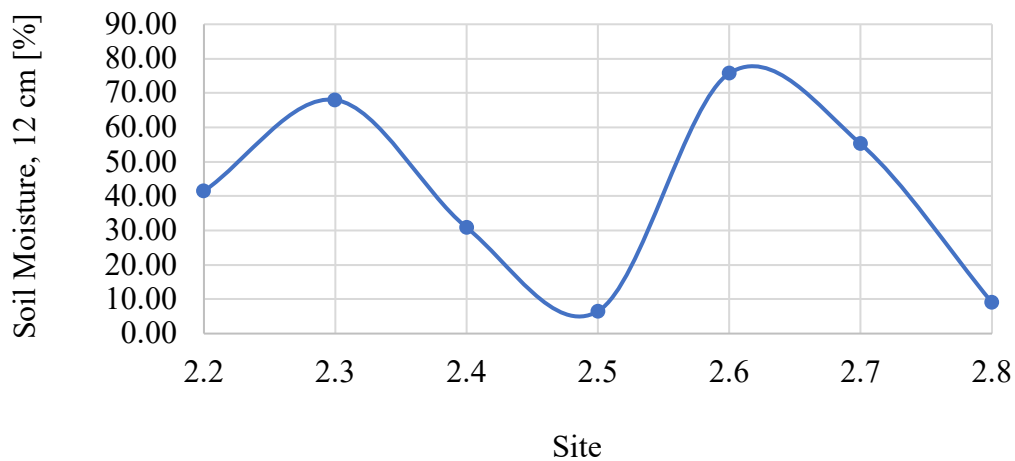

A 5: Average soil moisture in 12 cm [%] of transect 5 for the whole measuring period 2023.
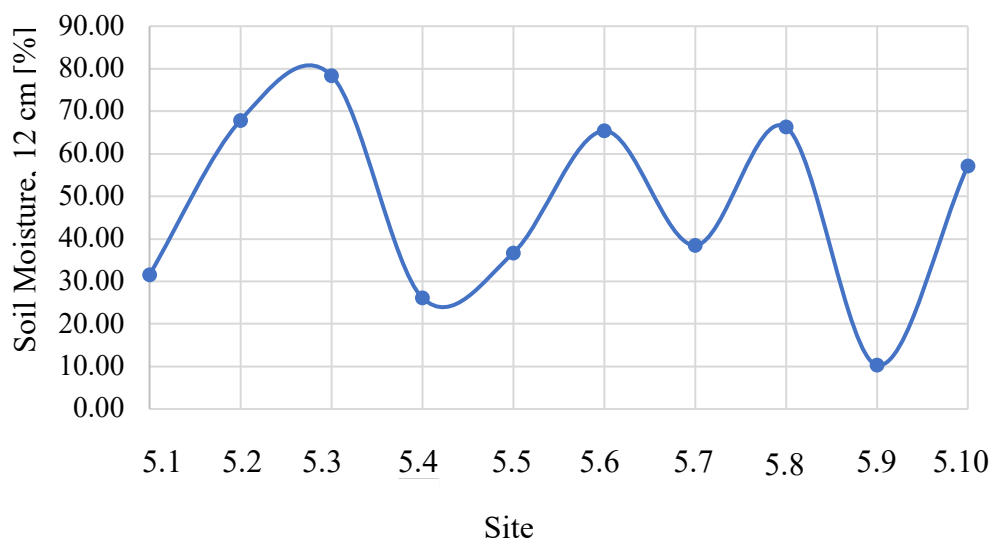
A 6: Setup for CO₂ chamber measurements. The 1) gas analyser is connected to the 2) chamber via various tubes and the 3) data logger via WiFi. Additional instruments used for the measurements are the 4) collar 5) cover sheet for dark measurements 6) steel rod for thawing depth 7) PAR sensor 8) soil moisture probe 9) soil temperature sensors (5, 10, 20, 30 cm) and 10) pH logger (photos: KÜCHENMEISTER, 2023; PCE INSTRUMENTS, 2024).
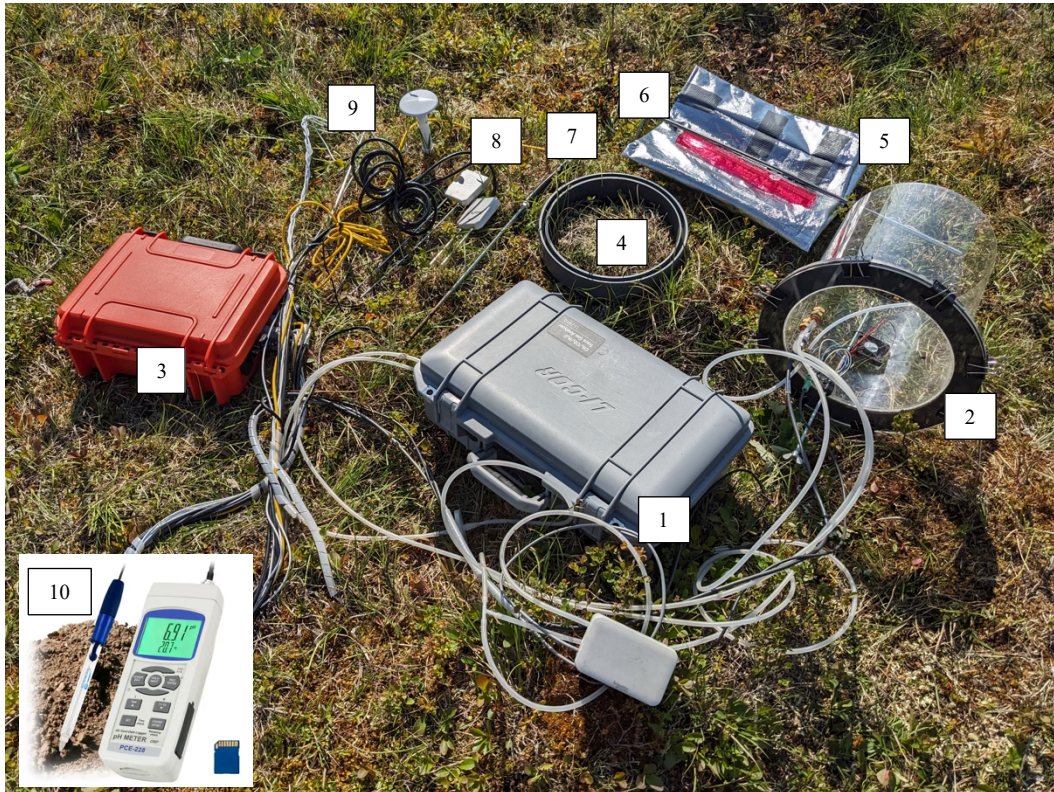
A 7: Differences in environmental conditions between Group 1,2, 3 and 4. The plots show the median value and variance of each environmental parameter according to each Group. Moreover, statistically significant differences between the Groups are shown in the bars above the violin plots.
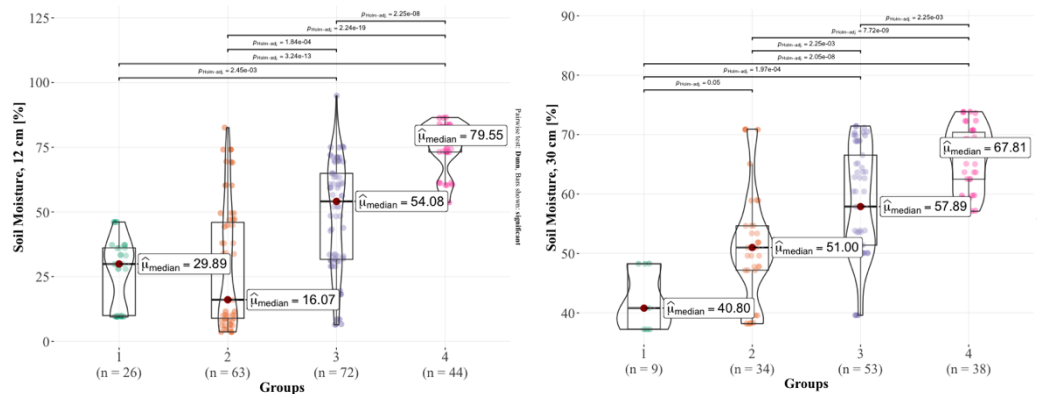
Continuing plots of A7: Differences in environmental parameters by groups 1, 2, 3 and 4.
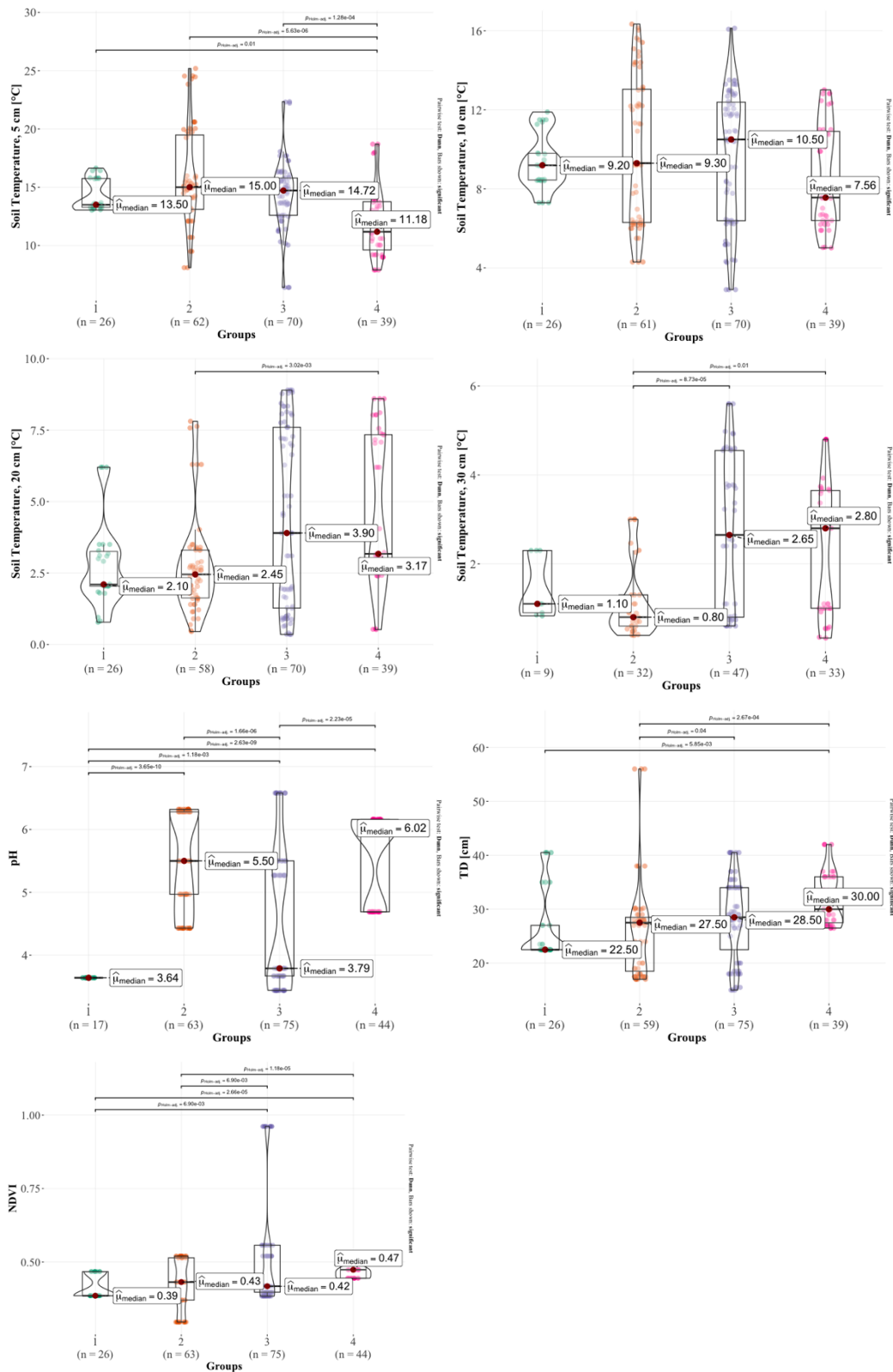
A 8: Timeline of NEE, ER and GPP fluxes of group 1 during the measuring period 2023. The plots show the different sites of each group (colored). The black line represents the mean flux of the whole group.
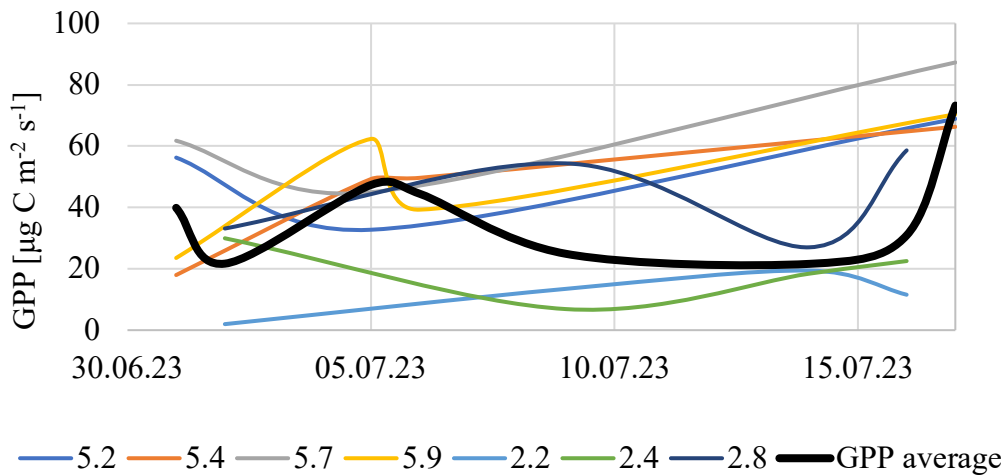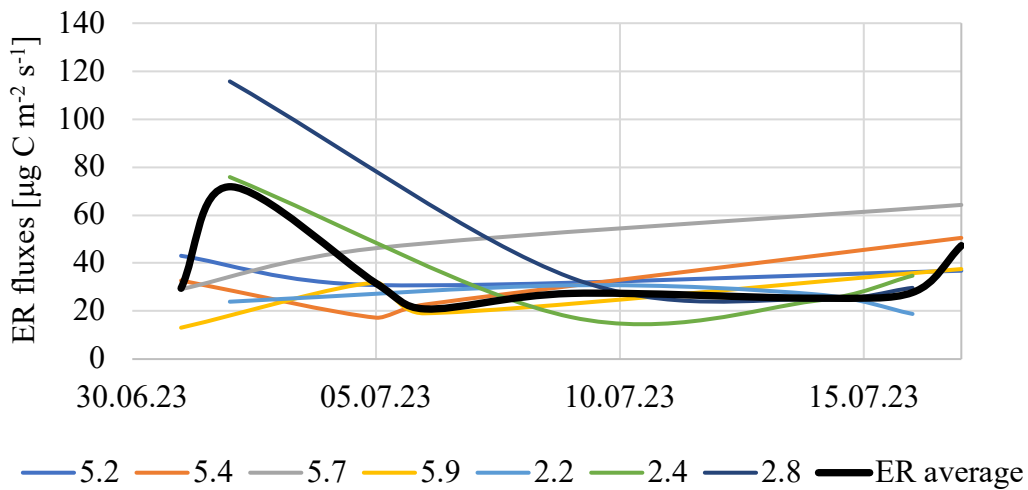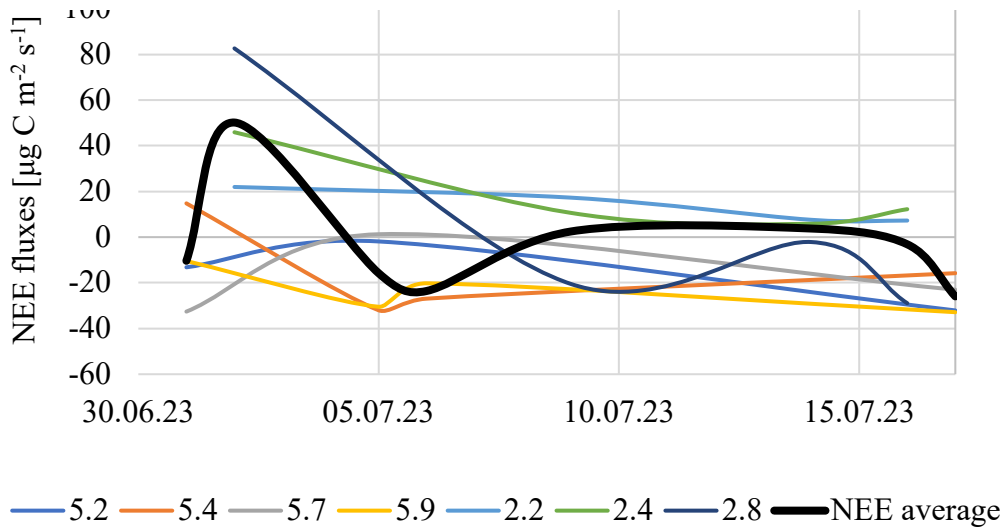
A 9: Timeline of NEE, ER and GPP fluxes of group 2 during the measuring period 2023. The plots show the different sites of each group (coloured). The black line represents the mean flux of the whole group.
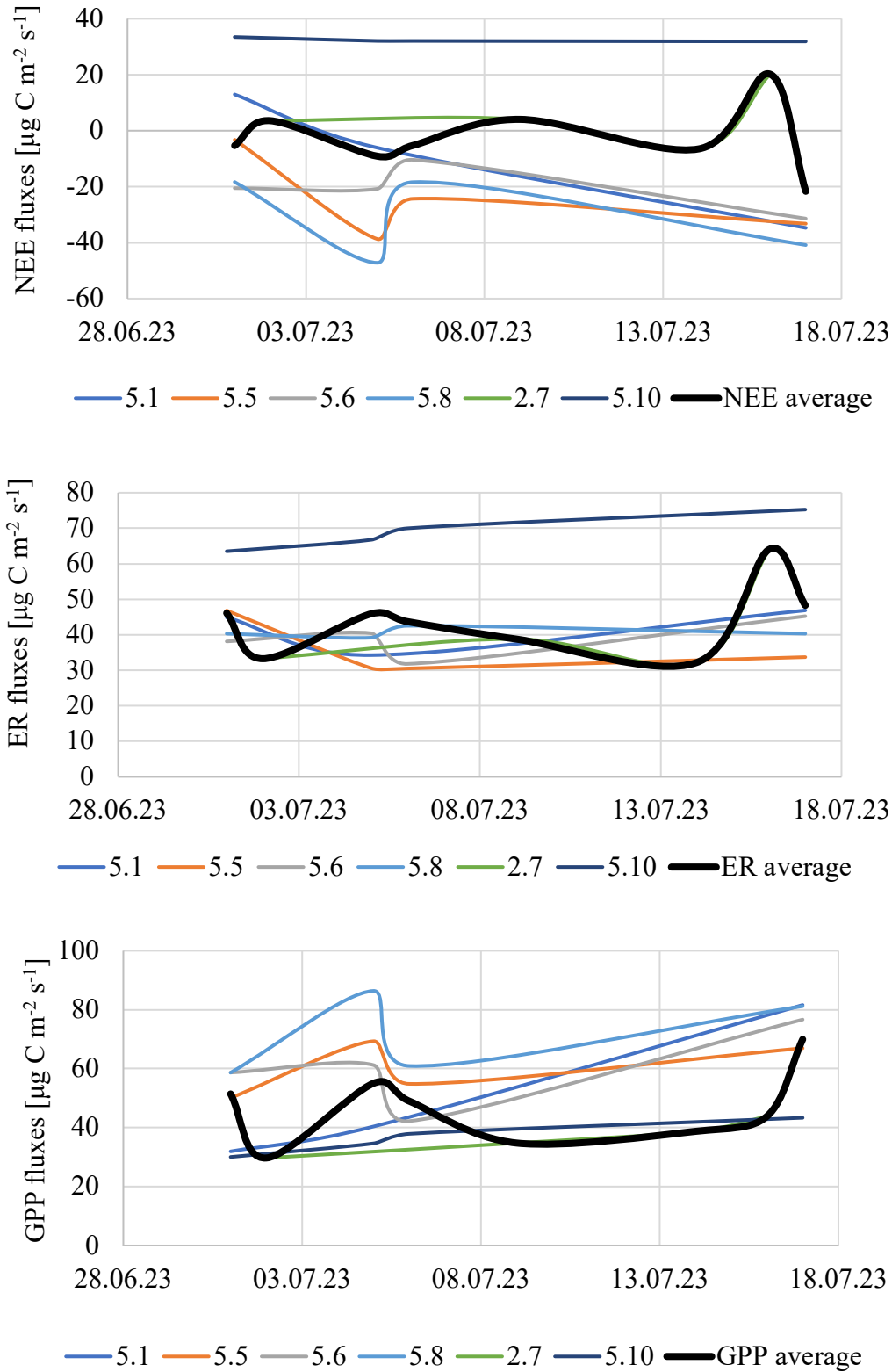
A 10: Timeline of NEE, ER and GPP fluxes of group 3 during the measuring period 2023. The plots show the different sites of each group (colored). The black line represents the mean flux of the whole group.
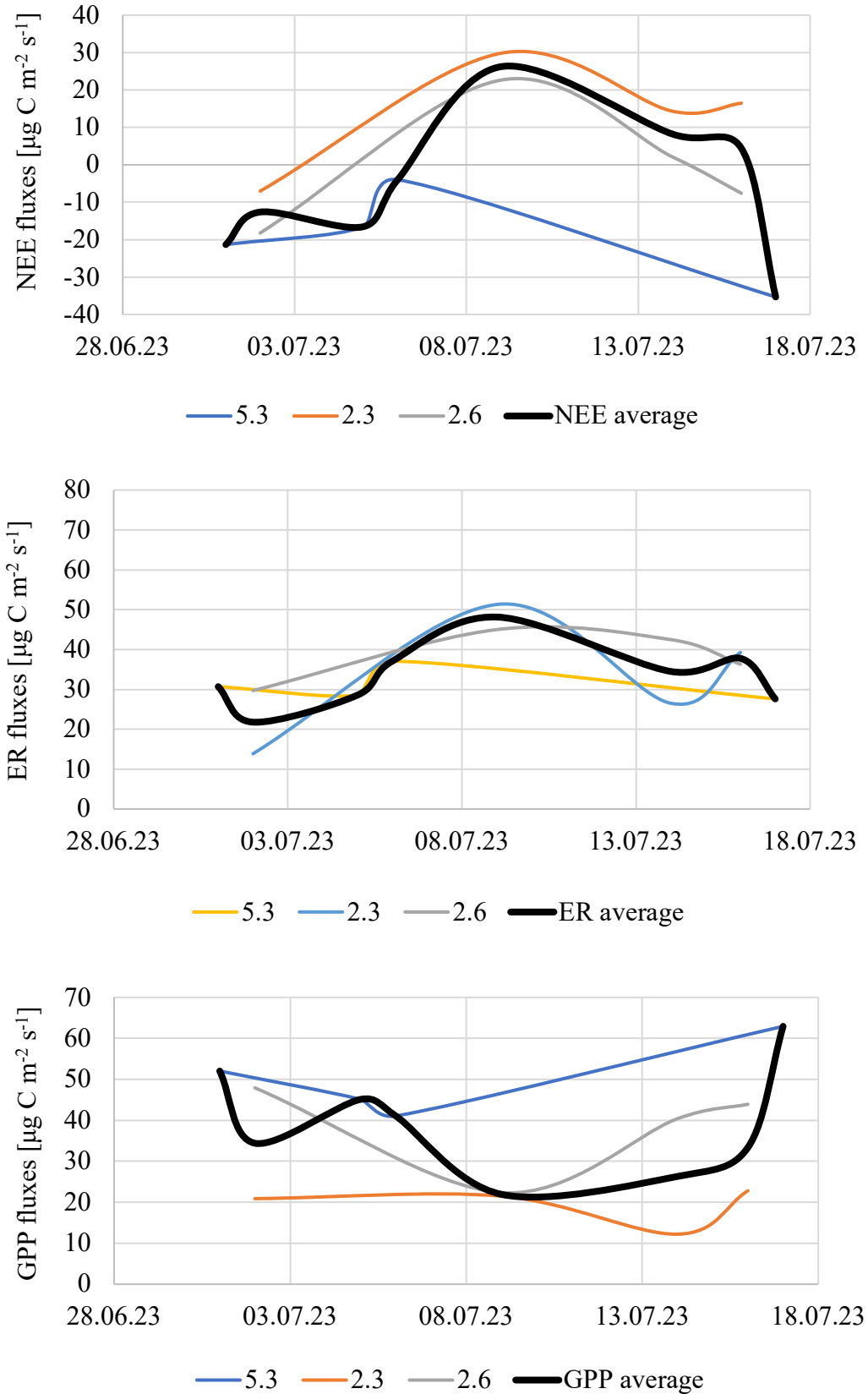
A 11: Statistical values of the linear model and the GAM model for soil moisture in 12 cm and 30 cm depth and NEE.

NEE	Soil Moisture, 12 cm [%]	Soil Moisture, 30 cm [%]
Group 1		
Linear model		
R^2	0.01	0.05
p-value < 0.05	3.5E-01	1.7E-01
p-value < 0.05 corrected	1.4E-01	7.0E-01
Significance	No	No
RMSE	30.01	31.09
MAE	23.97	23.01
GAM model		
R^2	0.48	**0.77**
p-value	3.5E-01	**2.0E-16**
RMSE	30.01	**11.06**
MAE	23.97	**8.63**
Group 2		
Linear model		
R^2	0.00	0.02
p-value < 0.05	8.6E-01	2.8E-01
p-value < 0.05 corrected	2.6E-02	8.6E-01
Significance	yes	No
RMSE	21.93	22.11
MAE	18.43	17.44
GAM model		
R^2	0.13	**0.01**
p-value	3.4E-01	**8.8E-02**
RMSE	21.64	**20.75**
MAE	18.40	**17.34**
Group 3		
Linear model		
R2	**0.17**	0.75
p-value < 0.05	**8.3E-03**	7.6E-12
p-value < 0.05 corrected	**3.4E-06**	1.7E-02
Significance	**Yes**	Yes
RMSE	**17.35**	15.40
MAE	**12.91**	9.93
GAM model		
R^2	**0.37**	0.76
p-value	**8.3E-03**	2.0E-16
RMSE	**17.35**	9.01
MAE	**12.91**	6.95

A 12: Statistical values of the linear model and the GAM model for soil moisture in 12 cm and 30 cm depth and ER.

ER	Soil Moisture, 12 cm [%]	Soil Moisture, 30 cm [%]
Group 1		
Linear model		
R^2	0.02	0.01
p-value < 0.05	2.8E-01	7.0E-01
p-value < 0.05 corrected	3.1E-02	2.8E-01
Significance	No	No
RMSE	21.73	22.21
MAE	15.31	14.50
GAM model		
R^2	-0.07	-0.02
p-value	3.2E-01	7.0E-01
RMSE	12.02	21.69
MAE	9.60	15.25
Group 2		
Linear model		
R^2	0.06	0.00
p-value < 0.05	1.2E-01	8.6E-01
p-value < 0.05 corrected	7.5E-01	1.2E-01
Significance	No	No
RMSE	13.14	13.62
MAE	10.96	10.10
GAM model		
R^2	0.07	-0.08
p-value	1.2E-01	8.6E-01
RMSE	13.14	12.63
MAE	10.96	8.96
Group 3		
Linear model		
R^2	0.09	0.21
p-value < 0.05	1.3E-01	2.9E-02
p-value < 0.05 corrected	6.6E-01	1.3E-01
Significance	No	No
RMSE	9.37	9.71
MAE	7.38	7.81
GAM model		
R^2	0.44	**0.01**
p-value	1.0E-01	**2.9E-02**
RMSE	8.81	**9.42**
MAE	7.25	**7.51**

A 13: Statistical values of the linear model and the GAM model for soil moisture in 12 and 30 cm depth and GPP.

GPP	Soil Moisture, 12 cm [%]	Soil Moisture, 30 cm [%]
Group 1		
Linear model		
R^2	0.00	0.00
p-value < 0.05	6.6E-01	6.6E-01
p-value < 0.05 corrected	1.8E-02	6.6E-01
Significance	No	No
RMSE	22.47	22.87
MAE	19.06	19.22
GAM model		
R^2	**0.06**	**0.32**
p-value	**5.1E-02**	**2.7E-04**
RMSE	**21.58**	**20.30**
MAE	**18.10**	**15.53**
Group 2		
Linear model		
R^2	0.01	0.03
p-value < 0.05	3.2E-01	2.0E-01
p-value < 0.05 corrected	2.1E-03	3.2E-01
Significance	Yes	No
RMSE	17.04	17.68
MAE	13.77	14.37
GAM model		
R^2	0.04	0.07
p-value	1.6E-01	1.1E-01
RMSE	16.91	14.15
MAE	13.48	12.35
Group 3		
Linear model		
R^2	**0.11**	**0.55**
p-value < 0.05	**4.4E-02**	**2.1E-07**
p-value < 0.05 corrected	**1.5E-09**	**8.8E-02**
Significance	**Yes**	**Yes**
RMSE	**14.62**	**12.17**
MAE	**12.70**	**10.12**
GAM model		
R^2	**0.08**	**0.55**
p-value	**4.4E-02**	**1.4E-06**
RMSE	**14.62**	**10.32**
MAE	**12.70**	**8.15**

A 14: Statistical values of the linear model and the GAM model for soil temperature (Tsoil) in 5, 10, 20 and 30 cm depth and NEE.

NEE	Tsoil, 5cm	Tsoil, 10 cm	Tsoil, 20 cm	Tsoil, 30 cm
Group 1				
Linear model				
R^2	0.01	0.03	**0.05**	0.08
p-value < 0.05	3.3E-01	1.2E-01	**3.9E-02**	6.9E-02
p-value < 0.05 corrected	1.0E+00	5.0E-01	**2.3E-01**	7.7E-02
Significance	No	No	Yes	No
RMSE	30.50	29.06	**29.86**	32.88
MAE	24.07	21.92	**22.40**	23.45
GAM model				
R^2	0.07	**0.33**	**0.11**	0.10
p-value	3.3E-01	**8.9E-03**	**3.9E-02**	8.0E-02
RMSE	30.06	**28.54**	**25.28**	17.58
MAE	23.85	**21.11**	**19.93**	15.42
Group 2				
Linear model				
R^2	0.01	0.21	**0.34**	**0.11**
p-value < 0.05	3.7E-01	6.3E-05	**1.1E-07**	**2.6E-02**
p-value < 0.05 corrected	5.7E-01	7.4E-01	**1.3E-04**	**2.3E-07**
Significance	No	no	Yes	Yes
RMSE	22.08	21.75	**18.74**	**24.75**
MAE	18.06	17.18	**15.22**	**19.13**
GAM model				
R^2	**0.08**	**0.05**	**0.06**	**0.10**
p-value	**1.9E-02**	**1.8E-04**	**1.7E-06**	**2.6E-02**
RMSE	**19.20**	**17.80**	**16.45**	**15.78**
MAE	**15.53**	**14.59**	**13.72**	**12.68**
Group 3				
Linear model				
R^2	**0.37**	**0.42**	**0.39**	**0.55**
p-value < 0.05	**1.25E-04**	**3.08E-05**	**8.03E-05**	**1.70E-06**
p-value < 0.05 corrected	**1.00E+00**	**2.49E-04**	**6.15E-05**	**1.61E-04**
Significance	Yes	Yes	Yes	Yes
RMSE	**17.71**	**18.98**	**18.73**	**19.91**
MAE	**14.84**	**15.17**	**15.60**	**16.89**
GAM model				
R^2	**0.41**	**0.51**	**0.69**	**0.57**
p-value	**2.7E-04**	**1.1E-04**	**1.7E-05**	**6.7E-06**
RMSE	**13.07**	**12.48**	**11.50**	**10.78**
MAE	**10.96**	**10.23**	**9.17**	**9.27**

A 15: Statistical values of the linear model and the GAM model for soil temperature (Tsoil) in 5, 10, 20 and 30 cm depth and ER.

ER	Tsoil, 5cm	Tsoil, 10 cm	Tsoil, 20 cm	Tsoil, 30 cm
Group 1				
Linear model				
R^2	0.01	0.01	0.03	**0.17**
p-value < 0.05	5.8E-01	4.3E-01	2.6E-01	**3.1E-02**
p-value < 0.05 corrected	2.5E-01	5.8E-01	4.3E-01	**2.6E-01**
Significance	No	No	No	**Yes**
RMSE	22.19	22.10	21.40	**23.67**
MAE	15.22	14.97	14.20	**16.60**
GAM model				
R^2	0.09	0.13	0.53	**0.44**
p-value	2.1E-01	4.3E-01	2.6E-01	**5.2E-02**
RMSE	21.66	22.42	15.61	**12.02**
MAE	14.89	16.15	11.54	**9.60**
Group 2				
Linear model				
R^2	0.02	0.07	0.04	0.00
p-value < 0.05	4.0E-01	9.7E-02	2.0E-01	7.5E-01
p-value < 0.05 corrected	6.7E-02	4.0E-01	9.7E-02	2.0E-01
Significance	No	No	No	No
RMSE	14.00	12.82	13.10	14.00
MAE	10.42	9.65	9.95	10.04
GAM model				
R^2	0.01	-0.08	-0.08	-0.08
p-value	4.0E-01	9.7E-02	2.8E-01	7.5E-01
RMSE	11.66	11.35	11.42	9.00
MAE	9.13	8.71	8.82	6.55
Group 3				
Linear model				
R^2	0.07	0.08	0.00	0.01
p-value < 0.05	1.99E-01	1.58E-01	8.49E-01	6.56E-01
p-value < 0.05 corrected	4.91E-01	1.99E-01	1.58E-01	8.49E-01
Significance	No	No	No	No
RMSE	9.61	9.43	9.81	9.98
MAE	7.47	7.37	7.88	7.96
GAM model				
R^2	-0.10	-0.11	0.18	0.00
p-value	2.0E-01	1.6E-01	4.5E-01	4.9E-01
RMSE	9.37	9.43	9.37	10.06
MAE	7.23	7.37	7.61	8.34

A 16: Statistical values of the linear model and the GAM model for soil temperature (Tsoil) in 5, 10, 20 and 30 cm depth and GPP.

GPP	Tsoil, 5cm	Tsoil, 10 cm	Tsoil, 20 cm	Tsoil, 30 cm
Group 1				
Linear model				
R^2	0.01	**0.06**	**0.14**	**0.14**
p-value < 0.05	3.5E-01	**2.7E-02**	**5.4E-04**	**1.8E-02**
p-value < 0.05 corrected	7.5E-02	**3.5E-01**	**2.7E-02**	**5.4E-04**
Significance	No	Yes	Yes	Yes
RMSE	22.63	**23.12**	22.35	**24.35**
MAE	19.18	**19.21**	18.76	**19.95**
GAM model				
R^2	0.01	**0.18**	**0.13**	**0.12**
p-value	4.5E-01	**1.8E-04**	**5.4E-04**	**1.8E-02**
RMSE	22.14	**20.00**	**21.03**	**23.23**
MAE	18.72	**14.49**	**17.51**	**19.02**
Group 2				
Linear model				
R^2	0.00	**0.13**	**0.30**	**0.19**
p-value < 0.05	7.5E-01	**2.1E-03**	**1.1E-06**	**2.1E-03**
p-value < 0.05 corrected	7.0E-04	**7.5E-01**	**2.1E-03**	**1.1E-06**
Significance	No	Yes	Yes	Yes
RMSE	17.47	**16.99**	**15.92**	**19.63**
MAE	14.03	**13.49**	**13.11**	**15.85**
GAM model				
R^2	**0.07**	**0.15**	**0.29**	**0.17**
p-value	**6.3E-02**	**3.5E-03**	**1.3E-06**	**2.1E-03**
RMSE	**16.94**	**16.17**	**14.90**	**13.05**
MAE	**13.48**	**12.85**	**12.47**	**10.76**
Group 3				
Linear model				
R^2	**0.40**	**0.49**	**0.56**	**0.73**
p-value < 0.05	**5.5E-05**	**4.2E-06**	**3.1E-07**	**7.5E-10**
p-value < 0.05 corrected	**4.0E-01**	**1.1E-04**	**8.3E-06**	**6.2E-07**
Significance	Yes	Yes	Yes	Yes
RMSE	**11.88**	**12.46**	**14.27**	**18.51**
MAE	**9.65**	**9.77**	**10.51**	**13.20**
GAM model				
R^2	**0.39**	**0.50**	**0.55**	**0.73**
p-value	**1.4E-04**	**1.9E-05**	**3.8E-07**	**2.0E-16**
RMSE	**11.75**	**10.56**	**10.11**	**8.06**
MAE	**9.58**	**8.78**	**8.01**	**6.64**

A 17: Statistical values of the linear model and the GAM model for pH, TD and NEE.

NEE	pH	TD
Group 1		
Linear model		
R^2	0.24	0.09
p-value < 0.05	5.0E-06	5.5E-03
p-value < 0.05 corrected	2.2E-02	1.0E-05
Significance	Yes	Yes
RMSE	29.37	31.13
MAE	20.84	25.22
GAM model		
R^2	0.79	0.17
p-value	2.7E-05	5.5E-03
RMSE	26.41	26.74
MAE	17.62	21.09
Group 2		
Linear model		
R^2	0.31	0.27
p-value < 0.05	2.2E-07	2.0E-06
p-value < 0.05 corrected	3.1E-05	2.2E-07
Significance	Yes	Yes
RMSE	18.25	18.79
MAE	13.53	14.64
GAM model		
R^2	0.38	0.19
p-value	2.0E-16	1.6E-05
RMSE	15.95	18.68
MAE	12.20	14.53
Group 3		
Linear model		
R^2	0.32	0.43
p-value < 0.05	1.8E-04	5.8E-06
p-value < 0.05 corrected	1.2E-01	3.2E-04
Significance	Yes	Yes
RMSE	15.76	14.41
MAE	13.73	11.66
GAM model		
R^2	0.39	0.62
p-value	5.5E-04	1.8E-05
RMSE	15.25	13.82
MAE	13.20	11.03

A 18: Statistical values of the linear model and the GAM model for pH, TD and ER.

ER	pH	TD
Group 1		
Linear model		
R^2	0.00	0.00
p-value < 0.05	7.3E-01	9.6E-01
p-value < 0.05 corrected	3.4E-01	7.3E-01
Significance	No	No
RMSE	21.89	21.95
MAE	14.61	14.90
GAM model		
R^2	0.10	0.65
p-value GAM	5.0E-01	7.7E-01
RMSE	21.68	22.14
MAE	14.10	15.21
Group 2		
Linear model		
R^2	0.00	0.02
p-value < 0.05	7.3E-01	3.7E-01
p-value < 0.05 corrected	3.4E-01	3.7E-02
Significance	No	No
RMSE	21.89	13.40
MAE	14.61	10.28
GAM model		
R^2	0.10	-0.08
p-value	5.0E-01	3.7E-01
RMSE	21.68	13.40
MAE	14.10	10.28
Group 3		
Linear model		
R^2	0.04	0.03
p-value < 0.05	3.1E-01	4.0E-01
p-value < 0.05 corrected	1.6E-01	6.3E-01
Significance	No	No
RMSE	9.62	10.09
MAE	7.54	7.98
GAM model		
R^2	0.04	-0.12
p-value	3.4E-01	4.0E-01
RMSE	9.28	9.86
MAE	7.36	7.71

A 19: Statistical values of the linear model and the GAM model for pH, TD and GPP.

GPP	pH	TD
Group 1		
Linear model		
R^2	0.23	0.17
p-value < 0.05	0.06	1.2E-05
p-value < 0.05 corrected	0.05	0.03
Significance	Yes	Yes
RMSE	22.85	20.55
MAE	19.39	17.45
GAM model		
R^2	0.42	0.17
p-value	2.0E-16	5E-04
RMSE	15.61	20.30
MAE	12.52	17.51
Group 2		
Linear model		
R^2	0.17	0.30
p-value < 0.05	2.9E-04	3.7E-07
p-value < 0.05 corrected	3.9E-06	2.9E-04
Significance	Yes	Yes
RMSE	15.92	14.59
MAE	12.35	11.76
GAM model		
R^2	0.15	0.29
p-value	2.9E-04	5.2E-07
RMSE	15.92	14.59
MAE	12.35	11.76
Group 3		
Linear model		
R^2	0.35	0.53
p-value < 0.05	8.3E-05	1.6E-07
p-value < 0.05 corrected	6.2E-03	8.3E-05
Significance	Yes	Yes
RMSE	12.50	10.60
MAE	10.89	7.56
GAM model		
R^2	0.52	0.53
p-value	1.1E-06	1.4E-06
RMSE	10.42	10.40
MAE	8.32	7.55

A 20: Statistical values of the linear model and the GAM model for NDVI and NEE.

NEE	NDVI
Group 1	
Linear model	
R^2	**0.07**
p-value < 0.05	**1.1E-02**
p-value < 0.05 corrected	**1.7E-01**
Significance	Yes
RMSE	**29.05**
MAE	**21.87**
GAM model	
R^2	**0.36**
p-value	**1.1E-02**
RMSE	**28.43**
MAE	**20.74**
Group 2	
Linear model	
R^2	0.21
p-value < 0.05	3.1E-05
p-value < 0.05 corrected	5.5E-01
Significance	No
RMSE	19.48
MAE	15.29
GAM model	
R^2	**0.58**
p-value	**2.0E-16**
RMSE	**17.13**
MAE	**12.99**
Group 3	
Linear model	
R^2	**0.25**
p-value < 0.05	**1.1E-03**
p-value < 0.05 corrected	**1.5E-11**
Significance	Yes
RMSE	**16.51**
MAE	**14.23**
GAM model	
R^2	**0.40**
p-value	**5.2E-05**
RMSE	14.36
MAE	11.98

A 21: Statistical values of the linear model and the GAM model for NDVI and ER.

ER	NDVI
Group 1	
Linear model	
R^2	0.02
p-value < 0.05	3.4E-01
p-value < 0.05 corrected	7.0E-01
Significance	No
RMSE	21.79
MAE	15.48
GAM model	
R^2	0.07
p-value	4.3E-01
RMSE	21.70
MAE	15.44
Group 2	
Linear model	
R^2	**0.01**
p-value < 0.05	**8.6E-01**
p-value < 0.05 corrected	**1.5E-03**
Significance	**yes**
RMSE	**13.49**
MAE	**10.43**
GAM model	
R^2	**0.19**
p-value	**4.9E-03**
RMSE	**11.74**
MAE	**9.13**
Group 3	
Linear model	
R^2	**0.08**
p-value < 0.05	**1.6E-01**
p-value < 0.05 corrected	**2.9E-02**
Significance	**yes**
RMSE	**9.44**
MAE	**7.50**
GAM model	
R^2	0.04
p-value	2.25E-01
RMSE	9.35
MAE	7.44

A 22: Statistical values of the linear model and the GAM model for NDVI and GPP.

GPP	NDVI
Group 1	
Linear model	
R^2	**0.06**
p-value < 0.05	**3.0E-02**
p-value < 0.05 corrected	**6.6E-01**
Significance	**Yes**
RMSE	**21.86**
MAE	**18.85**
GAM model	
R^2	**0.15**
p-value	**0.00**
RMSE	**20.49**
MAE	**17.69**
Group 2	
Linear model	
R^2	**0.25**
p-value < 0.05	**3.9E-06**
p-value < 0.05 corrected	**2.0E-01**
Significance	**Yes**
RMSE	**15.05**
MAE	**11.51**
GAM model	
R^2	**0.24**
p-value	**4E-06**
RMSE	**15.05**
MAE	**11.51**
Group 3	
Linear model	
R^2	**0.21**
p-value < 0.05	**3.1E-03**
p-value < 0.05 corrected	**4.3E-07**
Significance	**Yes**
RMSE	**13.71**
MAE	**11.86**
GAM model	
R^2	**0.64**
p-value	**2.0E-16**
RMSE	**9.02**
MAE	**7.07**

A 23: Statistical values of the linear model and the GAM model for air temperature, PAR and NEE.

NEE	Air temperature	PAR
Group 1		
Linear model		
R^2	0.00	0.00
p-value < 0.05	0.90	0.87
p-value < 0.05 corrected	1.00	1.00
Significance	No	No
RMSE	30.16	30.16
MAE	23.34	23.39
GAM model		
R^2	-0.01	0.13
p-value	0.90	0.87
RMSE	30.16	30.16
MAE	23.34	23.39
Group 2		
Linear model		
R^2	**0.01**	0.02
p-value < 0.05	**0.45**	0.29
p-value < 0.05 corrected	**0.00**	0.45
Significance	**yes**	No
RMSE	**21.87**	21.79
MAE	**18.36**	18.20
GAM model		
R^2	**0.08**	0.08
p-value	**0.03**	0.29
RMSE	**20.79**	21.79
MAE	**16.87**	18.20
Group 3		
Linear model		
R^2	0.01	0.00
p-value < 0.05	0.56	0.82
p-value < 0.05 corrected	0.63	1.00
Significance	No	No
RMSE	19.00	19.07
MAE	15.84	15.82
GAM model		
R^2	0.02	0.01
p-value	0.45	0.48
RMSE	18.50	18.54
MAE	15.64	15.31

A 24: Statistical values of the linear model and the GAM model for air temperature, PAR and ER.

ER	Air temperature	PAR
Group 1		
Linear model		
R^2	0.01	0.03
p-value < 0.05	0.57	0.25
p-value < 0.05 corrected	0.57	0.57
Significance	No	No
RMSE	21.91	21.70
MAE	14.63	14.88
GAM model		
R^2	0.01	-0.05
p-value	0.50	0.25
RMSE	21.56	21.70
MAE	14.72	14.88
Group 2		
Linear model		
R^2	0.10	0.08
p-value < 0.05	0.04	0.07
p-value < 0.05 corrected	0.52	0.08
Significance	no	No
RMSE	12.85	12.99
MAE	10.17	10.43
GAM model		
R^2	**0.08**	-0.01
p-value	**0.04**	0.07
RMSE	**12.84**	12.99
MAE	**10.16**	10.43
Group 3		
Linear model		
R^2	0.04	0.02
p-value < 0.05	0.35	0.49
p-value < 0.05 corrected	0.35	0.35
Significance	No	No
RMSE	9.65	9.73
MAE	7.84	7.77
GAM model		
R^2	0.01	0.46
p-value	0.46	0.61
RMSE	9.55	9.64
MAE	7.79	7.77

A 25: Statistical values of the linear model and the GAM model for air temperature, PAR and GPP.

GPP	Air temperature	PAR
Group 1		
Linear model		
R^2	0.01	0.04
p-value < 0.05	3.8E-01	7.5E-02
p-value < 0.05 corrected	6.4E-01	3.8E-01
Significance	No	No
RMSE	22.39	22.06
MAE	18.94	18.39
GAM model		
R^2	0.00	0.04
p-value	3.8E-01	1.3E-01
RMSE	22.39	21.90
MAE	18.94	18.30
Group 2		
Linear model		
R^2	0.02	**0.15**
p-value < 0.05	2.7E-01	**7.0E-04**
p-value < 0.05 corrected	8.5E-01	**2.7E-01**
Significance	No	**Yes**
RMSE	17.29	**16.10**
MAE	13.92	**12.48**
GAM model		
R^2	**0.07**	**0.13**
p-value	**5E-02**	**7E-04**
RMSE	**16.63**	**16.10**
MAE	**13.07**	**12.48**
Group 3		
Linear model		
R^2	0.04	0.02
p-value < 0.05	2.2E-01	4.0E-01
p-value < 0.05 corrected	6.4E-01	4.4E-01
Significance	No	No
RMSE	15.14	15.30
MAE	13.19	13.59
GAM model		
R^2	0.11	0.01
p-value	8.4E-02	4.8E-01
RMSE	14.26	15.05
MAE	12.62	13.57

A 26: Non-significant non-linear relations in all groups between soil moisture across all depths and CO₂ fluxes produced by the GAM model for the measuring period 2023. The plots are sorted by CO₂ fluxes in the respective groups.
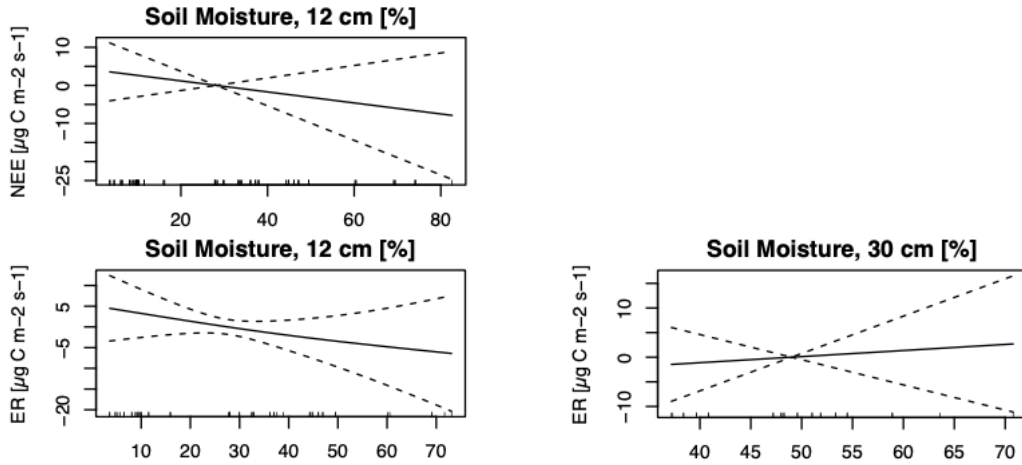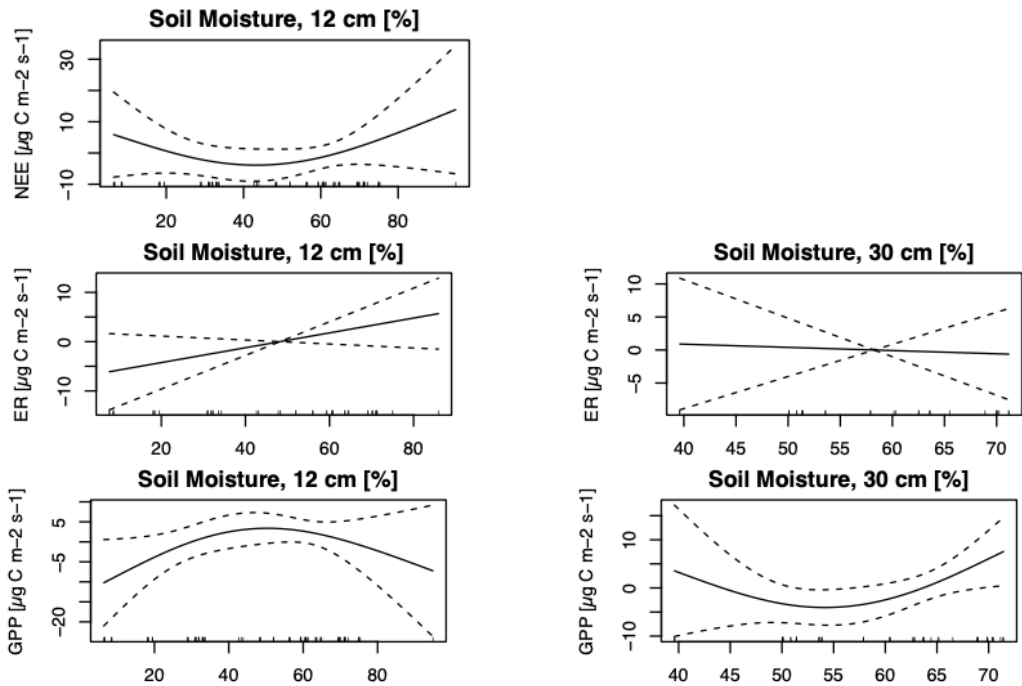
Group 1
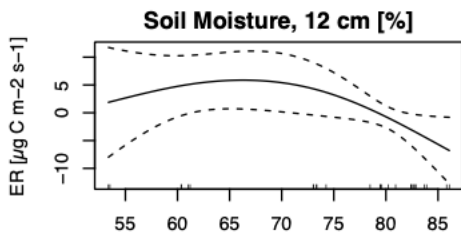
Group 2

Group 3

A 27: Non-significant non-linear relations in all groups between soil temperature across all depths and CO_2 fluxes produced by the GAM model for the measuring period 2023. The plots are sorted by CO_2 fluxes in the respective groups.
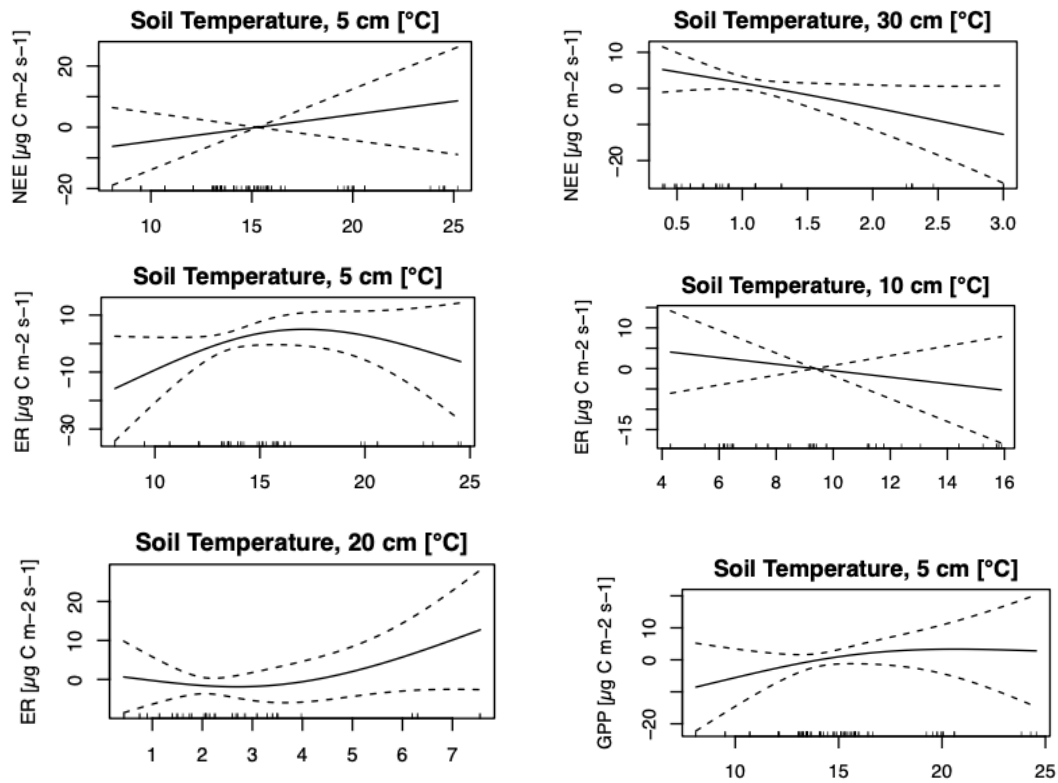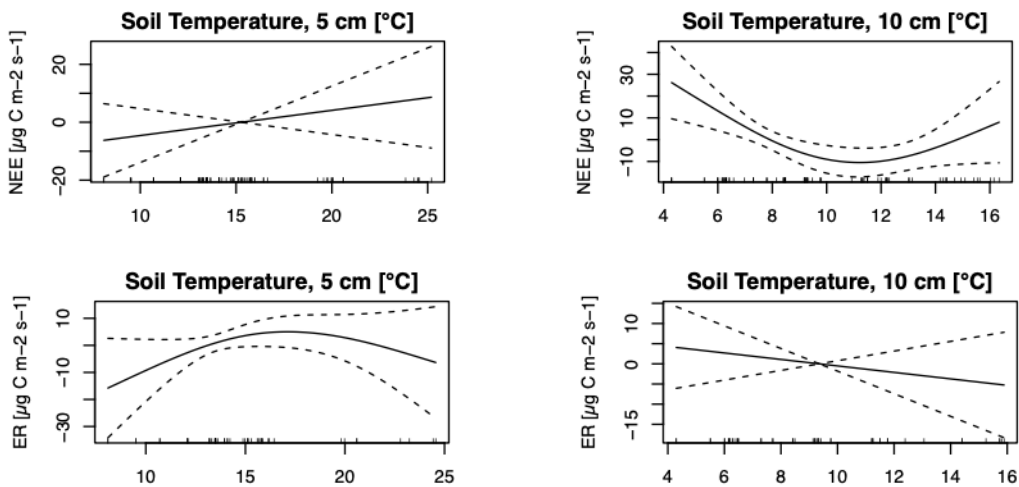
Group 1

Group 2

Continuing plot of A27: Non-significant non-linear relations in all groups between soil temperature across all depths and CO₂ fluxes produced by the GAM model for the measuring period 2023. The plots are sorted by CO₂ fluxes in the respective groups.
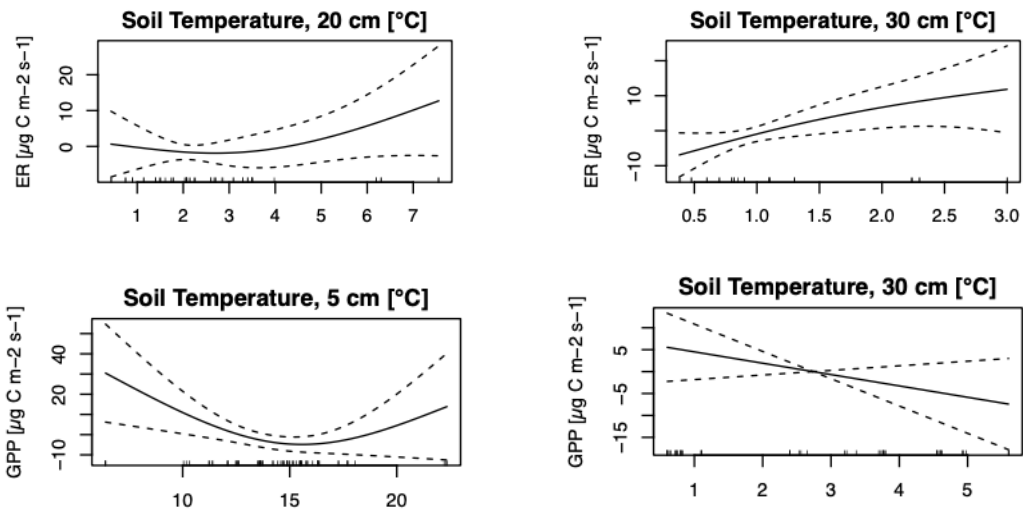
Group 3
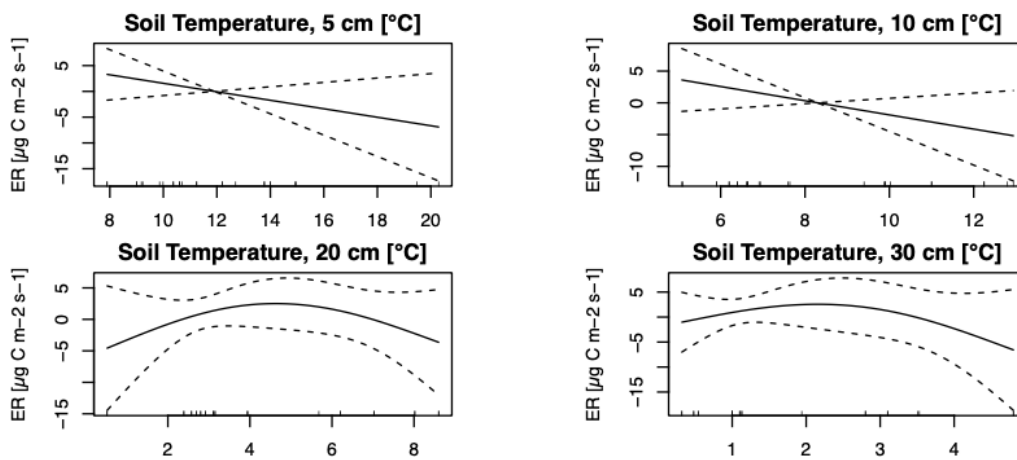
A 28: Non-significant non-linear relations in all groups between TD and CO$_2$ fluxes produced by the GAM model for the measuring period 2023. The plots are sorted by CO$_2$ fluxes in the respective groups.
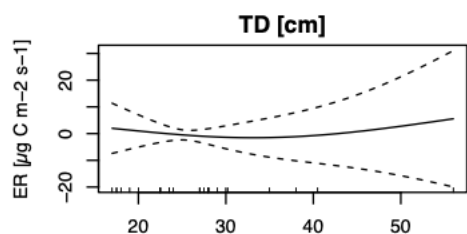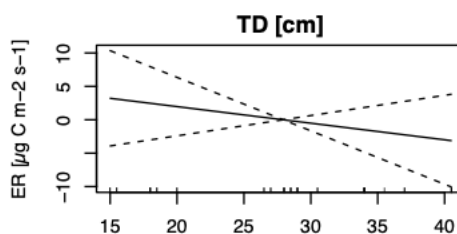
Group 1
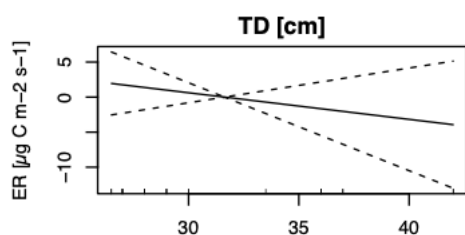
Group 2

Group 3

A 29: Non-significant non-linear relations in all groups between pH and ER flux produced by the GAM model for the measuring period 2023.

Group 1
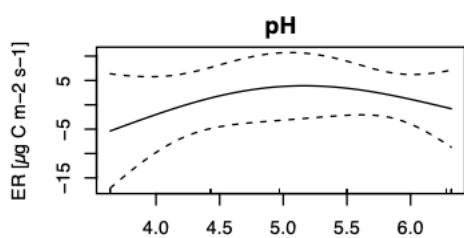
Group 2
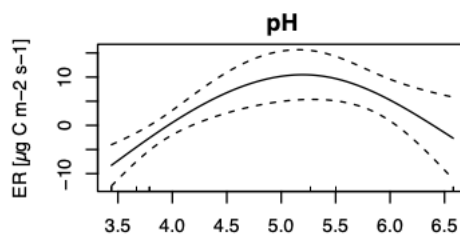
Group 3
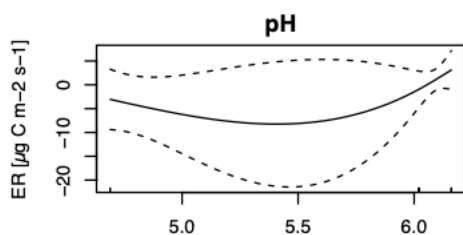
A 30: Non-significant non-linear relations in all groups between NDVI and CO_2 fluxes produced by the GAM model for the measuring period 2023.
The plots are sorted by CO2 fluxes in the respective groups.
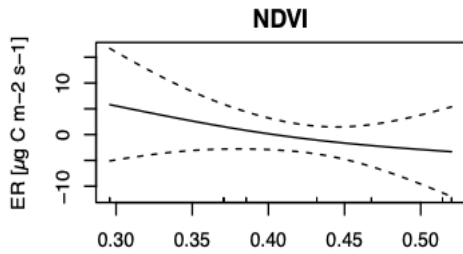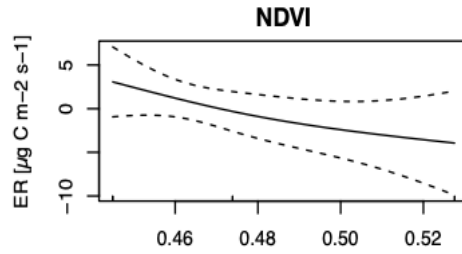
Group 1   Group 3

A 31: Non-significant non-linear relations in all groups between PAR and CO_2 fluxes produced by the GAM model for the measuring period 2023. The plots are sorted by CO2 fluxes (NEE, ER, GPP) in the respective groups.
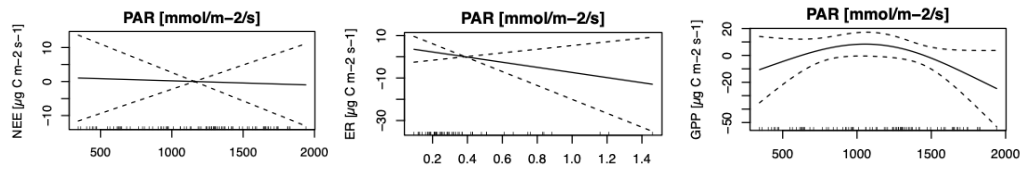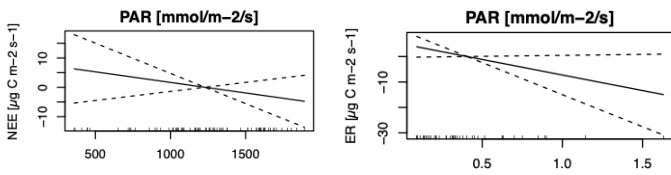
Group 1
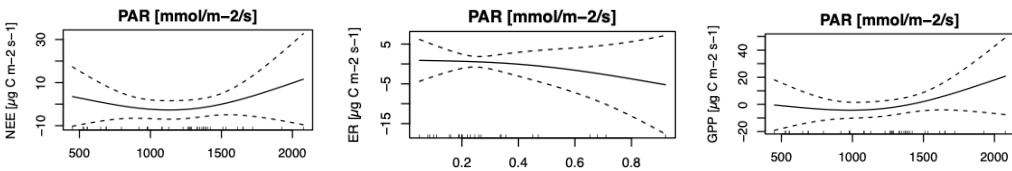
Group 2

Group 3

A 32: Non-significant non-linear relations in all groups between air temperature and CO₂ fluxes produced by the GAM model for the measuring period 2023. The plots are sorted by CO2 fluxes (NEE, ER, GPP) in the respective groups.
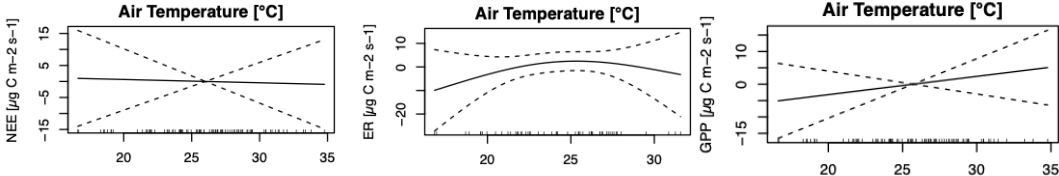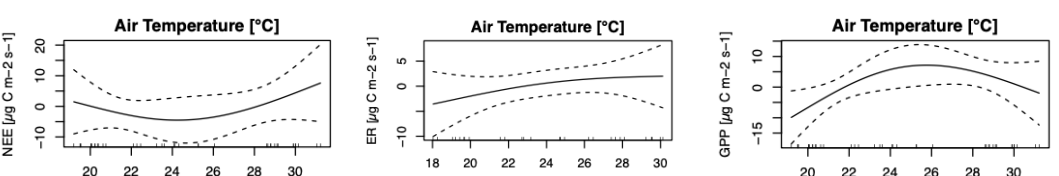
Group 1

Group 3

A 33: Linear regression plots with equation and corresponding p-value between NEE and soil moisture in 12 cm as well as 30 cm depth. The blue line represents the regression line and the dark grey area the confidence interval.
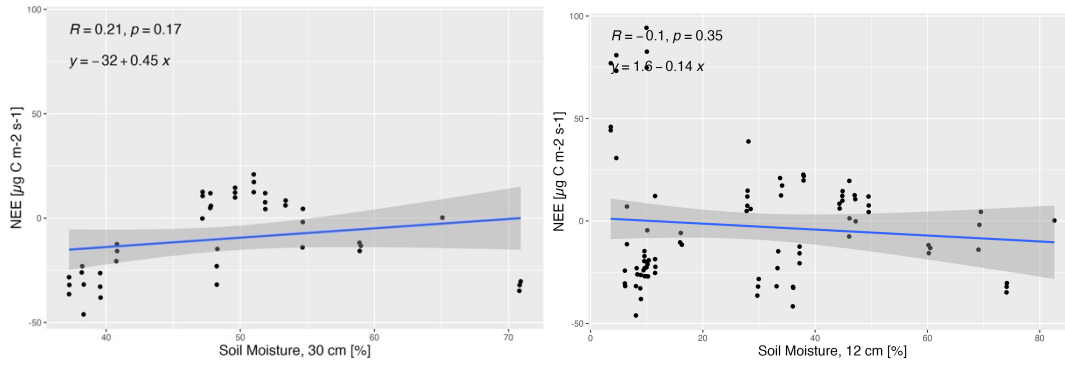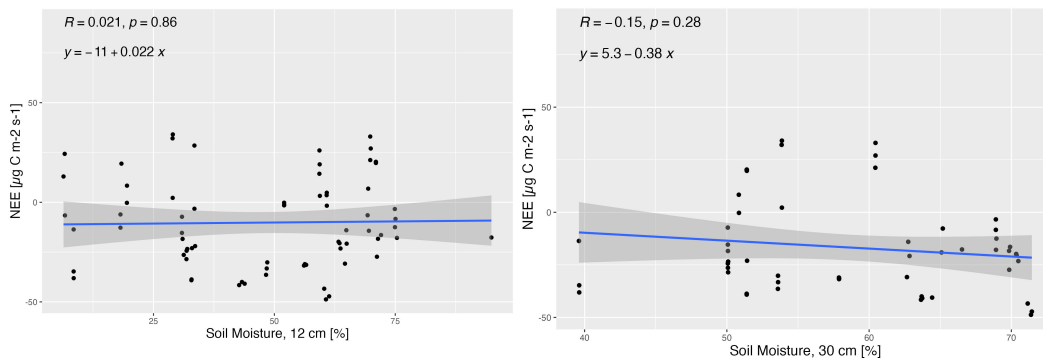
Group 1
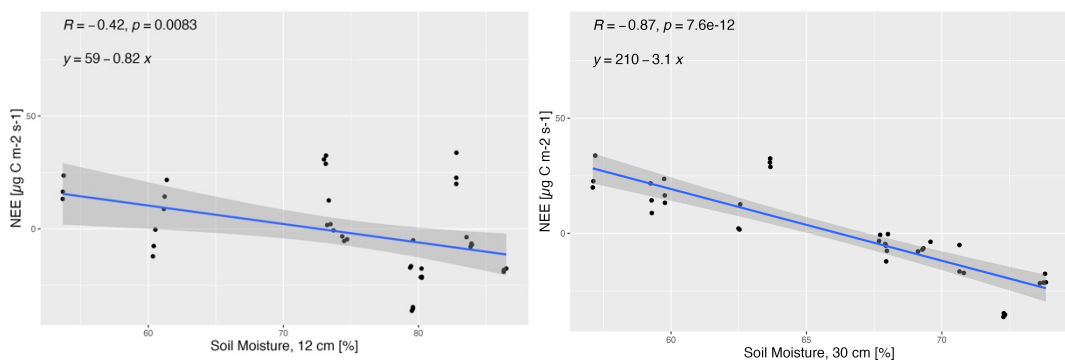
Group 2

Group 3

A 34: Linear regression plots with equation and corresponding p-value between ER and soil moisture in 12 cm as well as 30 cm depth. The blue line represents the regression line and the dark grey area the confidence interval.
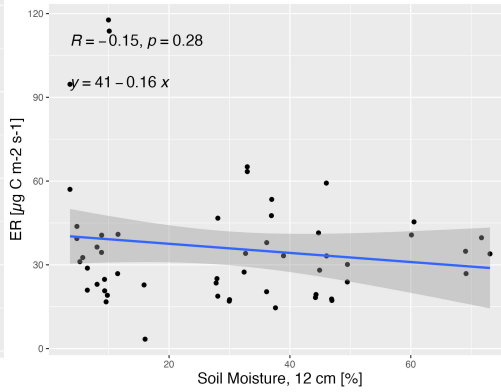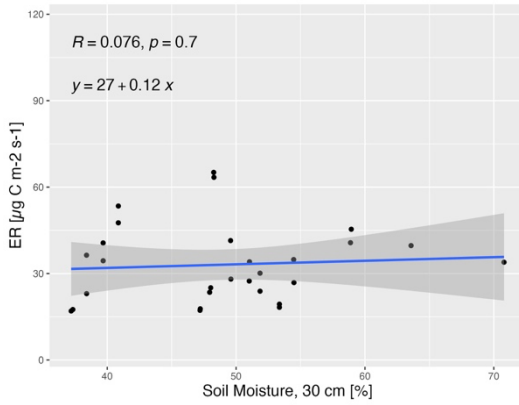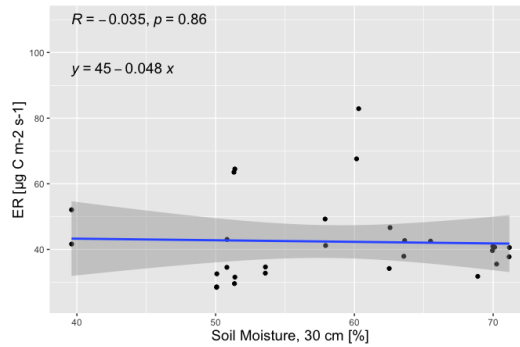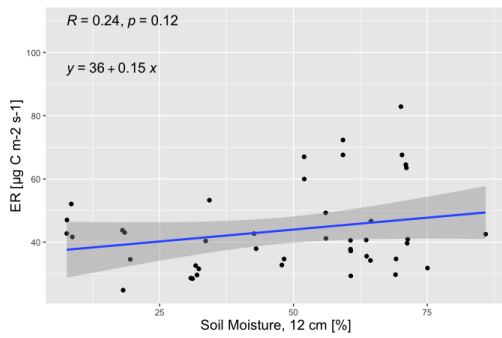
Group 1
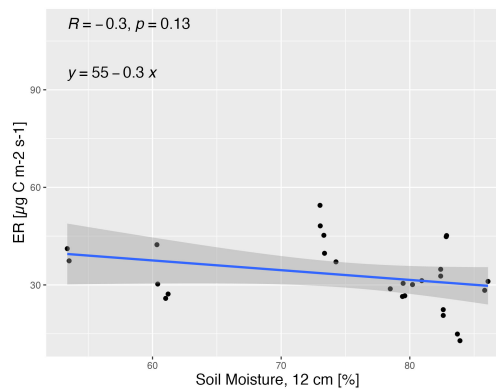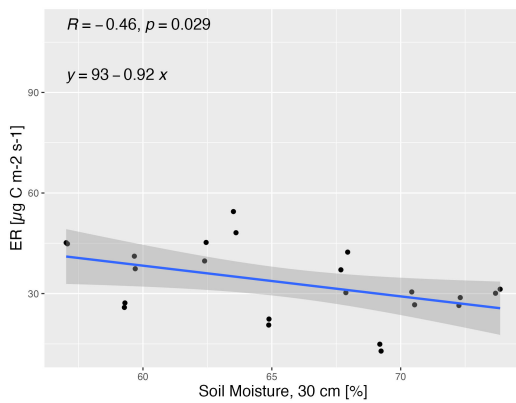
Group 2

Group 3

A 35: Linear regression plots with equation and corresponding p-value between GPP and soil moisture in 12 cm as well as 30 cm depth of the groups 1, 2 and 3. The blue line represents the regression line and the dark grey area the confidence interval.
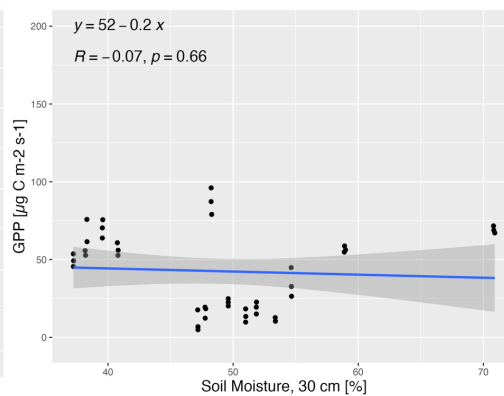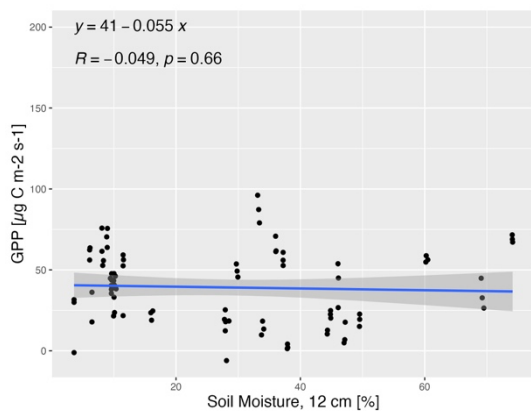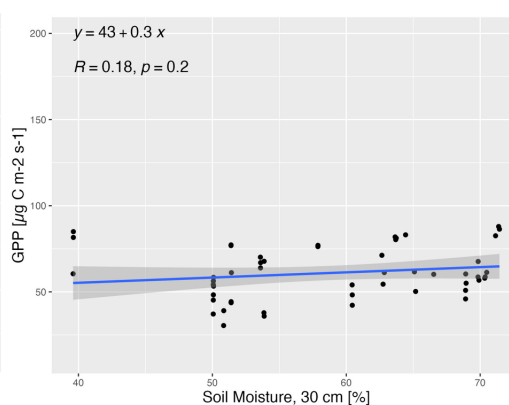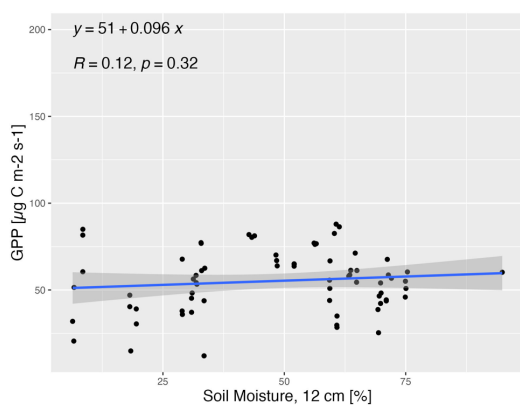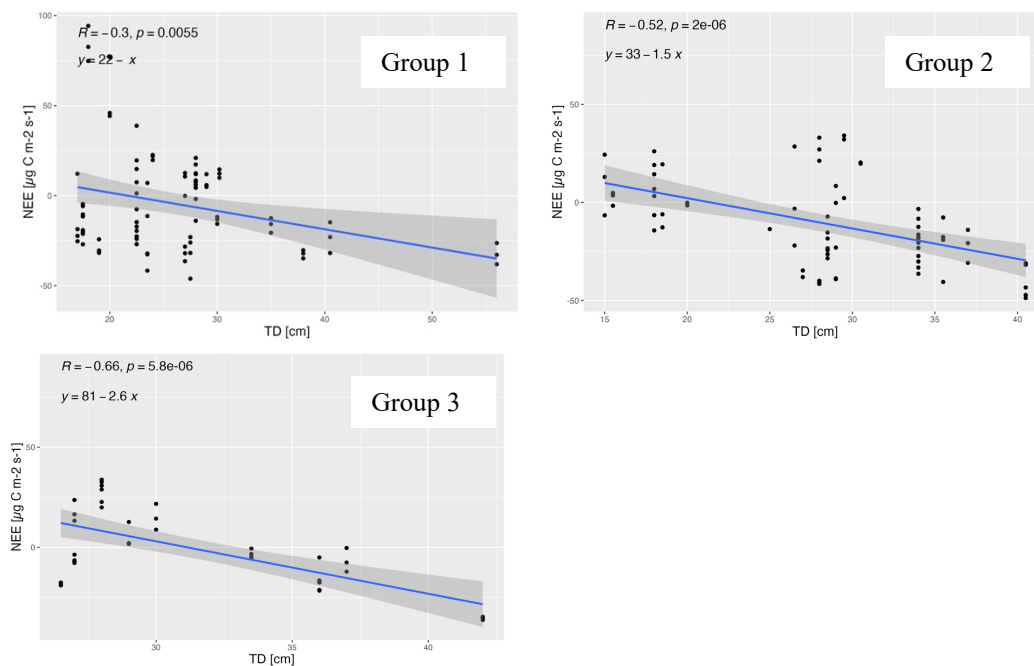
Group 1
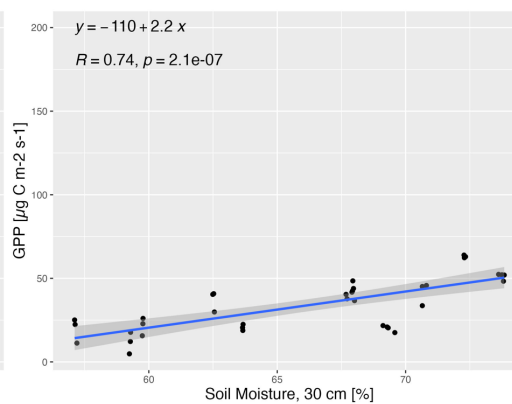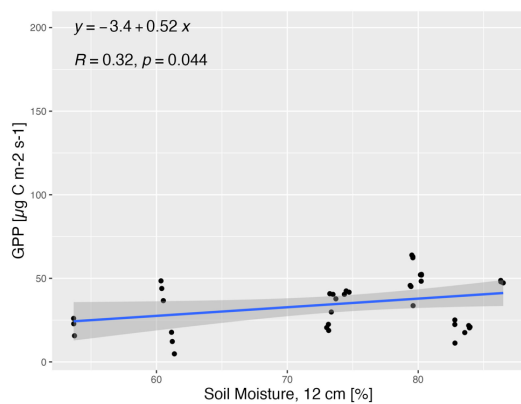
Group 2

Group 3

A 36: Linear regression plots with equation and corresponding p-value between NEE and soil temperature across all depths of Group 1. The blue line represents the regression line and the dark grey area the confidence interval.
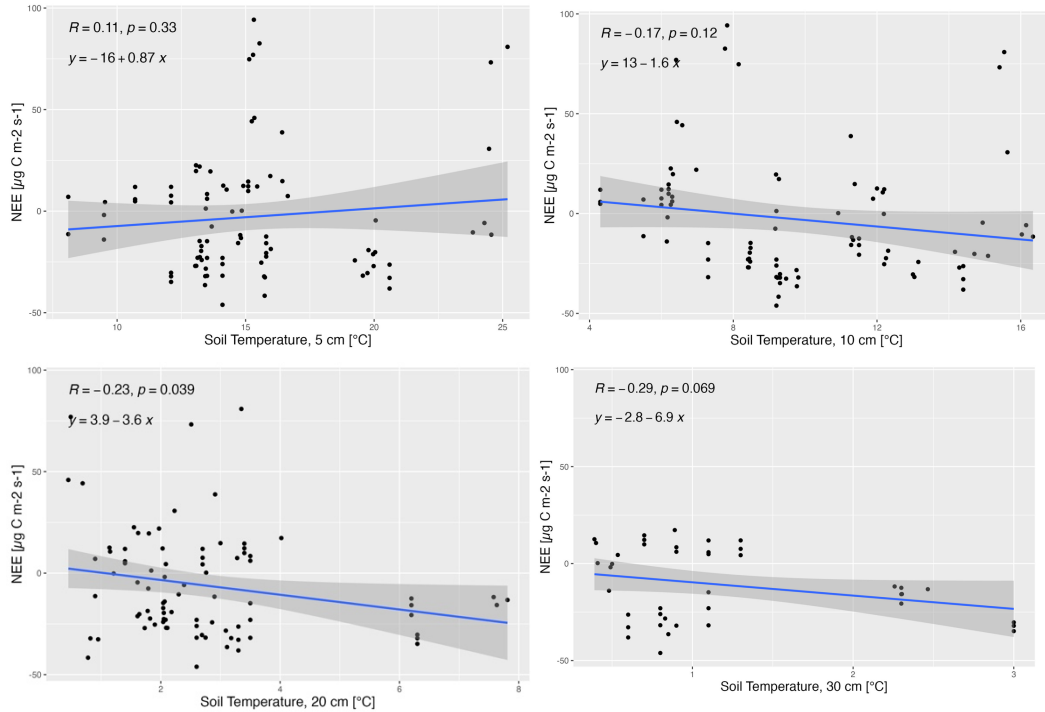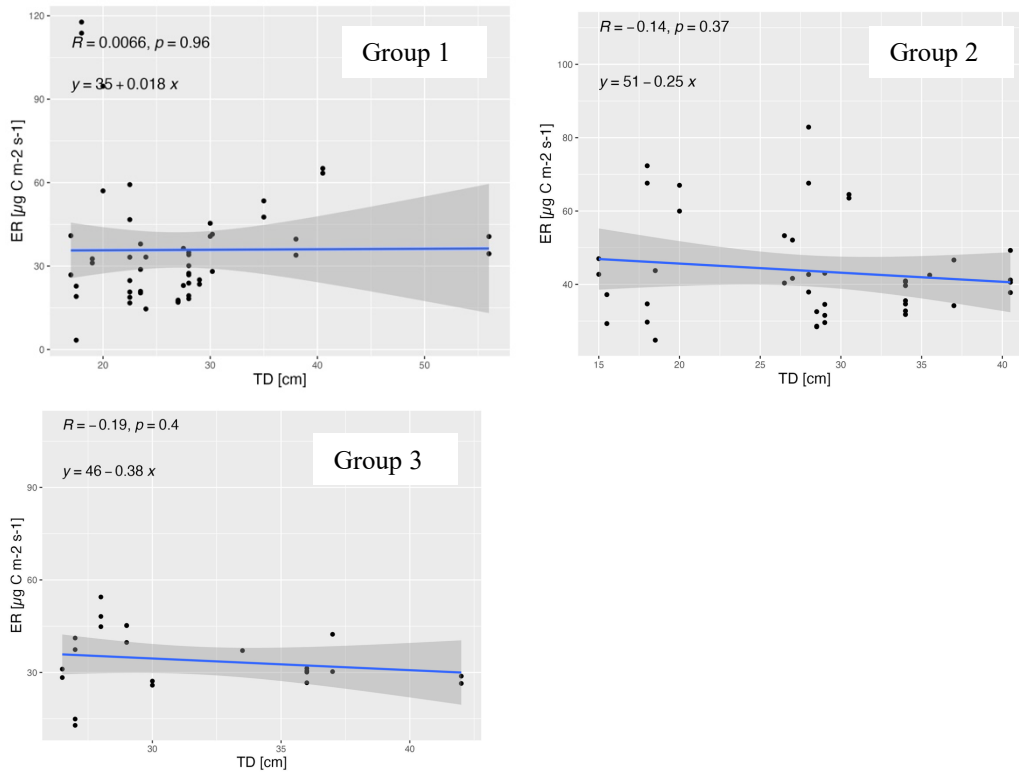

A 37: Linear regression plots with equation and corresponding p-value between NEE and soil temperature across all depths of Group 2. The blue line represents the regression line and the dark grey area the confidence interval.
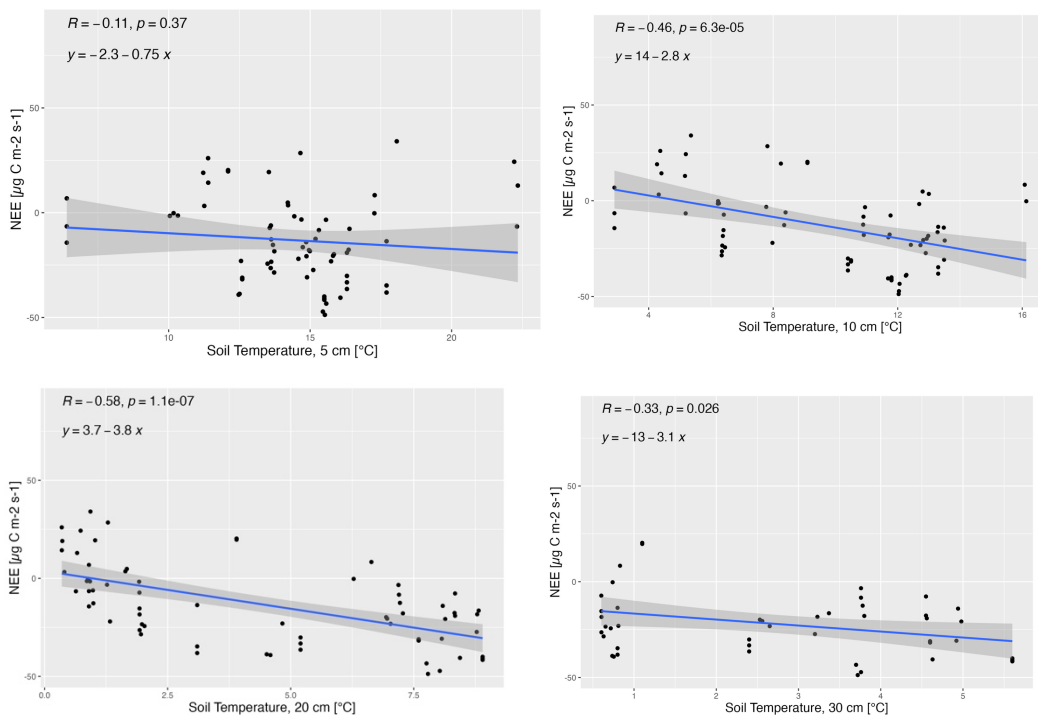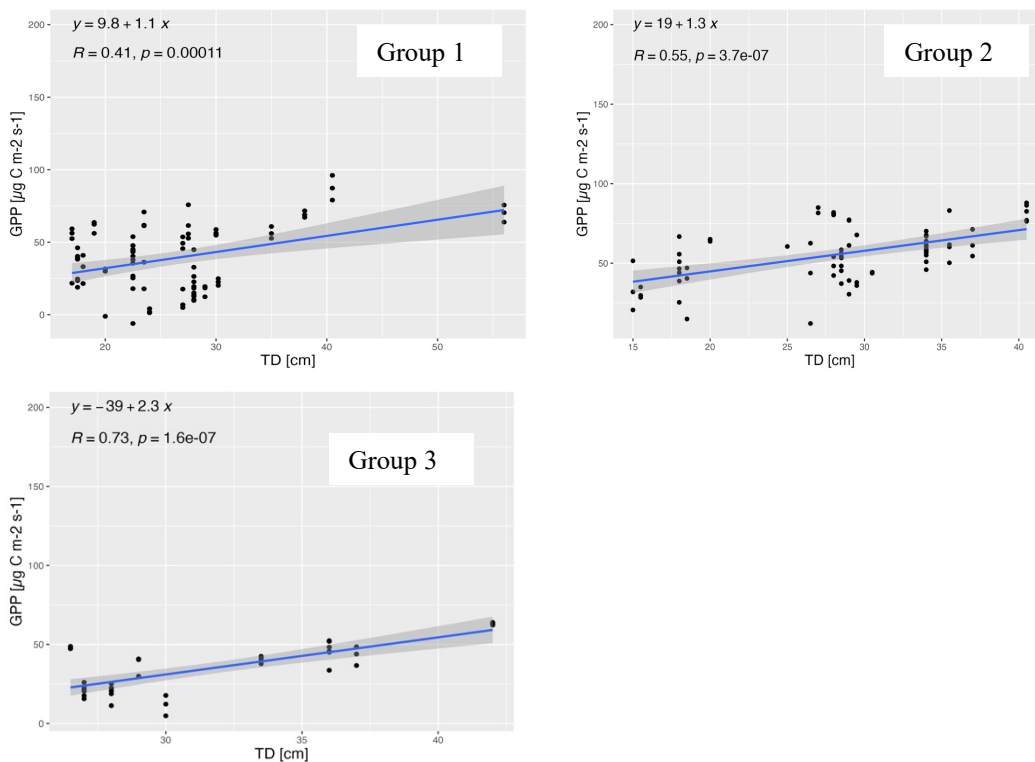
A 38: Linear regression plots with equation and corresponding p-value between NEE and soil temperature across all depths of Group 3. The blue line represents the regression line and the dark grey area the confidence interval.
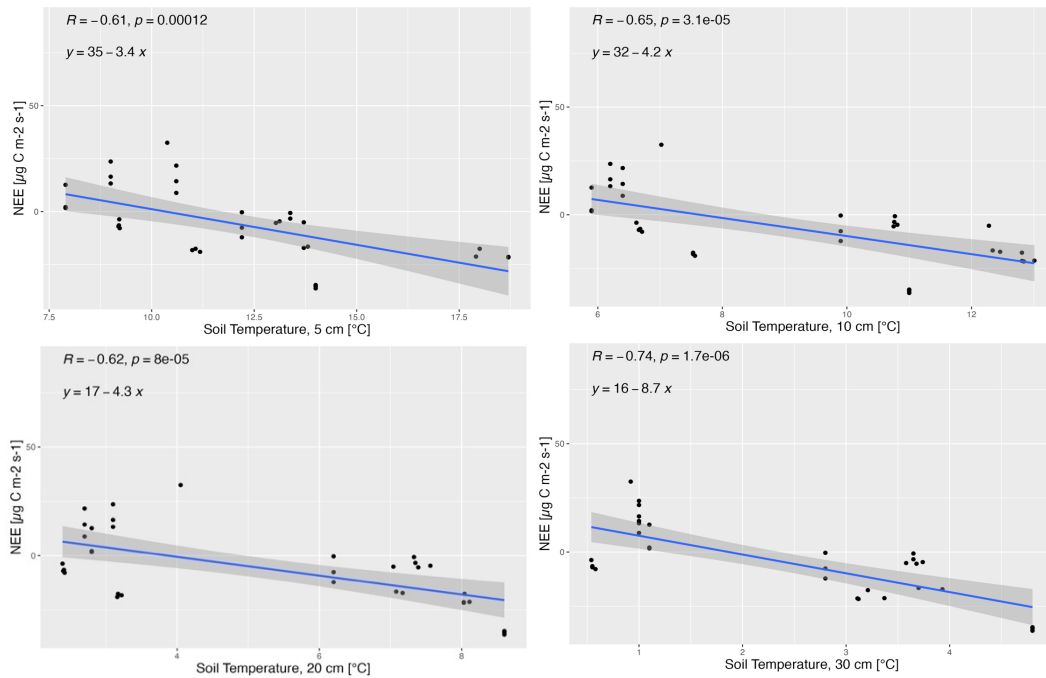
A 39: Linear regression plots with equation and corresponding p-value between ER and soil temperature across all depths of Group 1. The blue line represents the regression line and the dark grey area the confidence interval.
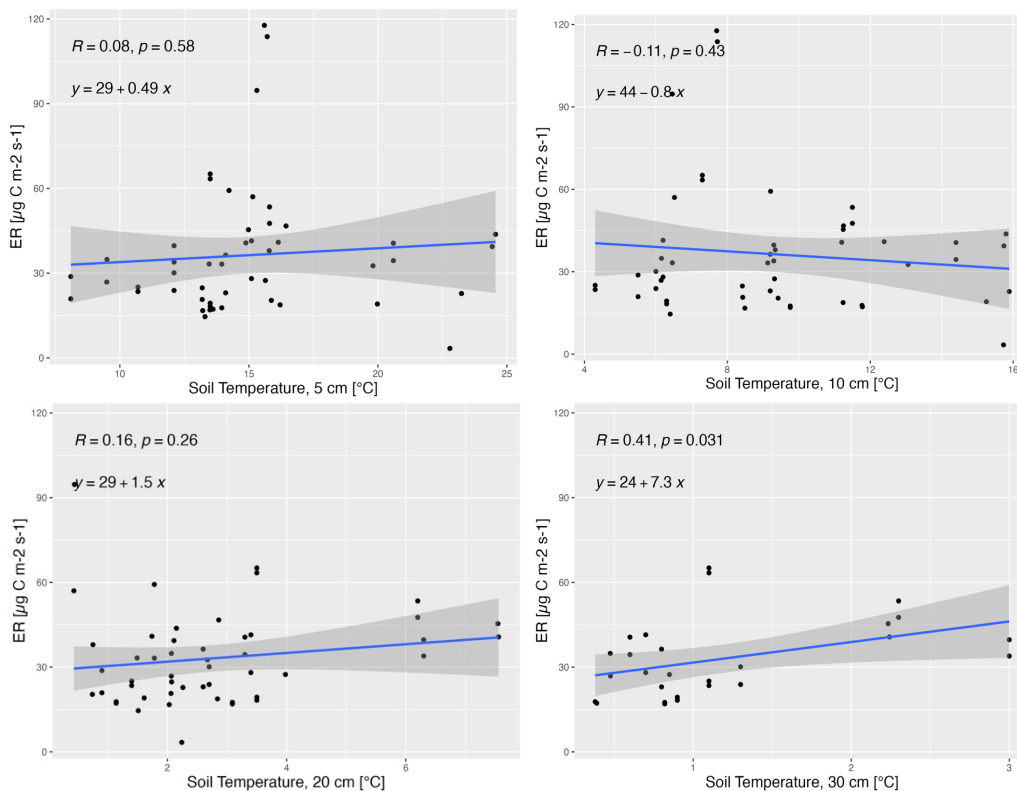
A 40: Linear regression plots with equation and corresponding p-value between ER and soil temperature across all depths of Group 2. The blue line represents the regression line and the dark grey area the confidence interval.
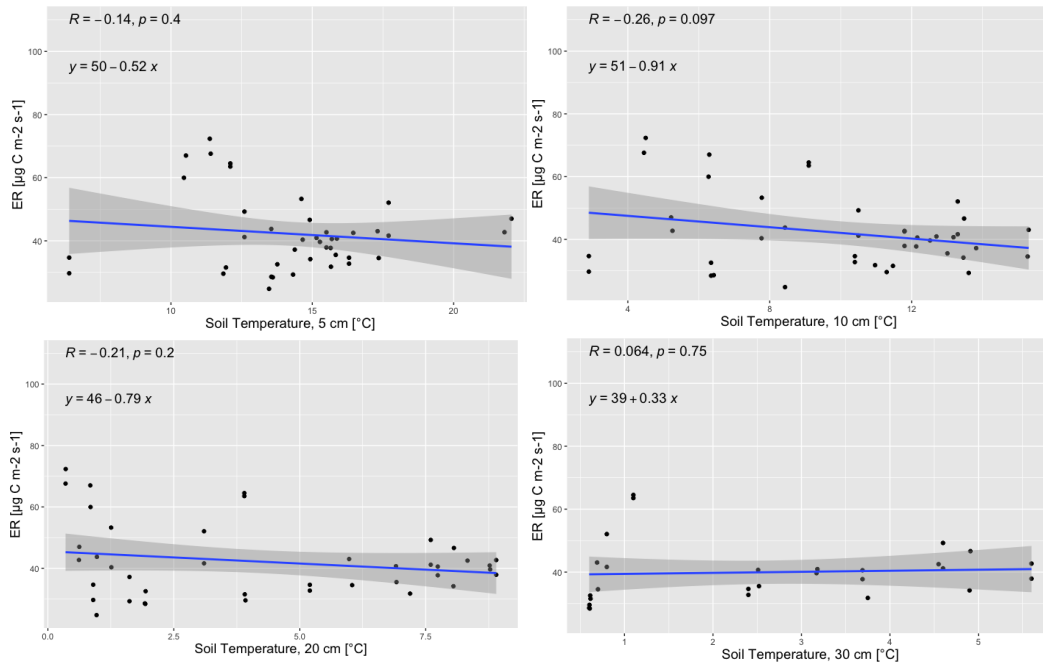
A 41: Linear regression plots with equation and corresponding p-value between ER and soil temperature across all depths of Group 3. The blue line represents the regression line and the dark grey area the confidence interval.
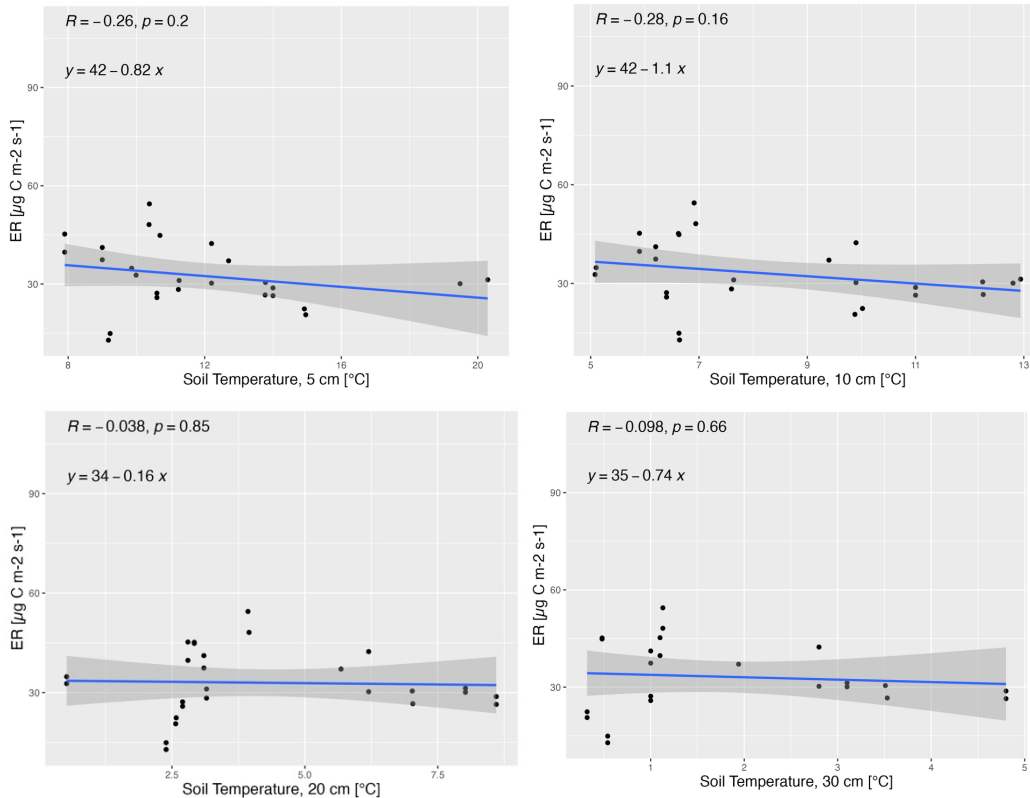
A 42: Linear regression plots with equation and corresponding p-value between GPP and soil temperature across all depths of Group 1. The blue line represents the regression line and the dark grey area the confidence interval**.**
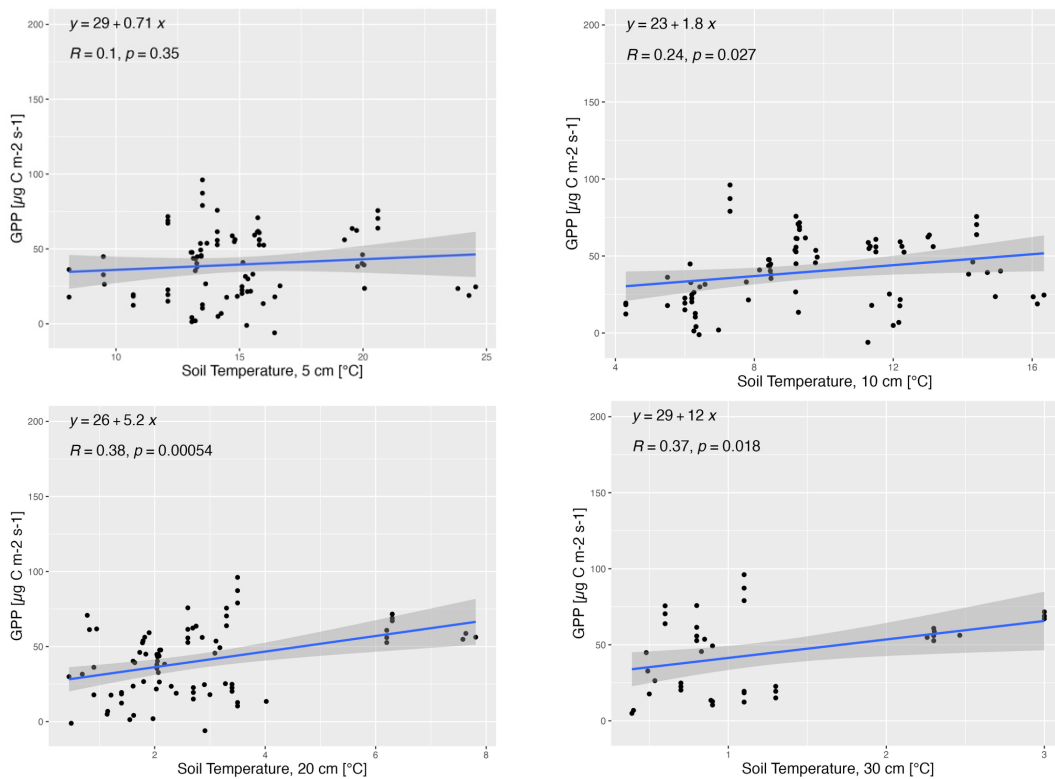
A 43: Linear regression plots with equation and corresponding p-value between GPP and soil temperature across all depths of Group 2. The blue line represents the regression line and the dark grey area the confidence interval.
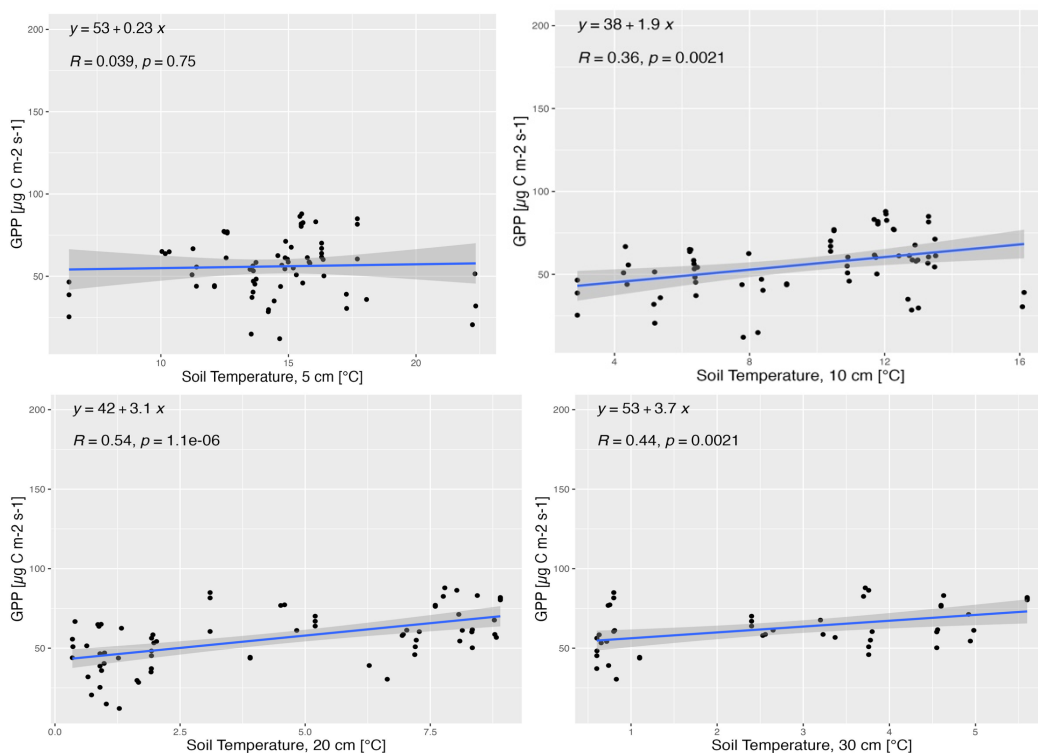
A 44: Linear regression plots with equation and corresponding p-value between GPP and soil temperature across all depths of Group 3. The blue line represents the regression line and the dark grey area the confidence interval.
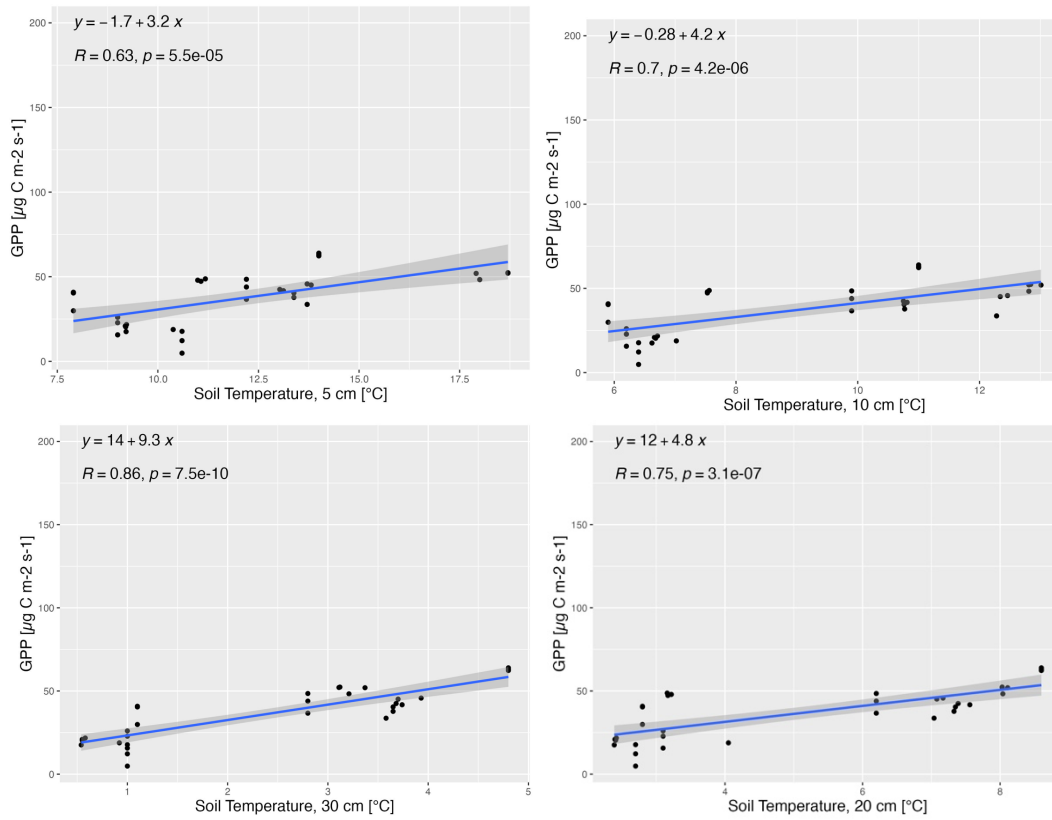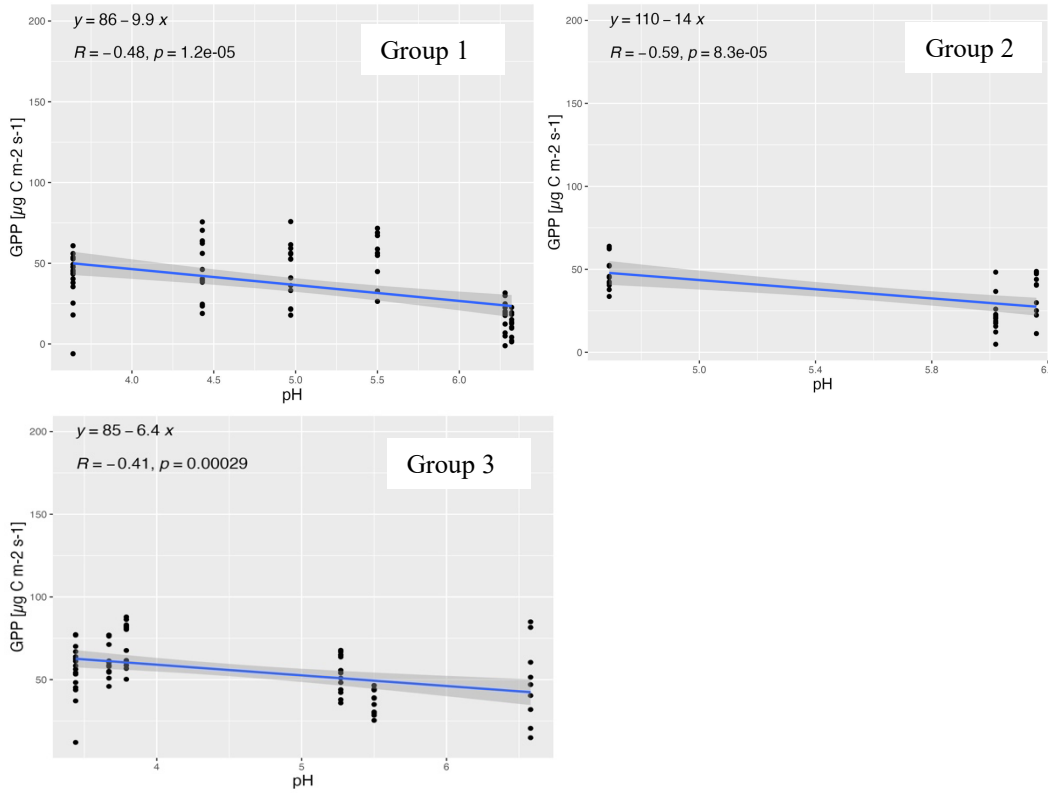

A 45: Linear regression plots with equation and corresponding p-value between NEE and TD of the groups 1, 2 and 3. The blue line represents the regression line and the dark grey area the confidence interval.
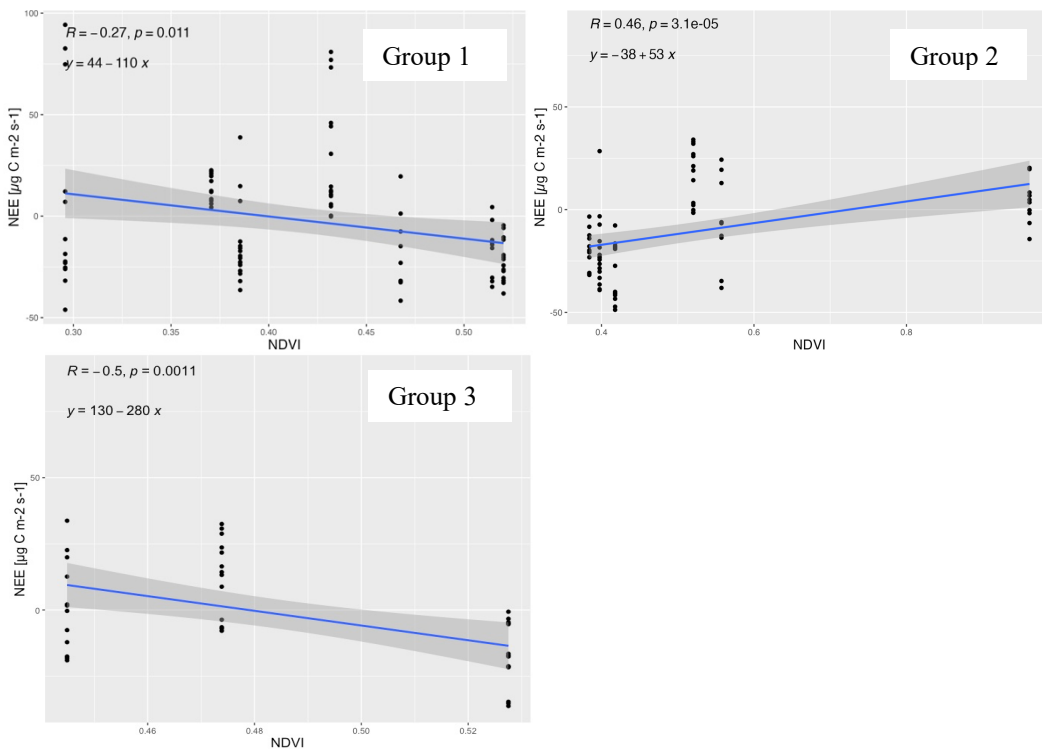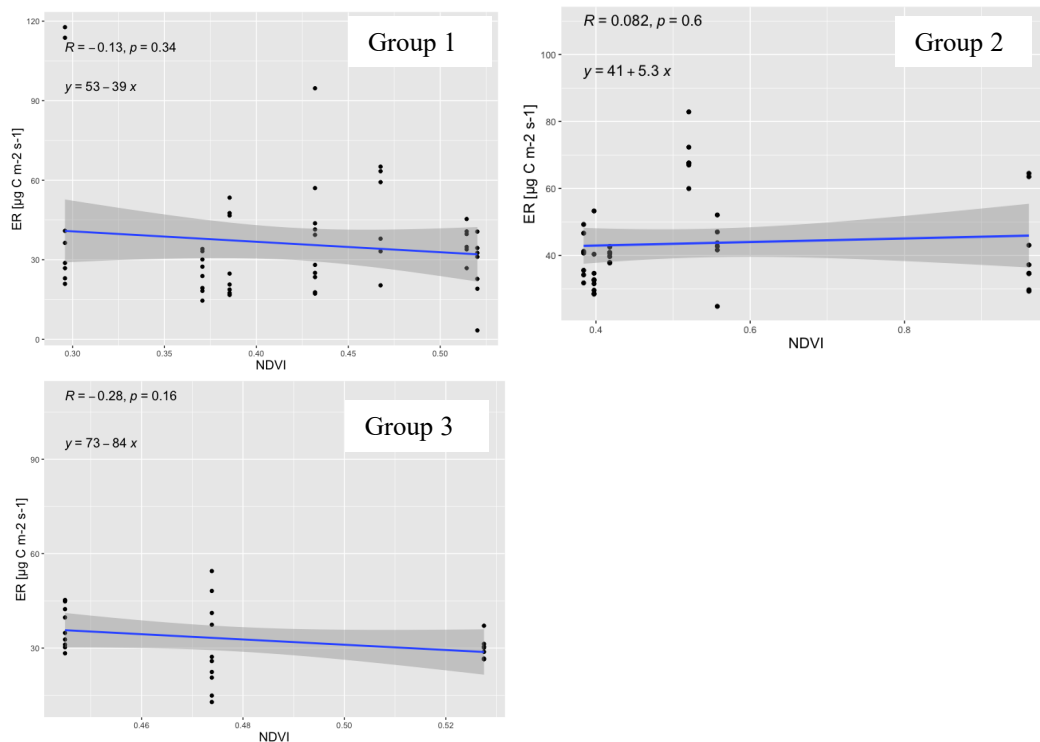
A 46: Linear regression plots with equation and corresponding p-value between ER and TD of the groups 1, 2 and 3. The blue line represents the regression line and the dark grey area the confidence interval.
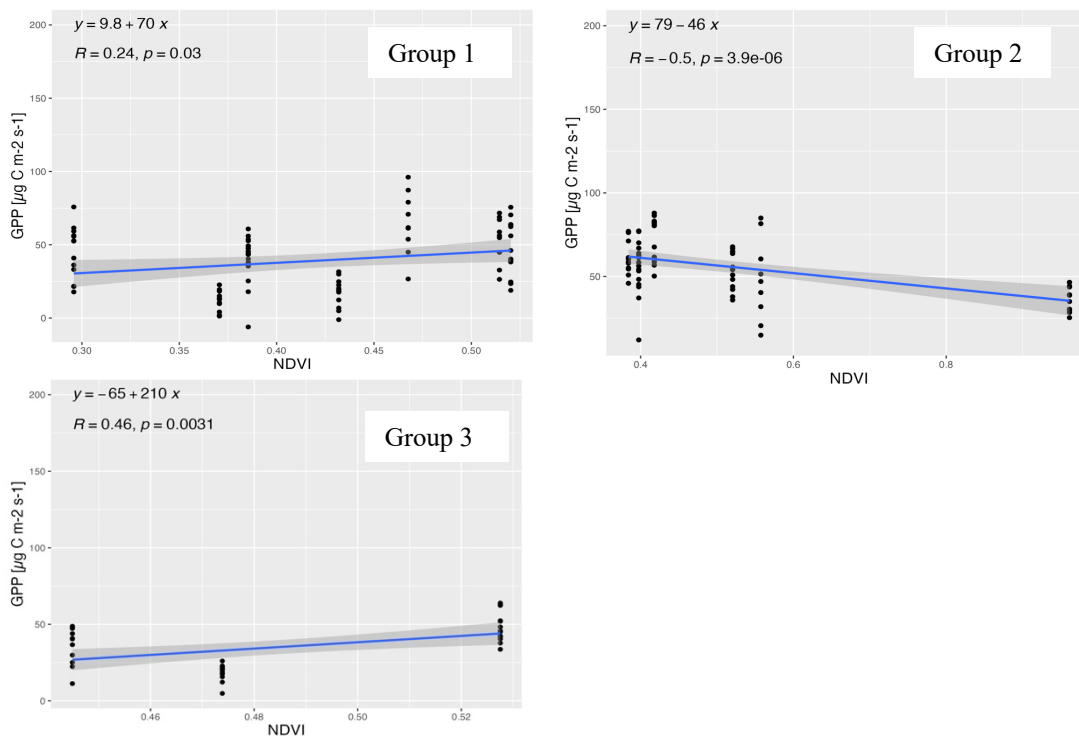

A 47: Linear regression plots with equation and corresponding p-value between GPP and TD of the groups 1, 2 and 3. The blue line represents the regression line and the dark grey area the confidence interval.

A 48: Linear regression plots with equation and corresponding p-value between NEE and pH of the groups 1, 2 and 3. The blue line represents the regression line and the dark grey area the confidence interval.
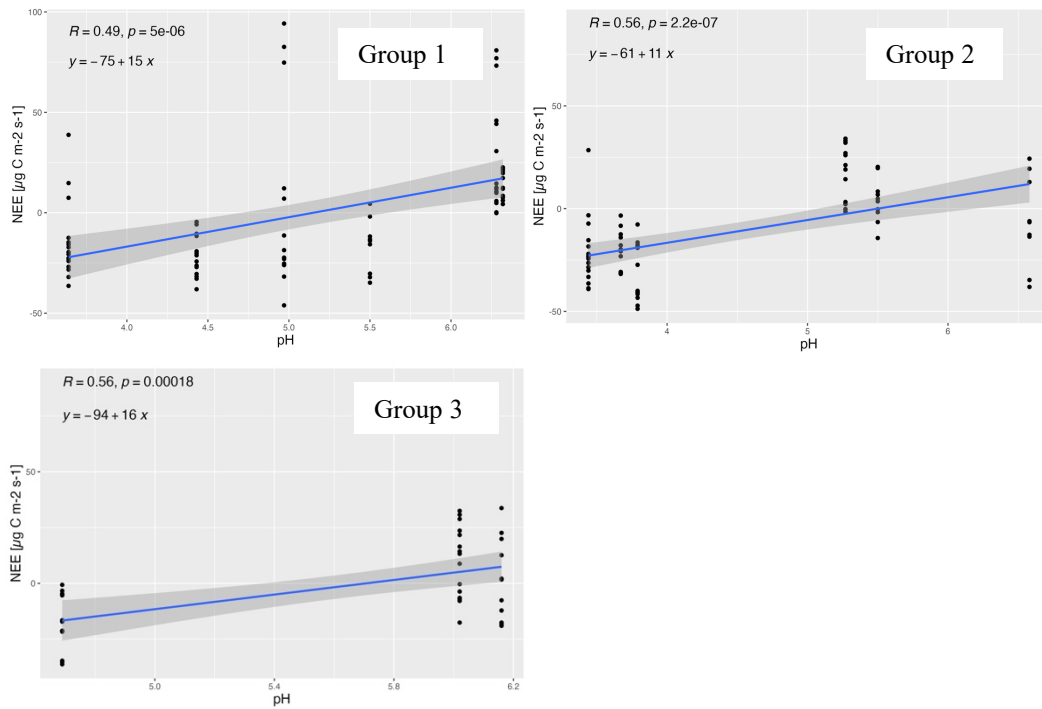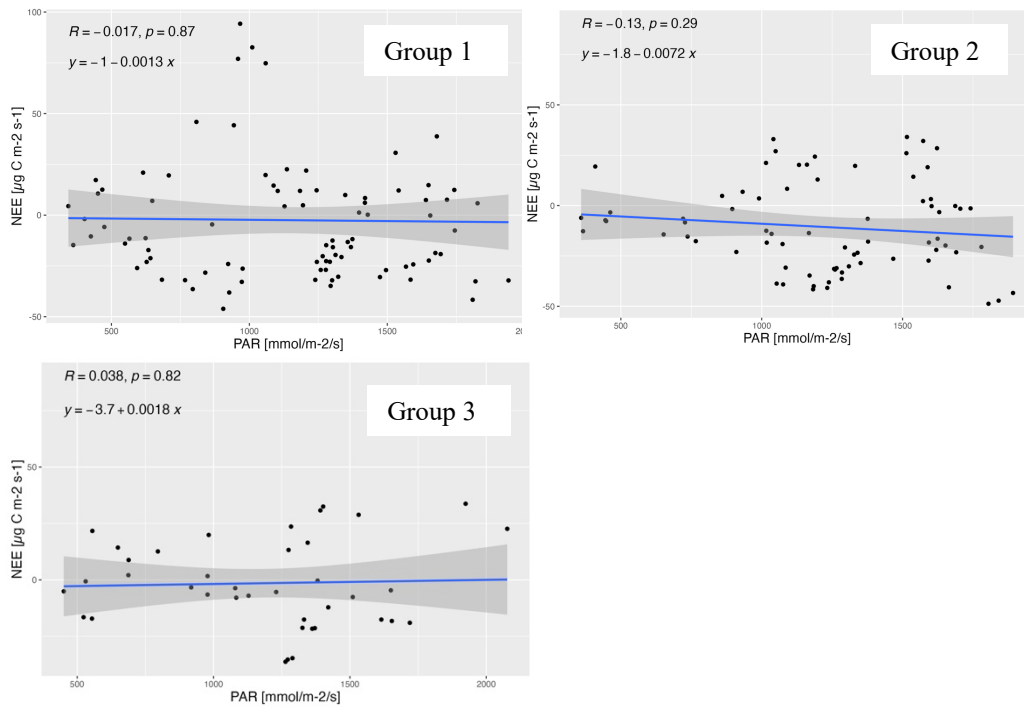

A 49: Linear regression plots with equation and corresponding p-value between ER and pH of the groups 1, 2 and 3. The blue line represents the regression line and the dark grey area the confidence interval.
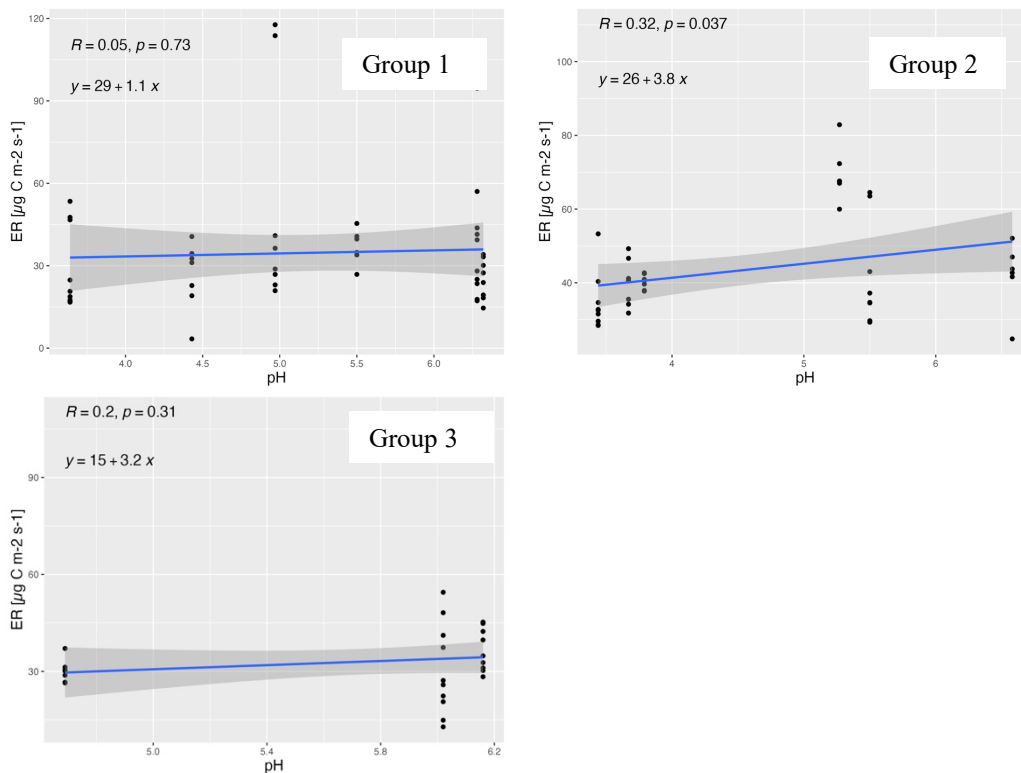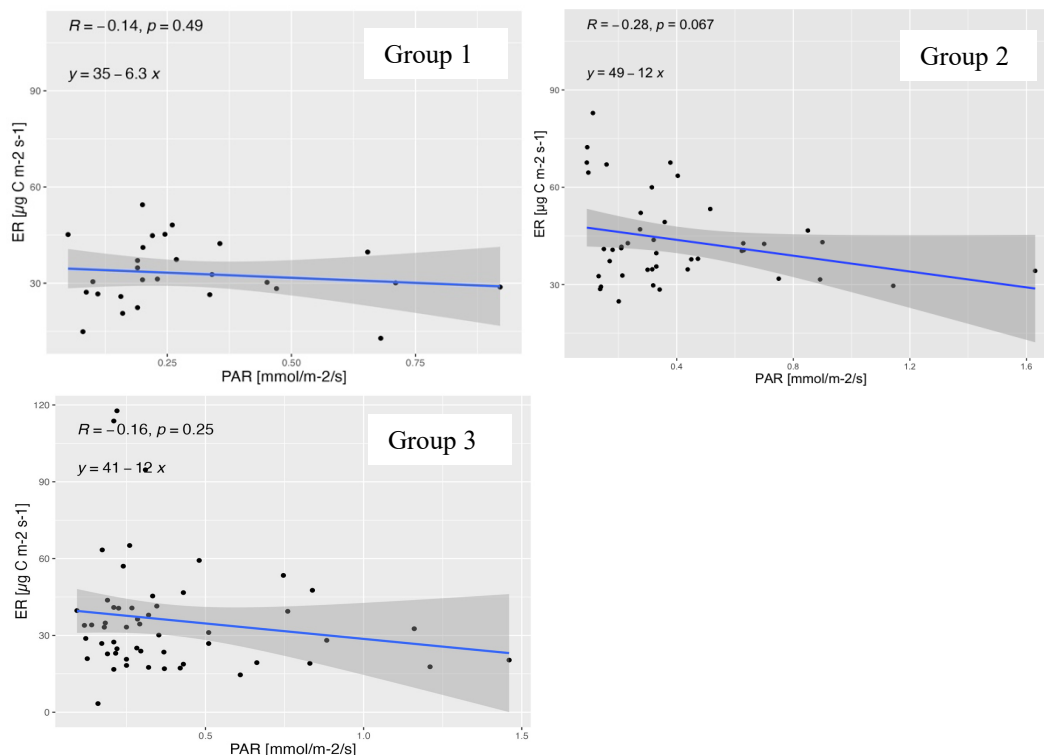
A 50: Linear regression plots with equation and corresponding p-value between GPP and pH of the groups 1, 2 and 3. The blue line represents the regression line and the dark grey area the confidence interval.

A 51: Linear regression plots with equation and corresponding p-value between NEE and NDVI of the groups 1, 2 and 3. The blue line represents the regression line and the dark grey area the confidence interval.
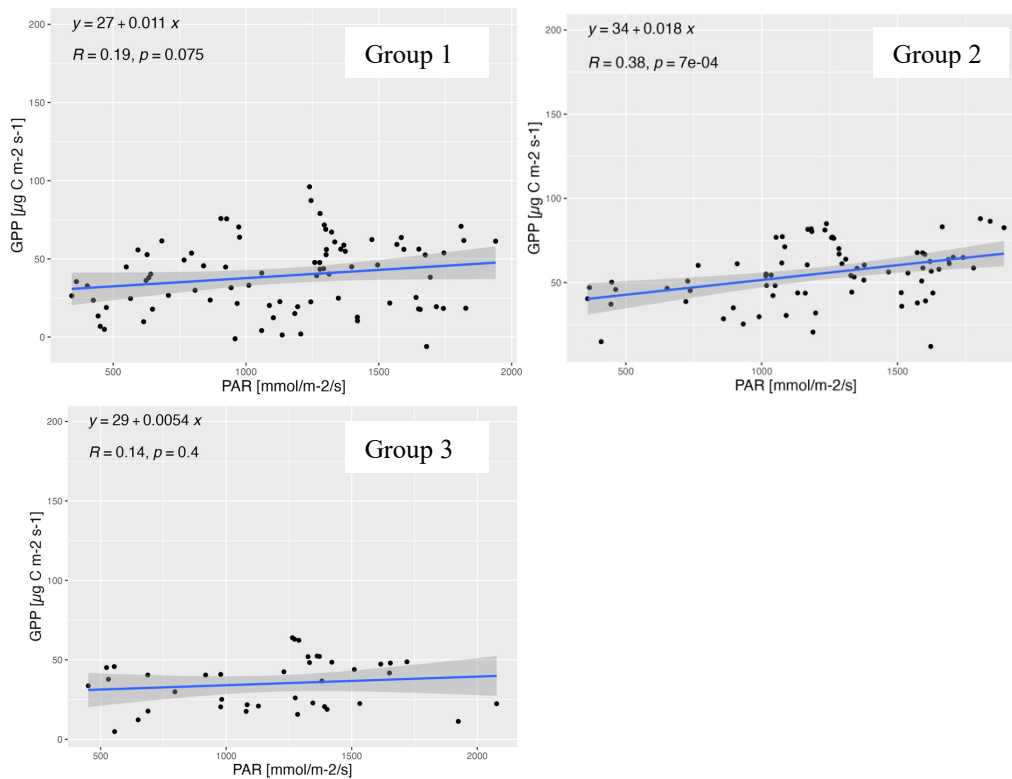
A 52: Linear regression plots with equation and corresponding p-value between ER and NDVI of the groups 1, 2 and 3. The blue line represents the regression line and the dark grey area the confidence interval.

A 53: Linear regression plots with equation and corresponding p-value between GPP and NDVI of the groups 1, 2 and 3. The blue line represents the regression line and the dark grey area the confidence interval.
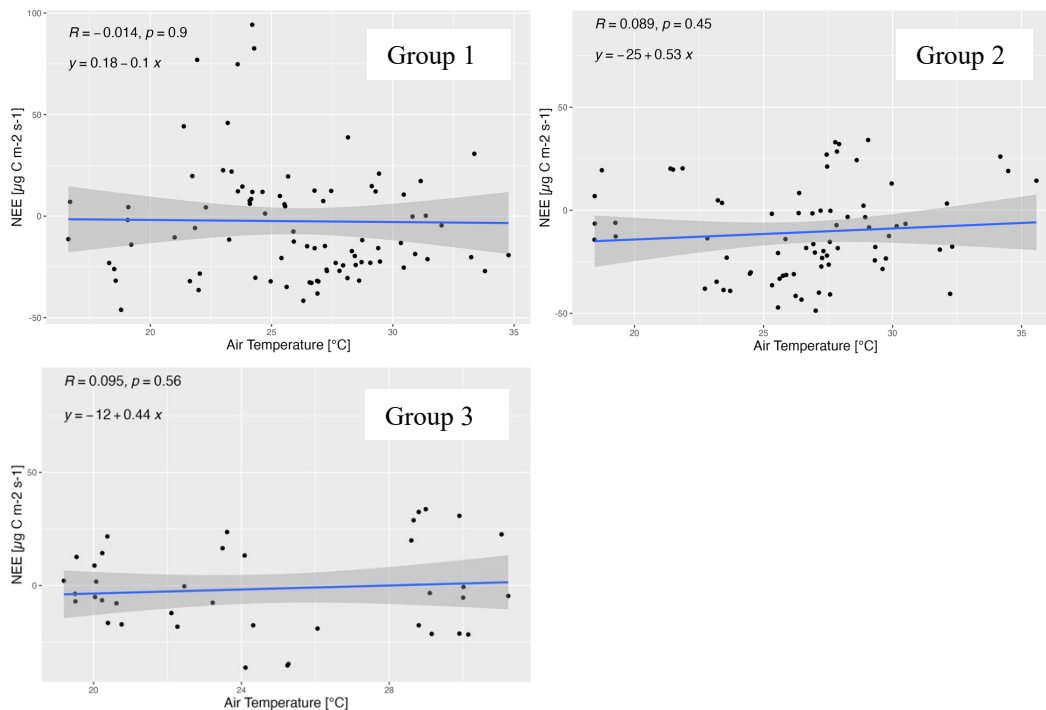
A 54: Linear regression plots with equation and corresponding p-value between NEE and PAR of the groups 1, 2 and 3. The blue line represents the regression line and the dark grey area the confidence interval.

A 55: Linear regression plots with equation and corresponding p-value between ER and PAR of the groups 1, 2 and 3. The blue line represents the regression line and the dark grey area the confidence interval.
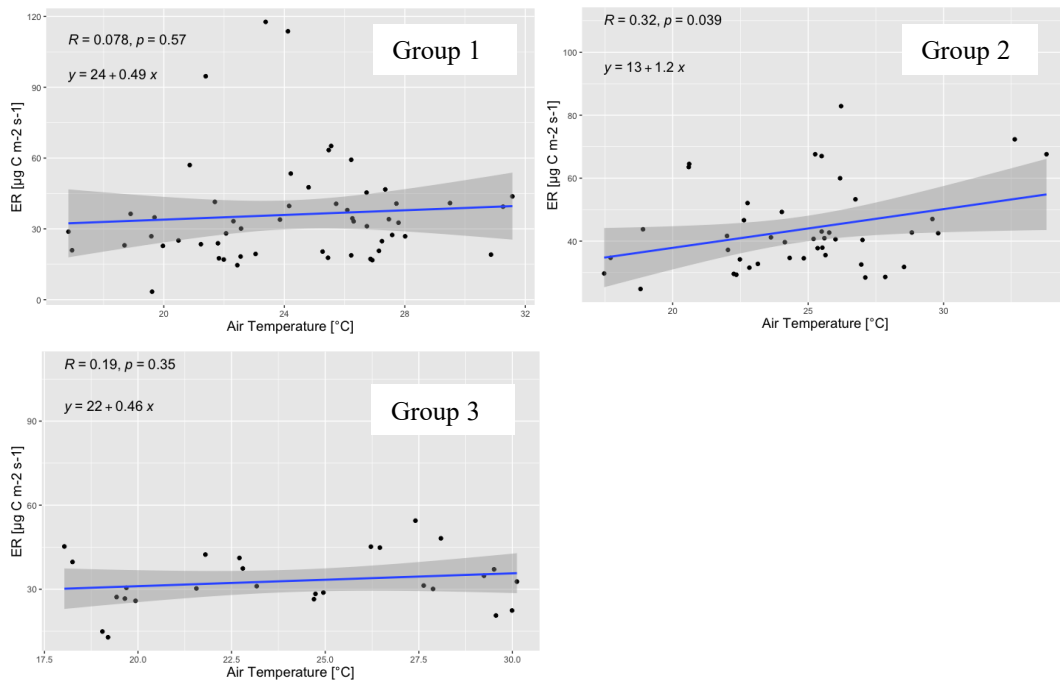
A 56: Linear regression plots with equation and corresponding p-value between GPP and PAR of the groups 1, 2 and 3. The blue line represents the regression line and the dark grey area the confidence interval.


A 57: Linear regression plots with equation and corresponding p-value between NEE and air temperature of the groups 1, 2 and 3. The blue line represents the regression line and the dark grey area the confidence interval.

A 58: Linear regression plots with equation and corresponding p-value between ER and air temperature of the groups 1, 2 and 3. The blue line represents the regression line and the dark grey area the confidence interval.

A 59: Linear regression plots with equation and corresponding p-value between GPP and air temperature of the groups 1, 2 and 3. The blue line represents the regression line and the dark grey area the confidence interval.
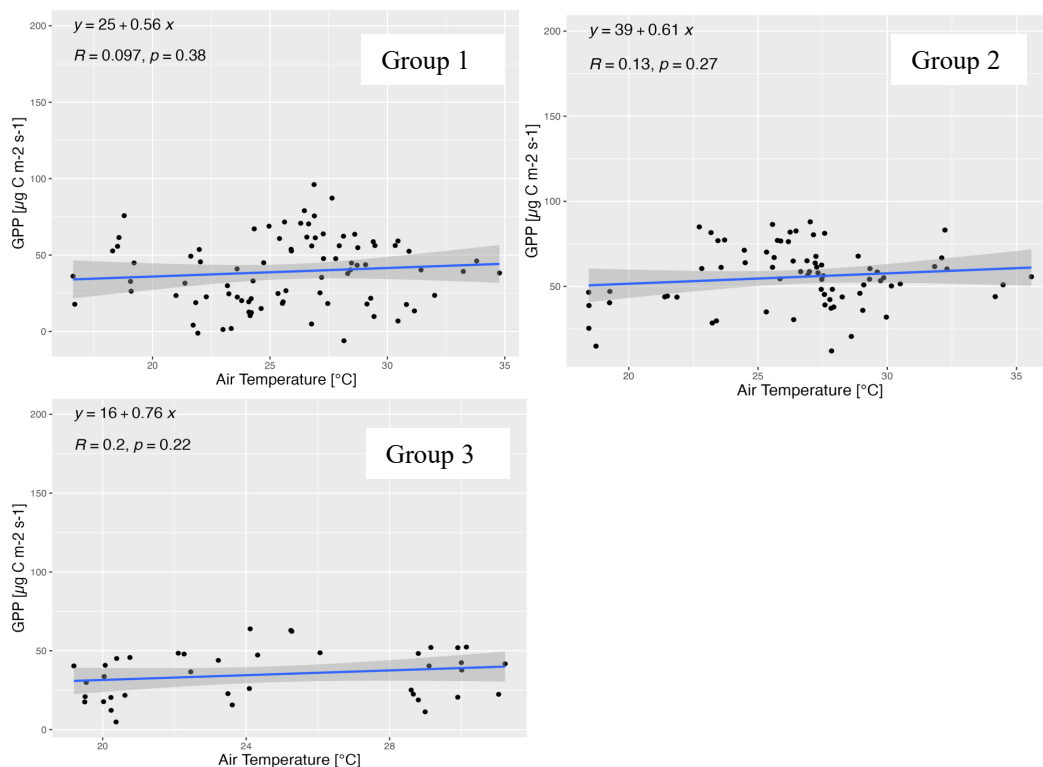
Eidesstattliche Erklärung

Ich, Annelen Küchenmeister, geb. am 28.08.1998, versichere, dass ich die vorliegende Arbeit ohne fremde Hilfe und ohne Benutzung anderer als der angegebenen Quellen angefertigt habe, und dass die Arbeit in gleicher oder ähnlicher Form noch keiner anderen Prüfungsbehörde vorgelegen hat. Alle Ausführungen der Arbeit, die wörtlich oder sinngemäß übernommen wurden, sind als solche gekennzeichnet.

Annelen Küchenmeister

28.04.2024, Unterbreizbach